Spring 2023

Phosphate and Borophosphate Glasses for optical and Biomedical Applications

Parker Tracy Freudenberger
Missouri University of Science and Technology

Department: Materials Science and Engineering

PHOSPHATE AND BOROPHOSPHATE GLASSES FOR OPTICAL AND BIOMEDICAL APPLICATIONS

by

PARKER TRACY FREUDENBERGER

A DISSERTATION

Presented to the Graduate Faculty of the

MISSOURI UNIVERSITY OF SCIENCE AND TECHNOLOGY

In Partial Fulfillment of the Requirements for the Degree

DOCTOR OF PHILOSOPHY

in

MATERIALS SCIENCE AND ENGINEERING

2023

Approved by:

Richard K. Brow, Advisor
Anthony Convertine
Michael Moats
Mark Schlesinger
Jay Switzer

PUBLICATION DISSERTATION OPTION

This dissertation consists of the following four articles, formatted in the style used by the Missouri University of Science and Technology:

"Spectroscopic and chromatographic analyses of zinc borophosphate glasses," found on pages 23-46, was published in *Physics and Chemistry of Glasses - European Journal of Glass Science and Technology Part B*, in December of 2018 in Volume 59 and Issue 6.

"Characterization of $20Na_2O \cdot 30((1-x)CaO \cdot xSrO) \cdot 50P_2O_5$ glasses for a resorbable optical fiber application," found on pages 47-82, was published in *International Journal of Applied Glass Science*, in February of 2019 in Volume 10.

"Network Structures and the Properties of Na-Ca-Sr-Borophosphate Glasses," found on pages 83-128, was published in the *Journal of Non-Crystalline Solids*, in January of 2023 in Volume 600.

"Dissolution Behavior of Borophosphate Glasses in Deionized Water and Simulated Body Fluid," pages 129-163, was accepted for publication to the *Journal of Non-Crystalline Solids: X* in March 2023.

ABSTRACT

The goal of this work was to connect the network structures of phosphate and borophosphate glasses to the compositional dependence of properties related to biomedical applications. The glasses were characterized by a variety of techniques, including phosphate ion chromatography, Raman spectroscopy, and ^{11}B and ^{31}P Magic Angle Spinning Nuclear Magnetic Resonance spectroscopy, which provide qualitative and quantitative information about the phosphate and borate moieties that constitute the network structures. The systematic addition of borate to a phosphate glass initially creates tetrahedral borate sites that replace P-O-P linkages with B-O-P linkages, and the properties of the resulting borophosphate glasses can be understood by modeling the number of bridging oxygen linkages between the borate and phosphate units; there are systematic increases in glass transition temperature with increases in the number of bridging oxygens per network former. The network structure also affects the dissolution rates of the glasses, but the nature of the crosslinking bonds is more important than their numbers. The substitution of SrO for CaO also decreases the dissolution rates of both Na-Ca/Sr-metaphosphate glasses as well as the borophosphate glasses, which are of interest for the use in biomedical applications. Finally, the systematic substitution of P_2O_5 for B_2O_3 in a series of Na-Ca/Sr-borophosphate glasses affects the dissolution rates of the glass in simulated body fluid, the pH of the SBF, and the nature of the phosphate phases that precipitate on the glass surface. It remains to be seen if these bioactive responses could be used to design new biomedical devices.

ACKNOWLEDGMENTS

The work found in this dissertation would not have been possible without the financial support of the National Science Foundation (DMR-1207520), International Materials Institute for New Functionality in Glass at Lehigh University (NSF DMR-0844014), and Graduate Assistance in Areas of National Need (GAANN) Fellowship (Department of Education). Nor without the hospitality of the Materials Processing Engineering Lab at Ehime University and the Project Planning Department at Nippon Electric Glass Co., Ltd.

One page certainly is not enough to thank everyone, but I'd like to start with my advisor, Dr. Richard K. Brow, for his guidance. I will be forever grateful for the opportunities that he has provided. Thanks also to my committee for their support, whether it was FactSage help, lending a book, or giving life lessons in the hall of MRC. A large piece of the puzzle for this work would have been lost without Randy Youngman's insight and encouragement. The staff of MRC and the MS&E Dept. (Patty, Sissy, Teneke, Dr. Bohannan, Fred, Ron, and Denise) are the best and deserve the world.

Jaime, Eric, Leiren, Rebekah, Jincheng, Paul (both of you), and Dr. Reidmeyer: I am appreciative of your friendships, past and present, especially since you all have gone or are going through this process yourselves. Dana, Melissa, Chandlee, Curtis, Em, Josh, Juniper, Alec, (another) Paul, Crystal, and Mike: thank you for listening and joining me in my outlets, whether it was DnD, art, travel, books, or video games.

And last but certainly not least, I'd like to thank my parents, Rich and Laurie, and my fiancé, Dolan. I have no words; I would not have finished if not for the three of you.

TABLE OF CONTENTS

LIST OF ILLUSTRATIONS

SECTION Page

PAPER I

PAPER IV

LIST OF TABLES

1. INTRODUCTION

The compositional-dependence of the properties of several different series of phosphate and borophosphate glasses, including properties relevant to biomedical applications, were related to the molecular-level structures of the glasses, determined by a variety of spectroscopic and chromatographic techniques. Structural models developed by Hermansen, Hoppe, and others, were extended to explain the composition-property trends. In general, properties were dependent on the relative numbers of bridging oxygens that link the neighboring phosphate and borate polyhedra that constitute the glass-forming network and on the type of metal cation that charge-balanced the anionic phosphate and borate sites.

In the borophosphate compositional series, the initial replacement of P_2O_5 by B_2O_3 created tetrahedral borate units and reduced the average size of the P-anions that constituted the original phosphate-glass structure. Trigonal borate sites were created in glasses with greater B_2O_3 contents, generally near compositions where the O/P ratio exceeded 4 and the dominant structural motif changed from borophosphate to borate. The structures of the zinc borophosphate (ZBP) glasses described in the Paper section were analyzed using the Hoppe model, which considers the availability of terminal oxygens to coordinate isolated metal polyhedra in a phosphate network.[1] Because boron is able to compete with phosphorus for oxygens, the model predictions for B-coordination in these ZBP glasses were not as good as they were for predictions of Al-coordination in an earlier study of zinc aluminophosphate glasses.[2] The structures of the Na-Ca/Sr-borophosphate glasses described in the Paper section were in general agreement with the

model of Hermansen, et al.[3, 4] who predicted the transition from a borophosphate network to a borate network when the former was saturated with tetrahedral borate sites. This structural transition was correlated with a break in the molar volume of the glasses and a minimum in the dissolution rates of the glasses in water and in simulated body fluid (SBF). The glass transition temperature (T_g) of these glasses was most dependent on the number of network cross-links, through bridging oxygens, between the P- and B-polyhedra, with the relative fraction of fully coordinated B-tetrahedra having the greatest effect on T_g. A similar explanation can be used for the effect of the B_2O_3-content on the T_g of a ZBP glass. Replacing CaO with SrO in the Na-Ca/Sr-phosphate glasses described in the Paper section decreased T_g and the isokom temperatures, an effect best explained by the lower field strength of the Sr^{2+} ions producing weaker ionic bonds between neighboring metaphosphate chains. There was no systematic effect of the type of alkaline earth on the T_g of an Na-Ca/Sr-borophosphate glass.

The dissolution characteristics of the Na-Ca/Sr-metaphosphate and -borophosphate glasses were studied in detail. The metaphosphate glasses were developed to produce bio-soluble fiber waveguides that were intended for implanted therapeutic and diagnostic devices that could be eventually resorbed by the body. The replacement of CaO by SrO increased the refractive index of the glasses in ways suitable for creating core-clad optical waveguides. Their dissolution rate in water decreased systematically when SrO replaced CaO and this was related to a decrease of the electronic asymmetry associated with the P-tetrahedra that constitute the metaphosphate chains, as indicted by the systematic changes in the infrared and Raman spectra of the glasses. The linear

dissolution kinetics were used to model the optical transmission characteristics of a fiber waveguide in a phosphate buffer solution.

For the Na-Ca/Sr-borophosphate glasses, the dissolution rates depended on several competing factors. The initial replacement of P_2O_5 by B_2O_3 decreased dissolution rates by several orders of magnitude, and this was related to the creation of tetrahedral borate sites that connect phosphate anions into a borophosphate network. The resulting smaller phosphate anions themselves are less soluble than long anions, like those from the metaphosphate glasses described in the Paper section. At the transition from a borophosphate network to a borate network with the further replacement of P_2O_5 by B_2O_3, the dissolution rates increased significantly because of the rapid hydrolysis of the borate network. The replacement of P_2O_5 by B_2O_3 increased the solution pH when boric acid, a weaker acid than phosphoric acid, was released to solution, and the dissolution kinetics of both phosphate and borate glasses are slower in pH neutral and basic solutions than in acidic ones. Finally, the precipitation of phosphate phases on the surfaces of the borophosphate glasses, in reacted in both water and in SBF, affected the release rates of ions from the dissolving glasses. The nature of the phosphate phases that formed on the surfaces of these reacting glasses, and their dependence on local pH, affects their use for biomedical applications.[5–7]

2. LITERATURE REVIEW

This literature review is intended to provide a general description of simple phosphate, borate, and borophosphate glass structures. The use of borate and phosphate glasses in biomedical applications are discussed. The compositional dependence of structure and the resulting effects on material properties are also described, with particular emphasis on the dissolution properties of these glasses.

2.1. GLASSES IN BIOMEDICAL APPLICATIONS

Bioactive silicate-based glasses were first developed by Hench in the late 1960s.[8] Glass is ideal for use in biomedical applications due in part to the fact that it can be produced in several different forms, from spheres to powders to a cotton-wool-like scaffolds.[9] Spheres are used in a product called Therasphere™, which is a yttrium doped aluminosilicate composition that has been used to increase the median life expectancy from 244 to 649 days and 64 to 302 days for Okuda stage I and stage II patients, respectively.[10] Additionally, glass spheres have also been reacted in a phosphate solution to produce hollow HAP microspheres, which have been shown to encourage bone regeneration.[11] Glasses in powder form (NovaMin) are utilized in toothpaste as a way to repair teeth by creating a HAP-like layer across exposed dentine and have also been used in bio-inks for the 3D printing of scaffolds.[12,13] Wound healing products made of cotton wool-like scaffolds like MIRRAGEN™ Advanced Wound Matrix are used to promote vascularization, penetration of cells and transport of nutrients throughout the scaffold in order to heal chronic wounds.[14]

Glasses are considered bioactive if hydroxyapatite (HA), a component of tooth enamel and bone, forms upon the surface of the glass when it reacts in physiological environments (*in vitro* or *in vivo*).[8,15-17] Borate-based glasses, like the 13-93B3 composition, have faster reaction rates.[16,18,19] and were found to be useful for drug release applications and promoted stem cell proliferation and differentiation *in vitro* and tissue infiltration *in vivo*.[19,20] Phosphate glasses have also been developed for biomedical applications, due in part to their chemical similarity to bone composition. Additionally, the solubility and bio-compatibility of phosphate glasses can be controlled by composition, and phosphate glasses have a relatively large glass forming region, so materials specifically tailored for biological applications can be designed.[21-24] Particularly, phosphate glasses and other bioactive glasses are also being investigated for the delivery of antibacterial ions and for tissue engineering.[15,16]

2.2. GLASS STRUCTURE

2.2.1. Phosphate Glass. Phosphate glasses have structures based on networks of phosphate tetrahedra that link to form anions through bridging oxygens.[25] These anions can be quantitatively described using the Pn notation, with n being the number of phosphate tetrahedra in the anion. These networks can also be classified by considering the types and relative concentrations of different P-tetrahedra using the Qi notation, where i is the number of bridging oxygens (i = 0, 1, 2, 3) associated with each tetrahedron. For example, a P_3 anion has three P-tetrahedra, one Q^2 tetrahedron that links two Q^1 tetrahedra. The size of a phosphate anion decreases with increasing oxygen-to-phosphorus (O/P) ratio. This ratio is conventionally used to compare and characterize

glasses over a wide compositional space and can be varied through the addition of other oxide components to the glass composition.[25] All these notations are summarized in Figure 2.1.

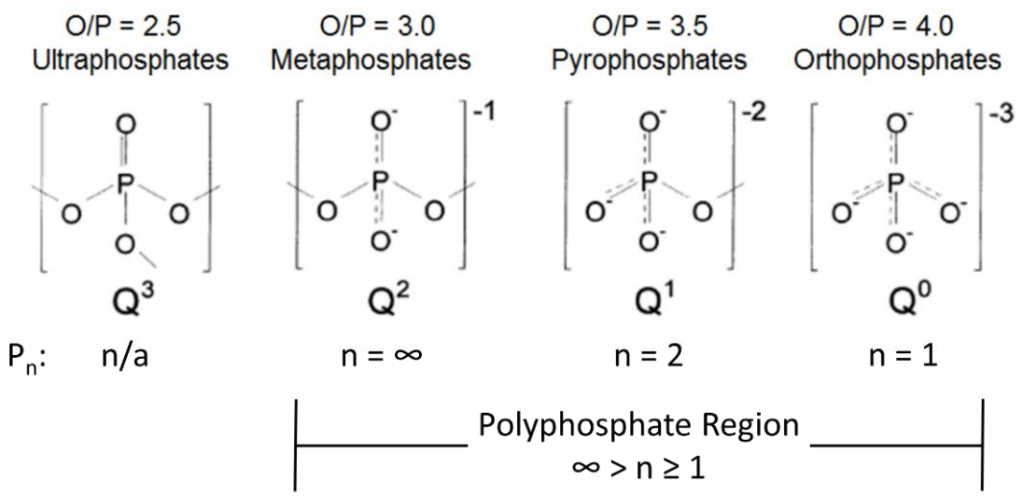

Figure 2.1. Demonstration of the notations used in describing phosphate glass structure.[25]

Phosphate glasses can be organized into different classifications based on the O/P ratio (Figure 2.1): ultraphosphates (2.5<O/P<3), metaphosphates (O/P=3), polyphosphates (3.0<O/P<4.0), pyrophosphates (O/P=3.5), and orthophosphates (O/P=4.0).[25] The categorization of phosphate glass compositions into sets based on structural units is one way to understand composition-property trends. When metal oxides are added to a phosphate glass, the additional oxygen is incorporated into the phosphate network as nonbridging oxygens, producing shorter anions with increasing O/P ratios. Because of this, phosphate glasses can have a wide variety of structures, from a fully

cross-linked network like vitreous P_2O_5 based on Q^3 tetrahedra, the polymeric structure of long P_n-anions (n>50) found in metaphosphate glasses, to short (n≤2) pyrophosphate and monophosphate units in glasses with O/P≥3.5.

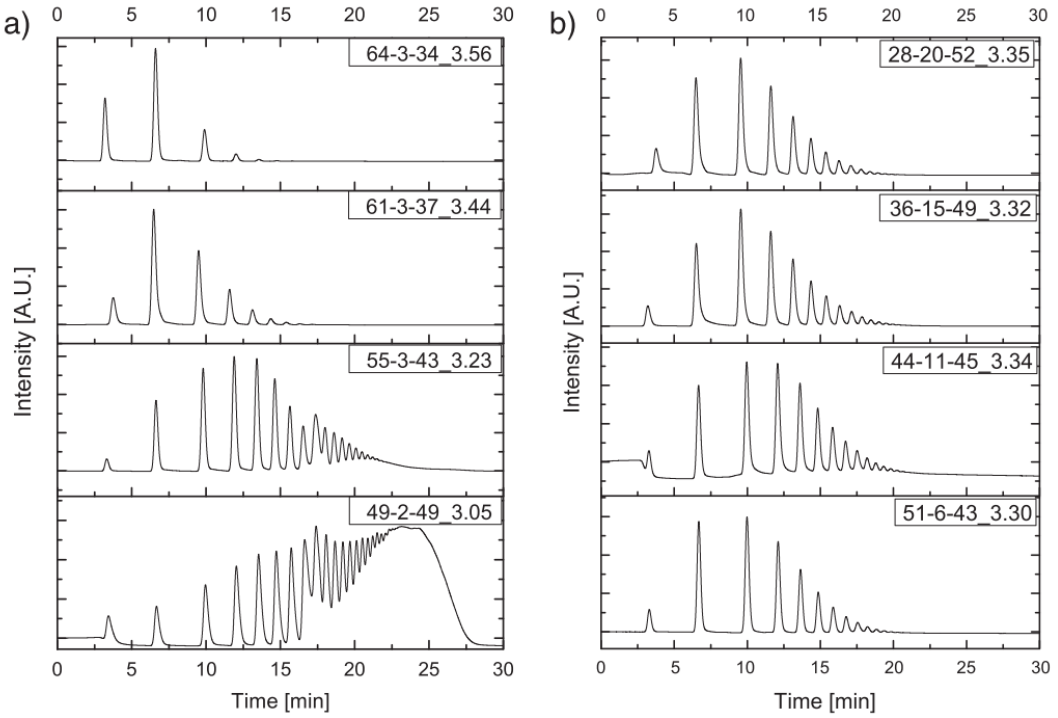

Figure 2.2. Example HPLC chromatographs of zinc aluminophosphate glasses with different O/P ratios (a) and a similar O/P ratio (b).[26] The labels in top right corner of each chromatograph identify the glass composition and the O/P ratio (ZnO-Al_2O_3-P_2O_5_O/P).

Sales *et al.*[27] established procedures for characterizing the structures of phosphate glasses using High Pressure Liquid Chromatography (HPLC). HPLC chromatographs provide information about the distribution of phosphate anions and the average phosphate anion size, for glasses with O/P>3. Glasses are dissolved in solutions that minimize the hydrolysis of the phosphate anions, and an assumption is made that the distribution of

anions analyzed in solution is representative of the anion distribution in the original glass. A typical set of chromatographs from glasses with a wide range of O/P ratios is shown in Figure 2.2.

Peaks in the chromatographs from left to right represent phosphate anions with increasing numbers (n) of tetrahedra, P_1, P_2, P_3, and on to P_n, released from the chromatography column after longer retention times.[27] The broad hump near 20 minutes in the chromatograph from the O/P = 3.05 glass is due to the continuous release of longer anions (n>12) that cannot be resolved by the HPLC system used.[19] HPLC cannot provide quantitative information about the structures of ultraphosphate glasses because the hydrolysis of Q^3 tetrahedra during the preparation of the chromatographic samples changes the P-anion distributions in the solutions from those in the original glass.

The properties of phosphate glasses also depend on the coordination environments of the metal cations that modify the glasses. Hoppe has shown that the number of terminal (nonbridging) oxygens per metal cation (N_{TO}) is related to the coordination number of those metal cations (CN_{Me}).[28] For a binary phosphate glass with the molar composition $x(Me_{2/\nu}O)\ (1\text{-}x)P_2O_5$, N_{TO} can be calculated from:

$$N_{TO} = \nu(x+1)/x \qquad [2.1]$$

In Equation [2.1, ν is the valence of the $Me^{\nu+}$ cation. When $N_{TO} \geq CN_{Me}$ (structural range I), isolated metal polyhedra are incorporated into the phosphate glass structure. With increasing $Me_{2/\nu}O$ content, the average coordination number of these polyhedra can decrease with decreasing N_{TO} to remain in isolated sites. When a minimum

value in CN_{Me} is reached, and so $N_{TO} < CN_{Me}$, then there are insufficient TO for the metal polyhedra to remain isolated and so those polyhedra must form a Me-O-Me subnetwork by sharing TO on the phosphate anions (structural range II). For many phosphate systems, there are breaks in the composition-property trends at the onset of the formation of the metal polyhedral subnetwork, as seen, for example, by the minima in packing densities for different binary phosphate glasses shown in Figure 2.3.[29]

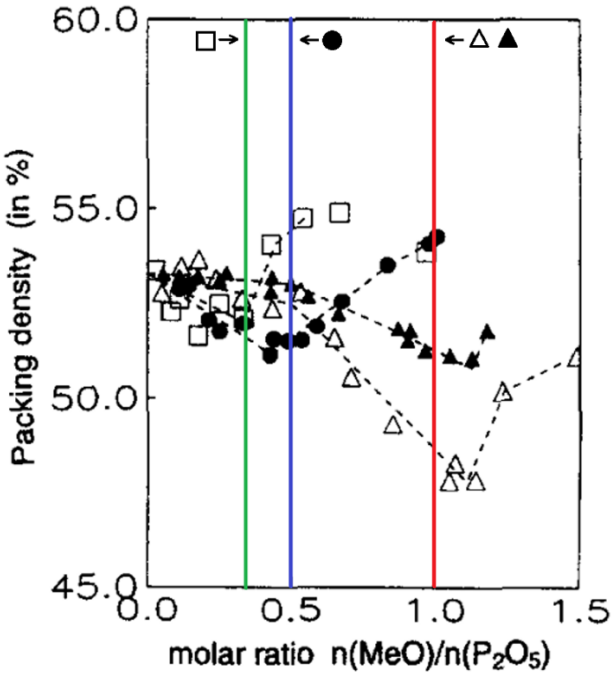

Figure 2.3. The packing densities of binary zinc (open triangles), magnesium (closed triangles), calcium (closed circles) and barium (open squares) phosphate glasses ($MeO-P_2O_5$) plotted against the molar ratio ($n[MeO]/n[P_2O_5]$).[29] Dashed lines are a guide to the eye. The lines indicating the transition between structural ranges are included for the purposes of this review and indicate the expected minima positions at 0.33 (green), 0.5 (blue), and 1.0 (red) for barium, calcium, and zinc and magnesium phosphate glasses, respectively.

Figure 2.4 demonstrates the effect of the changes in modifier coordination on density and glass transition temperature for lithium, sodium, and, less strongly, cesium ultraphosphate glasses.[30] The average coordination in both metaphosphate and ultraphosphate glasses[31,32] have been found to be tetrahedral and in the range of 4-5, respectively. For sodium, the coordination number is approximately 5.[33,34] Using Equation 2.1 and these coordination numbers, the transition from structural region I to structural region II is estimated to occur around 20-25 mol% for Li and Na ultraphosphate glasses, which is where the density and glass transition temperature minima occur. The coordination environment of cesium is not as well known, but based on the trends in Figure 2.4, the Cs^+ coordination number is estimated to be 6.[35]

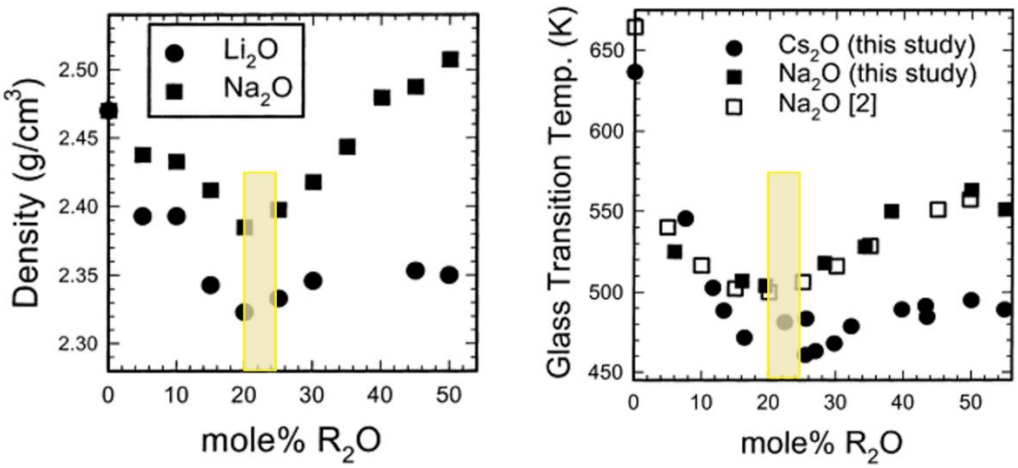

Figure 2.4. Density (left) and glass transition temperatures (right) of sodium, lithium, and cesium ultraphosphate glasses. The local minima in the properties indicate a transition from structural range I to structural range II in Hoppe's structural theory.[35] Yellow bars indicating the estimated transition between structural ranges based on 2.1 are used as emphasis for this review.

As the modifying metal oxide content is increased, the density and glass transition temperatures decrease due to the Q^3 network expanding to longer, weaker bonds to accommodate the additional cations. Once the modifier content has surpassed 20 mol %, the transition from structural range I ($N_{TO} \geq CN_{Me}$) to structural range II ($N_{TO} < CN_{Me}$) occurs, and therefore the alkali polyhedra must share TOs through corners and edges of Q^2 and Q^3 tetrahedra, increasing the density and glass transition temperatures through a tighter, stronger glass network. Through compositional modifications such as these, the solubility of phosphate glasses in aqueous solutions can be tailored to obtain a wide range of ion release rates, and will be discussed further on in this review.[36]

2.2.2. Borate Glass. A local minima or maxima can be observed in several properties of borate glasses due to the increase and subsequent decrease in cross-linking with increasing modifier content, and is described as the borate anomaly.[37] Figure 2.5 demonstrates the these changes in borate structure, estimated by Shelby in 1983, and the effect on glass properties.[38] Because of the borate anomaly, many alkali borate property trends are plotted as a function of the alkali content or quantity of $BØ_4^-$ units.

The structure of vitreous boric oxide is based on trigonal borate units ($BØ_3$) with bridging oxygens (Ø) that link to neighboring trigonal units. A large fraction of these trigonal units, 60-70%, form planar boroxol rings.[39] With the addition of metal oxides to B_2O_3, the additional oxygens are initially incorporated into the borate network by converting borate triangles to borate tetrahedra, ($(BØ_4)^-$) which are charge-balanced by the metal cations. The associated changes in glass properties, including increasing glass transition temperatures, decreasing thermal expansion coefficients, and slower dissolution kinetics, are expected from the increasingly cross-linked borate glass structures.[40-43]

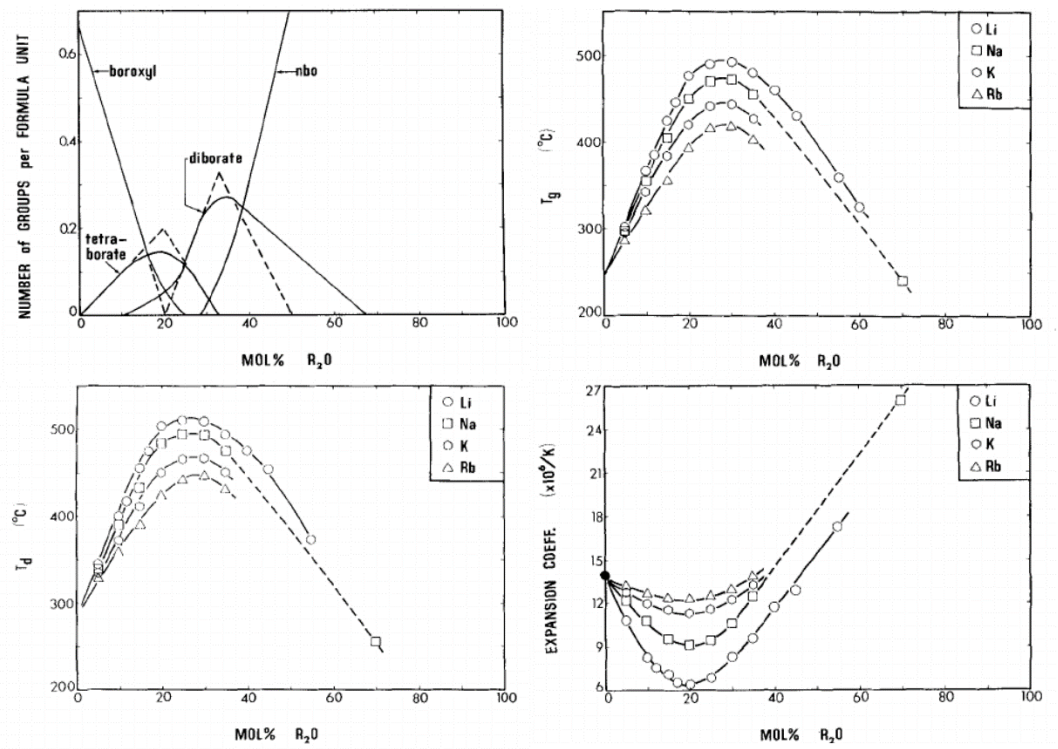

Figure 2.5. The borate anomaly as demonstrated by the formation of the different borate groups as modifying oxide is added (top left), and the resulting property trends in glass transition temperature (top right), dilatometric softening point (bottom left), and coefficient of thermal expansion (bottom right).[40]

When the O/B ratio reaches about 1.75, viz., the diborate composition, further additions of metal oxide create B-triangle with nonbridging oxygens and these replace the tetrahedral sites, reducing the extent of cross-linking in the borate network, with associated reversals in the composition-property trends. Equations 2.2[2.2] and 2.3 are used to calculate the relative fractions of borate tetrahedra that constitute the structures of xR_2O-$(100-x)B_2O_3$ glasses for $x \leq 33.3$ and for $x \geq 33.3$, respectively:[44]

$$N_4 = \frac{x}{100 - x} \qquad [2.2]$$

$$N_4 = \frac{300 - 4x}{500 - 5x} \qquad [2.3]$$

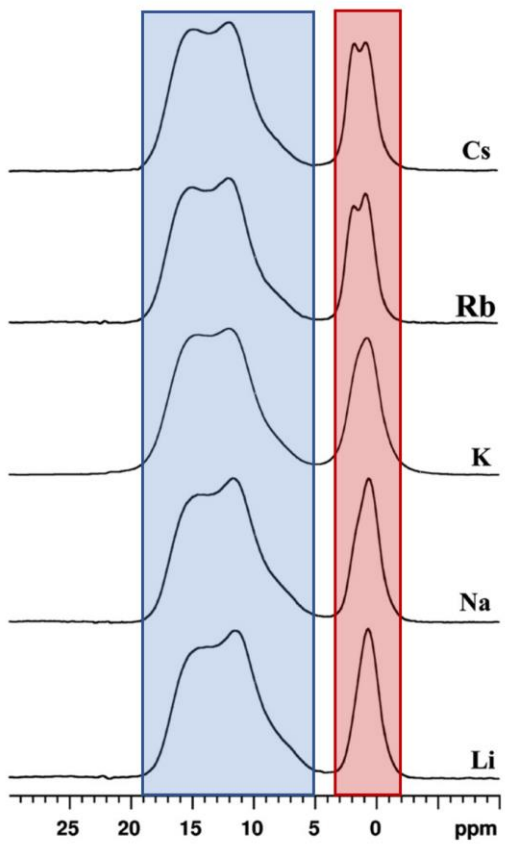

Figure 2.6. ^{11}B MAS NMR spectra of various alkaline borate glasses of the composition $Me_2O:B_2O_3 = 0.2$.[45] The blue and red boxes highlighting features attributed to the trigonal and borate species, respectively, are added for the purposes of this review.

^{11}B Magic Angle Spinning Nuclear Magnetic Resonance (MAS NMR) is a common tool used to quantify these borate anions that constitute glass structures. A

typical set of these spectra[39] for several alkali borate compositions are shown in Figure 2.6. Three coordinated boron sites—denoted by the blue highlighted area—typically have a substantial quadrupole coupling constant ($C_Q \approx 2.6$ MHz), which translates into the broad quadrupolar peak from 5 to 19ppm in the spectra.[46-48] In contrast, the peaks from approximately -2 to 3ppm indicate the presence of tetrahedral borate structures,[46,49] are narrow due to relatively high site symmetry, resulting in a significantly lower quadrupole coupling constant ($C_Q \approx 200$ kHz) as indicated by the red highlights, respectively. The doublets observed in the cesium and rubidium spectra are due to two distinct $(B\text{Ø}_4)^-$ species arising from medium-range order.[50]

2.2.3. Borophosphate Glass. B_2O_3 has been added to phosphate glasses for various reasons, including the enhancement of chemical durability, increasing ionic conductivity, and improving non-linear optical properties.[51-55] Christensen *et al.*[52] used ^{11}B and ^{31}P MAS NMR to investigate the effects of composition on the structures and properties of alkali borophosphate glasses.

The ^{11}B MAS NMR spectra of the glasses shown in Figure 2.7 demonstrate that tetrahedral borophosphate units, $B(\text{Ø}P)_4$, assigned to the symmetric peak near -5 ppm, form with the initial addition of B_2O_3. At greater concentrations, a second tetrahedral peak is evident at lower frequencies and assigned to borate sites with at least one borate polyhedron as a nearest neighbor.[55-59] Trigonal borate species are assigned to the broad, asymmetric feature between 10 and 15 ppm in the spectra from glasses with borate fractions of $x \geq 0.5$, and in the phosphate-free glass ($x=1$). Trigonal units constitute about half of the borate network, along with the tetrahedral borates, $B(\text{Ø}B)_4$, as expected from Equation 2.3.

In the ^{31}P MAS NMR spectra of the glasses shown in Figure 2.7, only phosphate structures having two (Q^2) and three bonding oxygens (Q^3) were identified by Christensen *et al.*, except in the spectra for the x = 0.9 composition, in which the small peak at approximately 15 ppm denotes the presence of Q^1 species. This indicates the propensity for large changes in shifts over compositional spaces.

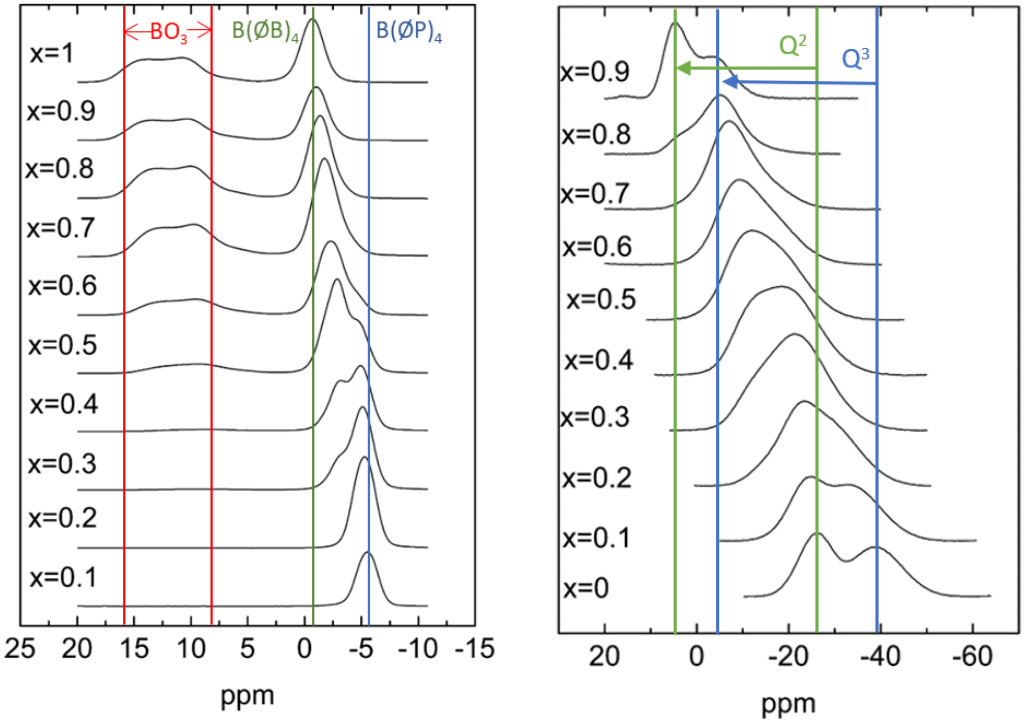

Figure 2.7. Representative borophosphate ^{11}B MAS NMR spectra (left) and ^{31}P MAS NMR spectra (right) from $0.35Na_2O + 0.65[xB_2O_3 + (1 - x)P_2O_5]$ compositions.[52] Peak demarcation is used as emphasis for this review.

Christensen *et al.*[52] noted the formation of a borophosphate tetrahedral network with the preferential association of alkali ions with the minority glass former. The formation of tetrahedral borate anions linked to the phosphate anions was consistent with

the theory that heteroatomic B-O-P bonds are more energetically favored[59] and were responsible for increased glass transition temperatures and durability and decreased coefficient of thermal expansion (CTE), when B_2O_3 was added to a phosphate glass.[51-55] An increase in chemical durability has been observed in studies where borate has been added in amounts as small as 1.25 mole percent to phosphate compositions.[60]

2.3. GLASS DISSOLUTION

2.3.1. Phosphate Glass Dissolution. The dissolution of phosphate glasses can be divided into two mechanisms: hydration and hydrolysis.[36,61] Hydration, the first step in dissolution, is an ion exchange process or diffusion of water into the network, in which the weakest bonds, between the NBO and metal cations, break first.[36,62] Ion exchange across the hydration layer and water penetration is dependent on the surface concentration of the interdiffusing ion, multicomponent interdiffusion coefficient, and the exchange potential at the exchange site.[63] The initial hydration rates are determined by the fraction of NBOs and the concentration of mobile ions (i.e. Na^+, Ca^{2+}, etc.).[64] With the depletion of alkali ions, intact phosphate anions are released into solution.[27]

Once the phosphate species have been hydrated and released into solution, hydrolysis—the cleavage of phosphorus to oxygen bonds—can occur (Equation 2.4). Phosphate chains have been found to be more stable in a basic pH environment, whereas phosphate rings are more stable in acidic conditions.[36,65] Additionally, longer chains hydrolyze more rapidly, and the rate of hydrolysis is also increased by the presence of alkali ions in solution.[66] In the former, the average charge on a NBO increases as a phosphate anion shortens, which results in an increase in average bond strength between

the metal cations and phosphate anions.[67] The latter can be linked to the pH of the leachate solution, which decreases as the phosphate chains are broken down into orthophosphates. A reaction (Equation 2.5) occurs between the alkali species in solution and a NBO oxygen site on a phosphate tetrahedron, releasing more H^+ ions into solution.[68]

$$R - P - O - P - R + H_2O \rightarrow R - P - OH + HO - P - R \qquad [2.4]$$

$$R - P - OH + M \rightarrow R - P - OM + H^+ \qquad [2.5]$$

Initial studies on alkali metaphosphate glasses by Bunker *et al.* established that the first stage of dissolution was controlled by surface hydration after observing a square root of time dependence ($t^{1/2}$) for weight loss.[36] The second stage is the hydration of intact polyphosphate chains from the glass surface and follows a linear time dependence. These stages can be observed in Figure 2.8. The dissolution rate in both stages is dependent on the solution pH and the concentration of other ions in the solution. In this case, with congruent dissolution, all the glass constituents are released from the glass at the same time, and the absorption and coprecipitation of the constituents is negligible, since solubility limits are not exceeded. Bunker concluded that the thickness of the hydrated layer would be controlled by the average chain length of the phosphate anions and remain constant with time.[36]

After this square root of time dependence dissolution mechanic was not observed in a few other studies, it became clear that dissolution kinetics are affected by several

other factors, including the surface topology and layer formation, saturation effects, solution chemistry, and the ratio of glass surface area to solution volume.[23,69] Delahaye *et al.* suggested that the $t^{1/2}$ time law in Bunker's model was due to a modification of the hydrated layer and increase in the electrostatic interactions between polyphosphate chains, resulting from an increase of the ionic strength of the solution and decrease in dissolution rate.[69] Additionally, it was shown that the developed hydrated layer of metaphosphate glass in an acidic solution has the same composition and structure as the surface of a pristine glass, and the dissolution reactions of the hydrated layer are affected by the metal chelating structure of the phosphate anions.[70] Moreover, work on alkali polyphosphate glasses by Lina *et al.* confirmed the dependence of dissolution kinetics on solution chemistry, as dissolution rates increased when leachate solution was replenished.[71]

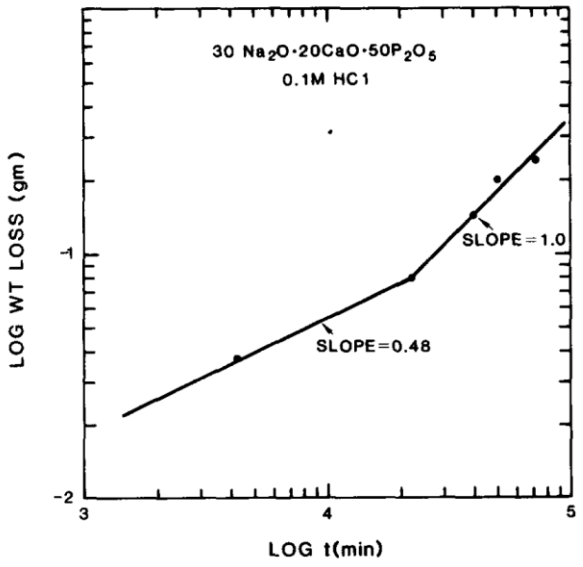

Figure 2.8. Log (weight loss) over log (time) for glass of the composition $30Na_2O$–$20CaO$–$50P_2O_5$ at 20°C and pH = 3 (HCl).[36]

Orthophosphates in solution, the products of hydrolysis, react with alkali ions, particularly calcium, in the solution to produce various species, several of which precipitate. The pH environment has an effect on which of these form. For example, amorphous calcium phosphate (ACP) and hydroxyapatite (HAP) are the stable phases in basic environments ($6 \leq pH \leq 12$), whereas crystalline calcium orthophosphate species such as dicalcium phosphate dihydrate (brushite, $CaHPO_4 \cdot 2H_2O$) and monocalcium phosphate monohydrate ($Ca(H_2PO_4)_2 \cdot H_2O$) form in more acidic conditions ($pH > 6$).[72] Amorphous calcium phosphate is a precursor to hydroxyapatite, and the rate of transition from ACP to HAP increases as the pH decreases from 12 to 6.[73] It is worth noting that the calcium to phosphorus (Ca/P) ratio in HAP is higher (Ca/P = 1.67) than that of its precursor, ACP (Ca/P ~1.5).

2.3.2. Borate Glass Dissolution. Although the dissolution of borate glasses also includes hydration and hydrolysis, these steps occur concurrently to one another, resulting in the hydration and release of the modifying metal cations. Goetschius et al. determined experimentally that while the overall dissolution rate (k_{dr}) is dependent on the rate of hydration ($k_{hydration}$), hydrolysis ($k_{hydrolysis}$), and transport (k_{trans}), as shown in Equation 2.6, the effects on khydrolysis from the concentration of $(BØ_4)^-$ units in the glass is stronger than those of alkali species on khydration.[74] This is due to the proton-catalyzed hydrolysis reactions (Equations 2.7 and 2.8) that involves the protonation of a bridging oxygen on a borate species by exchanging the proton for an alkali ion, destabilizing the bond and causing it to hydrolyze.[75] Zapol et al. used first principle calculations to explain that the bonds in $BØ_3$ units have an enhanced reactivity compared to those in $(BØ_4)^-$.[75] Furthermore, Bunker et al. have used the reactions described in

Equations 2.7 and 2.8 ($B\emptyset_3$ and $(B\emptyset_4)^-$, respectively) to demonstrate that these two steps—hydration and hydrolysis—occur simultaneously in borate glasses.[76]

$$\frac{1}{k_{dr}} = \frac{1}{k_{hydration}} + \frac{1}{k_{hydrolysis}} + \frac{1}{k_{trans}} \qquad [2.6]$$

Equations 2.7 and 2.8 describe the reactions of water with the modifying oxide ($R^{x+}O_{x/2}$) to neutralize $B\emptyset_2O^-$ (NBO on trigonal borate site) and $(B\emptyset_4)^-$ units, respectively.[67]

$$(R^{x+}[B\emptyset_4]_x^{x-})_{glass} + xH_2O \rightarrow x(H^+[B\emptyset_4]^-)_{glass} + (R^{x+} + xOH^-)_{soln} \qquad [2.7]$$
$$\rightarrow x(B\emptyset_2OH)_{glass} + (R^{x+} + xOH^-)_{soln}$$

$$(R^{x+}(B\emptyset_2O^-)_x)_{glass} + xH_2O \rightarrow x(B\emptyset_2OH)_{glass} + (R^x + xOH^-)_{soln} \qquad [2.8]$$

The dissolution behavior of binary lithium borate glasses were analyzed by Veléz *et al.*, who found that stirring rate has no effect on dissolution, dissolution rates are linked to the number of four coordinated boron, and that weight loss was linear with time.[42] More notably in the context of the current studies, it was determined that dissolution rates decreased with increasing solution pH.[42] This is consistent with Zapol's first principle calculations, as the activation energy of a protonated attack on borate sites is lower than that of a neutral or deprotonated attack, and contrasts with dissolution behavior of silicate glasses.[75]

The dissolution behavior of ternary borate glasses in the compositional series xNa_2O-$xCaO$-$(100-2x)B_2O_3$ glasses, where $5 \leq x \leq 20$ mole percent, was studied in water and other buffered solutions.[77] Through this study, it was confirmed that the sodium calcium borate glasses also dissolve congruently in deionized water and solutions buffered to a pH of 4, 7, and 10. A local minima in dissolution rate at glass modifier contents of 30 to 35 mole percent (x=15-17.5), which corresponds to the maxima in tetrahedral borate units in the glass structure, was also observed, similarly to what was seen by Veléz *et al.* Dissolution rate was also found to decrease with increasing pH, although it was noted that some compositions dissolved more slowly in deionized water than the solution buffered to a pH of 10.

The trends observed in the lithium borate and calcium borate series—including the trends with $(BØ_4)^-$ content (Figure 2.9), linear weight loss, and congruent dissolution—have also been confirmed across several ternary alkali-alkaline earth borate compositional series (Li, Na, Ca, K, Mg, Sr) by Goetschius *et al.* when dissolved in deionized water at 37°C.[43] Additionally, the contracting volume model was used to describe the kinetics of dissolution, indicating a reaction controlled mechanism (Equations 2.7 and 2.8), and dissolution rates increased in the order Li < Na < K and Ca < Sr ≈ Mg.

Although the dissolution rate is controlled by the fraction of tetrahedral borate species in the original glass, the borate species—H_3BO_3 and $(B(OH)_4)^-$—once in solution are dependent on the pH of the solution itself, and the ratio of these species can be used to accurately measure pH.[78] When borate glasses containing calcium are dissolved in

phosphate solutions, HAP or a carbonate substituted apatite has been observed to precipitate on the surface of the glass.[79,80]

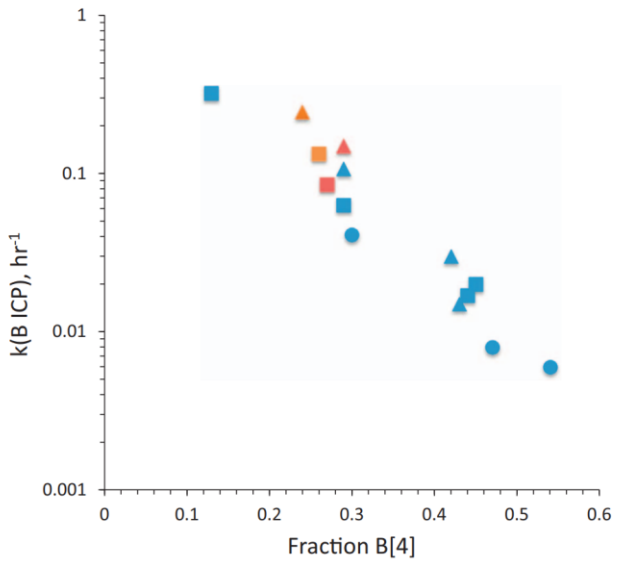

Figure 2.9. The dissolution rate, based on B ion release measured by ICP-OES, in deionized water at 37°C, related to the fraction of tetrahedral boron in the glass network for glasses of the xR_2O-$xR'O$-$(100-2x)B_2O_3$ compositional series, where R = Li (circles), Na (squares), or K (triangles), and R' = Mg (red), Ca (blue), or Sr (yellow) and x = 5, 10, 15 or 20 mol%.

PAPER

I. SPECTROSCOPIC AND CHROMATOGRAPHIC ANALYSES OF ZINC BOROPHOSPHATE GLASSES

Parker Freudenberger[1], Richard K. Brow[1]

[1]Department of Materials Science & Engineering, Missouri University of Science & Technology, Straumanis-James Hall, 1400 N. Bishop Ave, Rolla, MO 65409, USA

ABSTRACT

Thirteen zinc borophosphate glasses with analyzed compositions defined by constant O/P ratios of 3.1, 3.4, and 3.7 were prepared, and their structures were characterized by Raman spectroscopy, high pressure liquid chromatography (HPLC), and ^{11}B magic angle spinning nuclear magnetic resonance (MAS NMR) spectroscopy. ^{11}B MAS NMR spectra show that boron is predominantly incorporated into tetrahedral sites with four phosphate next-nearest neighbors, $B(OP)_4$, although some of these tetrahedra appear to have another borate unit as its next nearest neighbor, $B(OP)_3(OB)_1$. HPLC and Raman spectroscopy show that for glasses with an increasing O/P ratio, the phosphate anions that constitute the network structure become progressively smaller because of the formation of B-O-P bonds. The effects of composition on structure are discussed by considering the availability of oxygens on the phosphate anions to coordinate Zn- and B-polyhedra, and these structures are compared to those reported for zinc aluminophosphate glasses.

1. INTRODUCTION

Phosphate glasses are of interest for optical applications due to their large glass forming regions, transparency to ultraviolet (UV) light, and low thermo-optical coefficients, relative to silicate glasses.[1–3] Krause and Kurkjian showed that the tetrahedral structures of zinc phosphate glasses produced unusual thermal and mechanical properties like those possessed by fused silica. [4] Fletcher *et al.* showed that focused pulses of a femtosecond (fs) laser could be used to write optical waveguides into zinc phosphate glasses, particularly compositions with an oxygen to phosphorus (O/P) ratio of 3.25. When exposed to the fs-irradiation, the glass network is believed to densify, causing a local increase in refractive index.[5]

Zinc phosphate glasses possess generally poor chemical durability,[6] often limiting their applications. Smith *et al.* found that additions of alumina significantly improved the chemical durability of zinc phosphate glasses,[7] and waveguides could still be written into these more durable zinc aluminophosphate (ZAP) compositions.[8] The aluminum coordination number in the ZAP glasses depended on composition,[7] and for many compositions, could be predicted from the number of available terminal oxygens (TO), as described by Hoppe.[9]

Earlier studies have shown that the initial additions of B_2O_3 to Zn-metaphosphate and Zn-pyrophosphate glasses produce tetrahedral borate sites, although trigonal borons are present in glasses with greater B_2O_3 contents.[10, 11] The crosslinked network that forms in zinc borophosphate (ZBP) glasses with the incorporation of tetrahedral borons affects

properties, including decreasing the aqueous dissolution rates and the thermal expansion coefficients, and increasing glass transition temperatures. [1, 2, 10–12]

The purpose of the present study is to characterize the effect that B_2O_3 has on the properties and structure of ZBP glasses with fixed O/P ratios, to consider the compositional dependence of the structures of zinc borophosphate using Hoppe's terminal oxygen model,[9] and then to compare the structures of these glasses to those of zinc aluminophosphate glasses.

2. EXPERIMENTAL PROCEDURES

Zinc borophosphate (ZBP) glasses were prepared by mixing ZnO (99.5+%, Acros), H_3BO_3 (cert. ACS, Fisher), and H_3PO_4 (85%, Fisher) in appropriate amounts to obtain 75 grams of glass with nominal compositions that have O/P ratios of 3.0, 3.25, and 3.5 and that have a wide range of ZnO contents. Powders were gently ground for ten minutes using a mortar and pestle to break up clumps, and then phosphoric acid was added to the powder in a pure platinum crucible and calcined for 16-18 hours at 350°C. The calcined batch was then melted for two hours at 1000-1225°C, depending on the composition. The melt was stirred with a platinum stir rod at the half hour and hour marks to promote homogeneity, and then quenched in a pre-heated carbon mold. The resulting glasses were annealed for one hour at a temperature 10°C below the glass transition temperature, T_g, before being cooled in the furnace to room temperature. Glasses were confirmed to be fully amorphous by x-ray diffraction (XRD), using a

PANalytical X'Pert Multipurpose diffractometer utilizing a Cu K-α source and a PIXcel Detector.

Magic Angle Spinning (MAS) Nuclear Magnetic Resonance (NMR) Spectroscopy was performed with a Bruker Avance II 600 MHz (14.1 T) spectrometer with 4 mm zirconia rotors spinning at 12 kHz. To collect the ^{11}B spectra, the samples were scanned 512 times, with a pulse length of 2.5 μs and a delay time of 3 s at 193 MHz. The samples were indirectly referenced to a ^{1}H nucleus as recommended by IUPAC [13]. Peaks were fitted using the Multiple Peak Fit function in OriginPro 2017, using known assignments from literature; R^2 values for these fitted spectra were at least 0.999.

High Pressure Liquid Chromatography (HPLC) was done with a Dionex GP50-2 pump, an Ionpack AS7 4 × 250 mm Analytical Ion exchange column, and an AD25 absorbance detector. Glass samples were ground to < 125 μm particle size, dissolved overnight in a solution of 5 mM EDTA and 0.22 M NaCl (pH = 10), and analyzed within 24 h. At least two chromatographs per sample were collected over a linear solution gradient from 0.053 M NaCl to 0.5 M NaCl, both with 5 mM EDTA. The procedure was based on previously established processes to characterize phosphate anion chain lengths in glasses, described by Sales *et al.*[14]

Raman spectra were collected using a Horiba Jobin Yvon LabRAM ARAMIS micro-Raman spectrometer using a HeNe (632.8 nm) 17 mW laser with a 1200 grating at 10x magnification. Twenty 10 second scans were collected on each sample and the respective average spectra are reported.

Densities were measured using the Archimedes Method, with mineral oil as the buoyancy liquid. At least three samples from each composition were characterized. Molar volumes were calculated from the densities and the analyzed compositions, which were obtained using Inductively Coupled Plasma – Optical Emission Spectroscopy (ICP-OES), using a Perkin Elmer Avio 200 spectrometer. 50 mg of powdered samples (< 53 μm particle size) were completely dissolved in 50mL of 1% HNO_3, then diluted using 1% HNO_3 to obtain solutions with ion concentrations in the 1-10 ppm range. Samples were run in triplicate and compositional averages are reported.

Differential thermal analysis was performed with a Perkin Elmer Differential Thermal Analyzer 7 using Pyris Series - DTA 7 software. Samples were heated in a platinum crucible at a rate of 10°C/min to 900°C under nitrogen atmosphere, and at least two tests were performed on each sample to verify reproducibility.

3. RESULTS

Thirteen compositions batched with nominal O/P ratios of 3.0, 3.25, or 3.5 and with ZnO contents from 30 to 70 mol % were prepared, and the resulting glass compositions, obtained by ICP-OES are reported in Table 1. There was some phosphorus loss from many of the melts, and so the trends in properties and structure will be reported using the analyzed compositions which were organized to form three series of glasses with analyzed O/P ratios near 3.1, 3.4, and 3.7.

Table 1. As-batched compositions and analyzed compositions for the ZBP glasses, with standard deviations from triplicate ICP-OES measurements. The O/P ratios are calculated from the analyzed compositions.

	As Batched			*Analyzed (ICP-OES)*				
O/P	**ZnO** [mol %]	**B_2O_3** [mol %]	**P_2O_5** [mol %]	**ZnO** [mol %]	**B_2O_3** [mol %]	**P_2O_5** [mol %]	**O/P**	**TO/[B]**
3.5	70	0	30	69.9 ± 0.49	0.0	39.1 ± 0.49	3.66 ± 0.04	--
	50	10	40	55.2 ± 2.8	10.2 ± 0.36	34.6 ± 2.1	3.74 ± 0.07	0.98
	40	16	44	42.5 ± 2.6	17.3 ± 1.3	40.2 ± 2.9	3.67 ± 0.08	2.87
	30	22	48	32.4 ± 1.7	23.4 ± 0.96	44.1 ± 2.7	3.66 ± 0.07	3.50
3.25	60	0	40	62.1	0.0	37.9	3.32	--
	50	6	44	54.2 ± 2.5	6.5 ± 1.7	39.3 ± 2.3	3.44 ± 0.07	0.71
	43	9	48	47.2 ± 2.8	10.8 ± 0.43	42.1 ± 3.8	3.44 ± 0.10	2.53
	41	10	49	40.5 ± 1.4	10.2 ± 0.34	49.3 ± 1.5	3.22 ± 0.04	3.86
	40	11	49	42.4 ± 2.6	13.1 ± 0.57	44.5 ± 3.2	3.42 ± 0.08	3.16
	30	17	53	32.9 ± 1.5	18.5 ± 0.92	48.6 ± 2.9	3.41 ± 0.07	3.85
3.0	50	0	50	48.4 ± 1.0	0.93 ± 0.79	50.6 ± 1.3	3.00 ± 0.03	--
	40	5	55	43.6 ± 1.8	6.1 ± 0.65	50.3 ± 2.6	3.11 ± 0.06	4.10
	30	10	60	31.7 ± 1.7	11.0 ± 0.79	57.3 ± 2.1	3.06 ± 0.04	5.33

3.1. ^{11}B MAS-NMR

Two representative ^{11}B MAS NMR spectra are shown in Figure 1. Every ^{11}B MAS NMR spectrum is dominated by a peak at -3.8 ppm, indicating that tetrahedral boron is the preferred moiety.[15] A slight asymmetry on the low frequency side of this peak reveals a second peak centered near -3 ppm, consistent with other studies of

borophosphate glasses.[16–18] Based on those earlier studies, the peak near -3.8 ppm is assigned to tetrahedrally coordinated borons with four phosphate nearest neighbors ($B(OP)_4$), and the peak near -3 ppm is assigned to tetrahedral borons having at least one boron as a next nearest neighbor ($B(OP)_3(OB)_1$).[19, 20] Rinke and Eckert[17] have shown that, in alkali borophosphate glasses, heteroatomic bonds (such as B-O-P), are preferred over homoatomic bonds (like B-O-B), consistent with the preferential formation of $B(OP)_4$ units in these ZBP glasses. The broad, low intensity peak centered near 10 ppm in Figure 1 is assigned to trigonal borates.[15] This latter peak could be detected in only a few of the glasses.

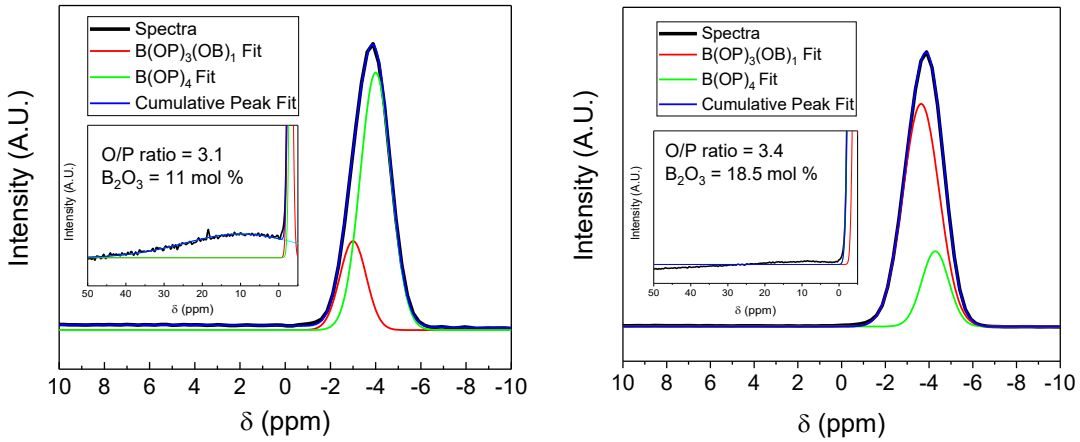

Figure 1. Representative ^{11}B MAS NMR spectra with fitted curves for the O/P = 3.1, B_2O_3 = 11 mol % and O/P = 3.4, B_2O_3 = 18.5 mol % glass.

Table 2 gives a summary of the compositional dependencies of the peak positions and relative areas of the two tetrahedral ^{11}B peaks used to fit each spectrum. Trigonal boron sites could be detected in several of the O/P≈3.1 and O/P≈3.7 glasses, but not in

the O/P ≈ 3.4 glasses. Due to the low intensity of the trigonal peak, and uncertainty in fitting the background of these spectra, these peak areas were not quantitatively evaluated. In general, the fraction of $B(OP)_3(OB)_1$ units increases at the expense of $B(OP)_4$ units with increasing B_2O_3 content. In addition, there is a general increase in shielding of the B-nuclei (more negative chemical shifts) as the boron content of the glass increases, similar to what has been observed in the ^{11}B NMR spectra of alkali borophosphate glasses.[19]

Table 2. Peak assignments for the ^{11}B NMR spectra with relative peak area values of the fitted peaks and calculated error of the fit. Compositions in which the trigonal boron peak at 10 ppm was detected have been noted with an asterisk.

Sample		**Peak Positions**		**Relative Peak Area**	
O/P ratio	*B content [mol %]*	*$B(OP)_3(OB)_1$ [ppm]*	*$B(OP)_4$ [ppm]*	*$B(OP)_3(OB)_1$ [%]*	*$B(OP)_4$ [%]*
3.67*	17.3	-2.8	-3.9	10.1 ± 4.1	89.9 ± 0.67
3.66*	23.4	-3.5	-4.2	47.3 ± 1.3	52.7 ± 1.2
3.44	6.5	-3.5	-4.1	64.2 ± 1.1	35.8 ± 1.5
3.44	10.8	-3.5	-4.2	72.3 ± 0.69	27.7 ± 1.3
3.22	10.2	-3.2	-4.1	34.3 ± 0.64	65.7 ± 0.41
3.42	13.1	-3.6	-4.3	79.9 ± 0.48	20.1 ± 1.2
3.41	18.5	-3.8	-4.4	88.5 ± 0.34	11.5 ± 1.5
3.06	6.1	-3.2	-4.1	37.0 ± 1.1	63.0 ± 0.80
3.11*	11.0	-3.1	-4.0	20.5 ± 0.51	79.5 ± 0.21

3.2. HIGH PRESSURE LIQUID CHROMATOGRAPHY

Figure 2 shows two sets of chromatographs obtained from the high performance liquid chromatography experiments, for glasses with different O/P ratios (left) and different B_2O_3 contents (right). Peaks in the chromatographs from left to right represent phosphate anions with increasing numbers (n) of tetrahedra, P_1, P_2, P_3, and on to P_n, released from the glass after longer retention times. The broad hump near 20 minutes in the chromatograph from the O/P≈3.1 glass is due to the continuous release of longer anions (n>12) that cannot be resolved by the chromatography system used here.[14]

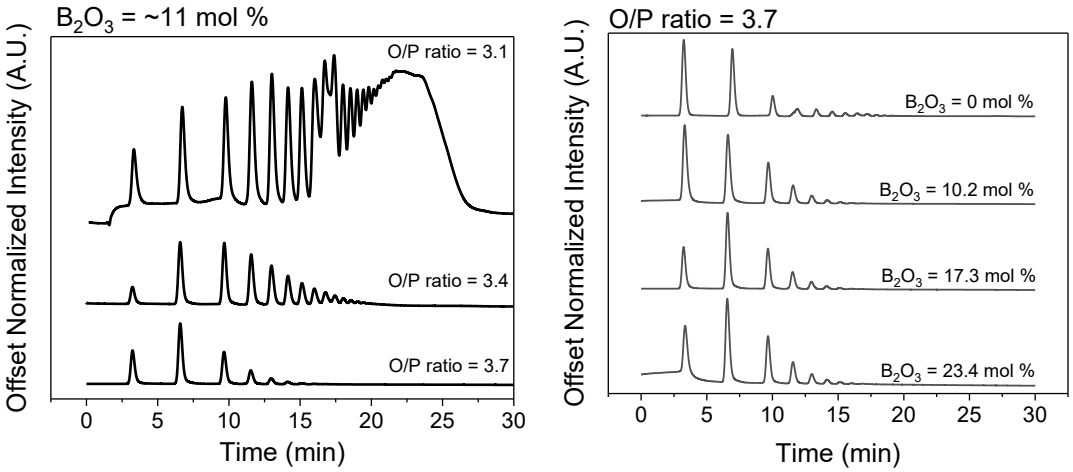

Figure 2. HPLC chromatographs for glasses with similar B_2O_3-contents but different O/P ratios (left) and for glasses with similar O/P ratios but different B_2O_3 contents (right). The average phosphate anion becomes shorter with increasing O/P ratio.

3.3. RAMAN SPECTROSCOPY

Figure 3 shows the Raman spectra for the ZBP glasses with O/P ≈ 3.1 (left), O/P ≈3.4 (center) and O/P ≈3.7 (right). The spectra are dominated by peaks in the ranges

between 900 and 1300 cm^{-1}, and between 600 and 800 cm^{-1}. The peak assignments from the literature are summarized in Table 3.

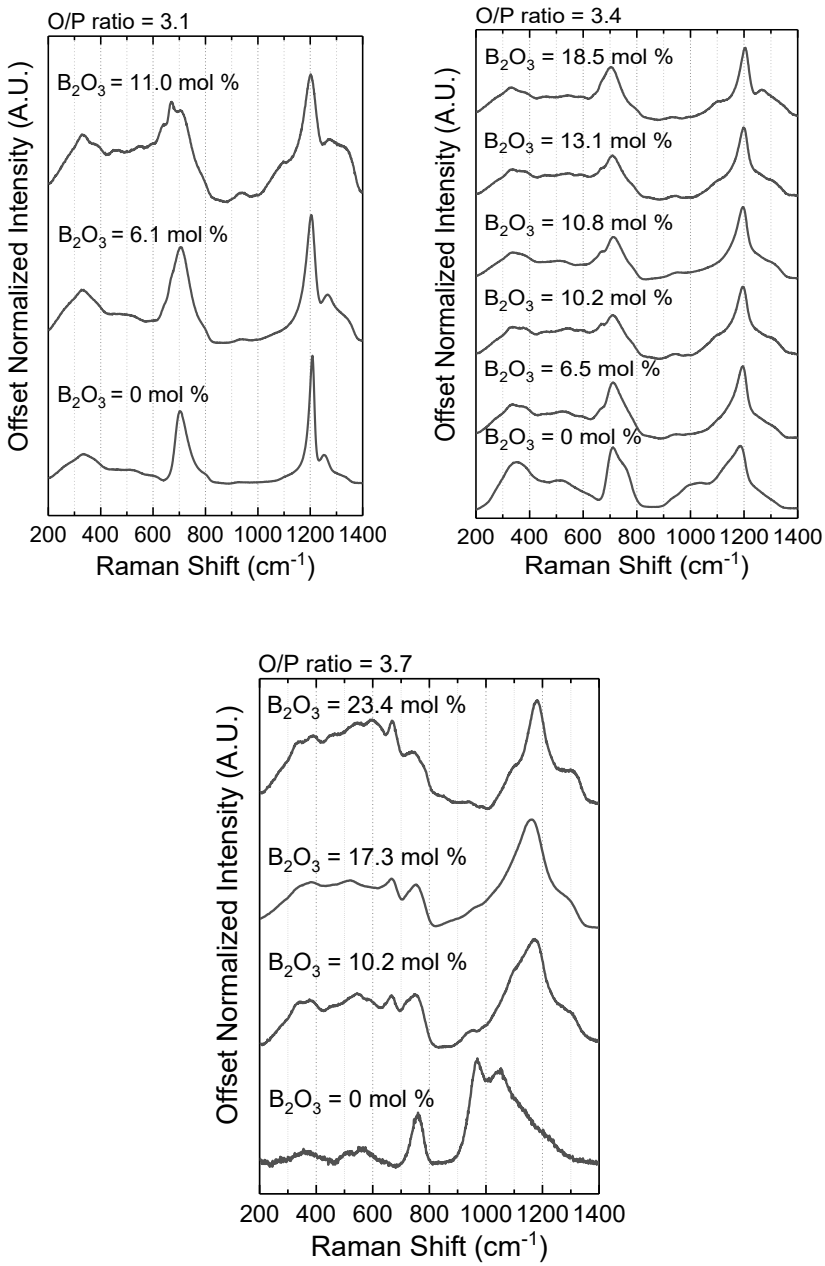

Figure 3. Raman spectra from glasses with similar O/P ratios: 3.1 (top left), 3.4 (top right), and 3.7 (bottom).

Table 3. Raman assignments from the literature.

Raman Shift (cm^{-1})	**Assignment**	**Reference**
350, 550	Zn-O-P linkages	3, 12, 21
650,720	P-O-B_{sym} stretch, P-O-P_{sym} stretch	22, 23
700	P-O-P_{sym} stretch (BO), Q^2 units	7, 10, 22, 24
758	P-O-P_{sym} stretch (BO), Q^1 units	7, 10, 22, 24
970	$(PO_4)_{sym}$ stretch (NBO), Q^0 units	3, 7, 10
1010	P-O stretch, Q^1 units	7
1067	P-O_{asym} stretch ($B(OP)_4$), Q^0 units	25
1116	P-O_{sym} stretch ($B(OP)_4$), Q^0 units	25
1140	$(PO_3)_{sym}$ stretch (NBO), Q^1 units	3, 7, 10
1200	$(PO_2)_{sym}$ stretch (NBO), Q^2 units	7, 10, 22, 23
1250	$(PO_2)_{asym}$ stretch (NBO), Q^2 units	7, 10, 22, 23
1300	$(PO)_{sym}$ stretch (NBO), Q^3 units	21, 26

The most intense peaks in the Raman spectra are near 1200 cm^{-1} and these peaks broaden from glasses with increasing B_2O_3 contents, and broaden and shift to lower frequencies with increasing O/P ratio. From earlier studies of binary Zn-phosphate glasses, the peak at 1200 cm^{-1} is assigned to the symmetric stretching modes of non-bridging oxygens on Q^2 tetrahedra and the smaller peak at 1250 cm^{-1} is due to the asymmetric stretching modes.[7, 10, 22, 23] (Here, the Q^x formalism refers to P-tetrahedra with 'x' bridging oxygens to a neighboring P-tetrahedron.[2]) Symmetric stretching modes for nonbridging oxygens on Q^1 and Q^0 P-tetrahedra have been assigned to peaks near 1140

and 970 cm^{-1}, respectively [3, 7, 10] and are the dominant features in the spectrum from the $70ZnO\text{-}30P_2O_5$ glass. A peak near 700 cm^{-1} in the Raman spectra from binary Zn-phosphate glasses is due to symmetric stretching modes associated with the bridging oxygens between Q^2 tetrahedra, and the one near 750 cm^{-1} is due to symmetric stretching modes associated with bridging oxygens that link at least one Q^1 tetrahedron. [7, 21, 27] The increase in the intensity of the 750 cm^{-1} peak relative to the 700 cm^{-1} peak in the spectra of the B-free glasses in Figure 3 with increasing O/P ratio is consistent with the decrease in the average P-anion size, and so an increase in the relative numbers of chain-terminating Q^1 units.

There are some systematic changes in the three sets of Raman spectra shown in Figure 3 from glasses with increasing B_2O_3-contents. In particular, there are increases in the relative intensities of peaks near 1300 cm^{-1} for all three sets of glasses, and these are assigned to the stretching modes associated with short $P\text{-}O^-$ bonds.[24, 27] The narrow peaks (or shoulders) near 650-670 cm^{-1} have been seen in earlier studies of alkali borophosphate glasses and are assigned to bridging oxygen stretching modes associated with borophosphate units.[28, 29] In addition, peaks in the range between about between 1000 and 1200 cm^{-1} associated with the stretching modes assigned to nonbridging oxygens on P-tetrahedra become broader, although the broad peaks near 1000 cm^{-1} in the spectra from glasses in the O/P≈3.4 and 3.7 series decrease in intensity, and disappear, with increasing B_2O_3 contents. This is particularly notable for the O/P≈3.7 series where the peaks due to the P-O stretching modes of Q^0 (970 cm^{-1}) and Q^1 (1010 cm^{-1}) phosphate units are replaced by higher frequency peaks near 1100 cm^{-1}, associated with

borophosphate units. The development of the 1067 cm^{-1} peak is also notable in the O/P≈3.1, B_2O_3=11 mol % spectrum.[3, 7, 10, 30]

The Raman peaks near 350 cm^{-1} in every spectrum are assigned to vibrational modes associated with Zn-O-P linkages,[7, 27] as are the broad peaks near 550 cm^{-1} in the spectra from low (<10 mol %) B_2O_3 glasses.[21] With increasing B_2O_3 contents, new peaks in the latter frequency range develop that are due to vibrational modes associated with various borate and borophosphate groups.[22]

3.4. PROPERTIES

The compositional dependence of the molar volume (left) and the glass transition temperature (right) for the ZnO-B_2O_3-P_2O_5 glasses are shown in Figure 4.

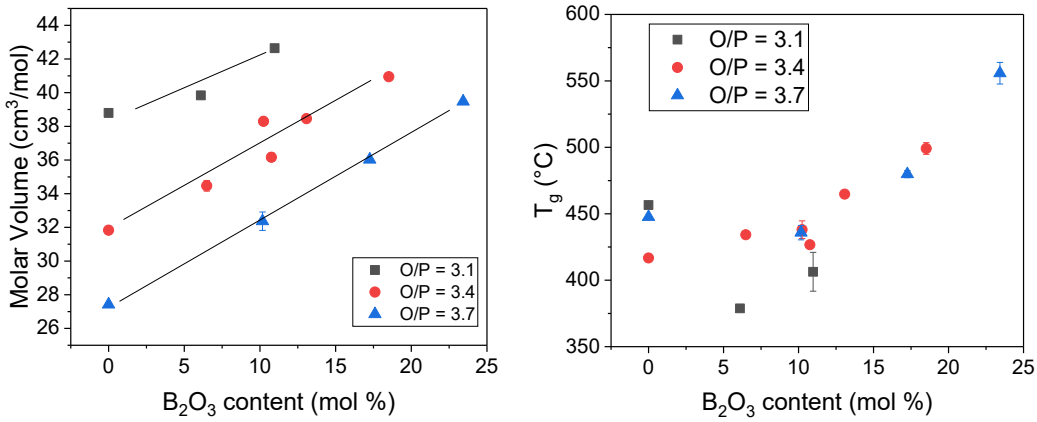

Figure 4. The molar volume (left) and glass transition temperatures (right). Both increase with increasing boron content when O/P ratio is maintained. However, the molar volume also has a dependence on O/P ratio, and lines are drawn to guide the eye for each O/P ratio. Symbols may be larger than error bars.

Molar volume increases with increasing boron content for each compositional series, and decreases in the order (O/P≈3.1) > (O/P≈3.4) > (O/P≈3.7). The glass transition temperature increases with increasing boron content with little dependence on the O/P ratio, with the exception of the B-free glass in the O/P≈3.1 series, which has a T_g greater than the two B-doped glasses in this series.

4. DISCUSSION

The more efficient packing of shorter P-anions in glasses with increasing O/P ratios explains the decrease in molar volume among the three series of glasses shown in Figure 4. Within each series, the molar volumes increase with increasing B_2O_3-content, indicating that the creation of the $B(OP)_4$ sites expands the glass structure. Koudelka and Mošner[20] showed that for ZBP glasses with constant ZnO contents, the replacement of P_2O_5 by B_2O_3 decreased molar volumes. However, their data is consistent with the molar volume trends shown in Figure 4 when the concomitant increase in O/P ratio in their series is considered. The development of the borophosphate network also increases T_g, as was reported by Koudelka and Mošner.[20]

The spectroscopic results show that when B_2O_3 is added to the Zn-phosphate glasses, a borophosphate network is created. For example, the ^{11}B spectra (Figure 1 and Table 2) are consistent with the formation of $B(OP)_4$ units and these units systematically reduce the average P-anion size with increasing concentration of B_2O_3, as indicated by the changes in the HPLC chromatographs (Figure 2) and the changes in the Raman spectra (Figure 3).

The structures of the ZBP glasses can be considered as phosphate anions, the average length of which depends on the O/P ratio, linked by individual B- and Zn-polyhedra. Hoppe has described the effects of composition on the polyhedral arrangements that constitute such structures. In particular, he has shown that the coordination number of metal cations (CN_{Me}) incorporated into a phosphate glass can vary with the number of terminal (nonbridging) oxygens (N_{TO}) associated with the P-tetrahedra.[9] For a binary phosphate glass with the molar composition $x(Me_{2/\nu}O)$ $(1-x)P_2O_5$, N_{TO} can be calculated from:

$$N_{TO} = \nu(x+1)/x \qquad [1]$$

Here, ν is the valence of the $Me^{\nu+}$ cation. When $N_{TO} \geq CN_{Me}$ (compositional range I), isolated metal polyhedra are incorporated into the phosphate glass structure, and the average coordination number of these polyhedra decreases with decreasing N_{TO} to remain in isolated sites. When a minimum value in CN_{Me} is reached and so $N_{TO} < CN_{Me}$, then there are insufficient TO for the metal polyhedra to remain isolated and so they begin forming a subnetwork by sharing TO on the phosphate anions (compositional range II). For many phosphate systems, including the binary ZnO-P_2O_5 system, there are breaks in the composition-property trends at the onset of the formation of the metal polyhedral subnetwork.

Recently, Smith *et al.* showed that the Hoppe Model could be used to explain the systematic changes in CN_{Al} when Al_2O_3 was added to zinc phosphate glasses.[7] They

assumed that all zinc ions were incorporated into the glasses in tetrahedral sites, consistent with diffraction studies of Zn-phosphate glasses,[30–32] and then they modified Equation 1 to calculate the number of terminal oxygens that remained after accounting for the isolated ZnO_4 species, using the molar fractions of each oxide in the analyzed composition (Equation 2). They found that Equation 2, where M=Al, predicted values for CN_{Al} for all compositions where $4 \leq (TO/[Al]) \leq 6$ (compositional range I). For glasses with relatively large Al_2O_3 or ZnO contents, the relationship no longer was valid and a subnetwork of Al- and Zn-polyhedra sharing TO was expected to form in the glass structure (compositional range II).

$$\frac{TO}{[M]} = \frac{[P_2O_5] + 3[M_2O_3] - [ZnO]}{[M_2O_3]} \qquad [2]$$

Table 1 shows the calculated values for TO/[B] for the ZBP glasses, assuming all Zn-ions are incorporated in isolated tetrahedral sites. Several of the compositions in the O/P≈3.7 and O/P≈3.4 series have (TO/[B])<3 and tetrahedral borate units are the predominant site in these glasses (Table 3.2). Because of the paucity of "free" TO, these glasses must have structures that include two Zn-polyhedra sharing a common terminal oxygen on a phosphate tetrahedron (compositional range II). Most of the glasses in the O/P≈3.4 series have 3<(TO/[B])<4; however, the ^{11}B NMR spectra from those glasses indicate that CN_B is independent of composition and that tetrahedral borate sites are also preferred. The two borate containing glasses in the O/P ≈3.1 series have (TO/[B])>4,

indicating that there are sufficient TO available to support isolated B- and Zn-tetrahedra in the glass structure (compositional range I).

There is evidence that some oxygens in the ZBP glasses are not associated with phosphate units, and so are not accounted for by the Hoppe Model. For example, the peak near -3 ppm in the ^{11}B spectra (Figure 1, Table 2) assigned to $B(OP)_3(OB)_1$ units indicates that some oxygens in the glass structure must not be linked to P-anions. The chromatographic data can be used to estimate the fraction of oxygens that are not associated with the phosphate anions. The areas under the chromatographic peaks, like those shown in Figure 2, can be used to quantify the P-anion distributions and calculate the average P-anion chain length ($\bar{n}$), which then can be compared to a predicted average P-anion size from the glass composition, using Equation 3,[14] where $[M_j]$, [P], and v_j, are the relative atomic fractions of the metal ions and phosphorus, and the valence of the metal oxide, respectively.

$$\bar{n} = \frac{2}{\sum_j \frac{[M_j][v_j]}{[P]} - 1} \qquad [3]$$

Figure 5 shows that the analyzed average P-anion size for glasses (solid symbols) with O/P > 3.2 follows the predicted compositional trend, but is typically greater than the predicted values. (This analysis was not done for the P-rich glasses when large (n>12) P-anions could not be resolved by chromatography.) If the oxygens associated the with B-O-B bonds in the $B(OP)_3(OB)_1$ units detected by NMR (Table 2) are removed from the

O/P ratio calculations, however, then there is a closer fit (open symbols) to the predicted average P-anion size for most of the compositions.

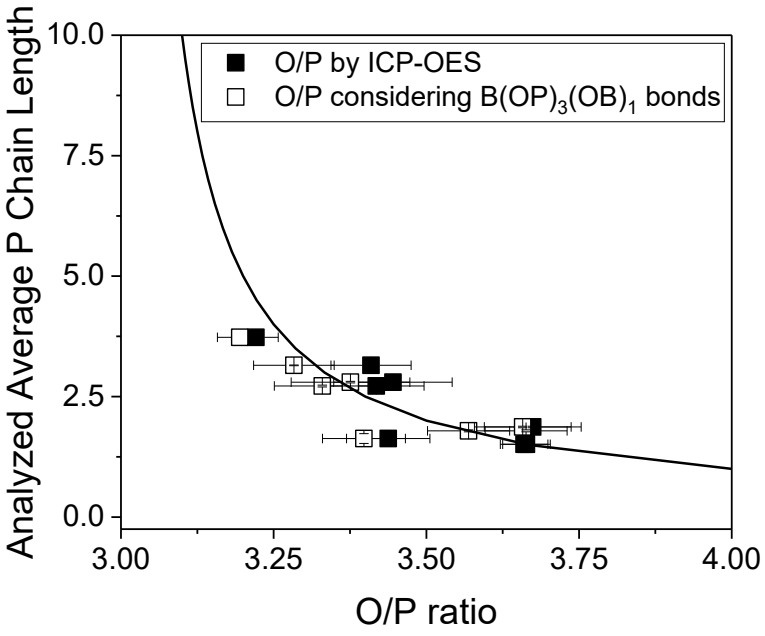

Figure 5. Solid symbols show the average P chain length analyzed by HPLC plotted against the analyzed O/P ratio (ICP-OES). The solid line is the expected relationship, from Equation 3. Open symbols assume that oxygens in B-O-B bonds do not contribute to the O/P ratio.

B_2O_3 is a more acidic oxide than Al_2O_3 and so can more effectively compete with P_2O_5 for bonds with the available oxygens that then determine the polyhedral arrangements that constitute the glass structure.[33] As a result, the types and relative fractions of the B-polyhedra in the ZBP glasses cannot be predicted from the bonding rules established by Hoppe in the way that the average Al-coordination could be for the ZAP glasses.[7, 9] However, Hoppe's model still provides some qualitative understanding for the compositional dependence of the ZBP glass structures. For example, the greater

than predicted value of CN_B and the removal of some oxygen from the phosphate anions will reduce the overall number of terminal oxygens available to coordinate the Zn-polyhedra, meaning that more of these terminal oxygens must be shared by two Zn-polyhedra which then form a Zn-O subnetwork. The vibrational modes associated with the terminal oxygen on a Q^1 P-tetrahedron that is linked to one Zn-polyhedron will produce a Raman peak at a different frequency than a terminal oxygen that is linked to two Zn-polyhedra, and those frequencies will be further affected if that P-tetrahedron is also bonded to a borate tetrahedron, or if the coordination number of the zinc changes to accommodate the number of available terminal oxygens. This variety of possible local polyhedral arrangements contributes to the complexity of the Raman spectra in the 1000-1300 cm^{-1} range (Figure 3).

5. CONCLUSION

The structures and properties of thirteen zinc borophosphate glasses were described by considering their respective O/P ratios and B_2O_3-contents. ^{11}B MAS NMR spectra show that boron was incorporated into the glass principally in tetrahedral borophosphate sites, $B(OP)_4$ and $B(OP)_3(OB)_1$. The formation of B-O-P bonds reduces the average size of the phosphate anions, described qualitatively by changes in the Raman spectra and more quantitatively by HPLC chromatographs. These polyhedral arrangements can be understood using the structural model proposed by Hoppe that considers the availability of terminal oxygens to coordinate metal polyhedra in a phosphate network. However, the model predictions for B-coordination in these ZBP

glasses are not as good as they were for predictions of Al-coordination in an earlier study of zinc aluminophosphate glasses. The ability of boron to compete with phosphorus for oxygens helps explain those differences.

ACKNOWLEDGEMENTS

The authors thank Deborah Watson and others at Iowa State University for their assistance with NMR measurements. This research was funded by the National Science Foundation (DMR-1207520) and a Graduate Assistance in Areas of National Need (GAANN) Fellowship.

REFERENCES

1. Kreidl NJ, Weyl W a. Phosphates in Ceramic Ware: Iv, Phosphate Glasses*. *Journal of the American Ceramic Society*. 1941;24(11):372–378. https://doi.org/10.1111/j.1151-2916.1941.tb15444.x

2. Brow RK. Review: the structure of simple phosphate glasses. *Journal of Non-Crystalline Solids*. 2000;263–264:1–28. https://doi.org/10.1016/S0022-3093(99)00620-1

3. Brow RK, Tallant DR, Myers ST, Phifer CC. The short-range structure of zinc polyphosphate glass. *Journal of Non-Crystalline Solids*. 1995;191:45–55. https://doi.org/10.1016/0022-3093(95)00289-8

4. Krause JT, Kurkjian CR. Vibrational Anomalies in Inorganic Glass Formers. *Journal of the American Ceramic Society*. 1968;51(4):226–227. https://doi.org/10.1111/j.1151-2916.1968.tb11880.x

5. Fletcher LB, Witcher JJ, Troy N, Reis ST, Brow RK, Krol DM. Direct femtosecond laser waveguide writing inside zinc phosphate glass. *Optics Express*. 2011;19(9):7929. https://doi.org/10.1364/OE.19.007929

6. Takebe H, Baba Y, Kuwabara M. Dissolution behavior of ZnO-P2O5 glasses in water. *Journal of Non-Crystalline Solids*. 2006;352(28–29):3088–3094. https://doi.org/10.1016/j.jnoncrysol.2006.04.002

7. Smith CE, Brow RK, Montagne L, Revel B. The structure and properties of zinc aluminophosphate glasses. *Journal of Non-Crystalline Solids*. 2014;386:105–114. https://doi.org/10.1016/j.jnoncrysol.2013.11.042

8. Hernandez-Rueda J, Semenov V, Troy N, Smith CE, Brow RK, Krol DM. All-optical characterization of fs-laser induce refractive index changes in bulk and at the surface of zinc phosphate glasses. *Proceedings of SPIE*. 2015

9. Hoppe U. A structural model for phosphate glasses. *Journal of Non-Crystalline Solids*. 1996;195(1–2):138–147. https://doi.org/10.1016/0022-3093(95)00524-2

10. Brow RK, Tallant DR. Structural design of sealing glasses. *Journal of Non-Crystalline Solids*. 1997;222:396–406.

11. Brow RK. An XPS study of oxygen bonding in zinc phosphate and zinc borophosphate glasses. *Journal of Non-Crystalline Solids*. 1996;194(3):267–273. https://doi.org/10.1016/0022-3093(95)00500-5

12. Koudelka L, Mošner P. Borophosphate glasses of the ZnO – B 2 O 3 – P 2 O 5 system. *Materials Letters*. 2000;42(January):194–199.

13. Becker ED, S SMCDEME, W ROGFO, R PGGE. Commission on Molecular Structure and Spectroscopy *. 2001;73(11):1795–1818.

14. Sales BC, Boatner LA, Ramey JO. Chromatographic studies of the structures of amorphous phosphates: a review. *Journal of Non-Crystalline Solids*. 2000;263–264:155–166. https://doi.org/10.1016/S0022-3093(99)00644-4

15. Yun YHH, Bray PJJ. Nuclear magnetic resonance studies of the glasses in the system K2OB2O3P2O5. *Journal of Non-Crystalline Solids*. 1978;30(1):45–60. https://doi.org/10.1016/0022-3093(78)90055-8

16. Svenson MN, Youngman RE, Yue Y, *et al.* Volume and Structure Relaxation in Compressed Sodium Borate Glass. *Phys Chem Chem Phys Physical Chemistry Chemical Physics Physical Chemistry Chemical Physics Accepted Manuscript*. 2016;18:29879–29891. https://doi.org/10.1039/C6CP06341A

17. Raskar D, Rinke MT, Eckert H. The Mixed-Network Former Effect in Phosphate Glasses: NMR and XPS Structural Studies of the Connectivity Distribution in the Glass System (NaPO3)1-x(B2O3)x. *The Journal of Physical Chemistry C*. 2008;112:12530–12539. https://doi.org/10.1039/c0cp01590c

18. Lim JWW, Schmitt MLL, Brow RKK, Yung SWW. Properties and structures of tin borophosphate glasses. *Journal of Non-Crystalline Solids*. 2010;356(28–30):1379–1384. https://doi.org/10.1016/j.jnoncrysol.2010.02.019

19. Carta D, Qiu D, Guerry P, *et al.* The effect of composition on the structure of sodium borophosphate glasses. *Journal of Non-Crystalline Solids*. 2008;354(31):3671–3677. https://doi.org/10.1016/j.jnoncrysol.2008.04.009

20. Koudelka L, Mošner P, Pospíšil J, Montagne L, Palavit G. Structure and properties of titanium-zinc borophosphate glasses. *Journal of Solid State Chemistry*. 2005;178(6):1837–1843. https://doi.org/10.1016/j.jssc.2005.03.025

21. Scagliotti M, Villa M, Chiodelli G. Short range order in the network of the borophosphate glasses: Raman results. *Journal of Non-Crystalline Solids*. 1987;93(2–3):350–360. https://doi.org/10.1016/S0022-3093(87)80180-1

22. Hidi IJ, Melinte G, Stefan R, Bindea M, Baia L. The study of the structure and bioactivity of the $B_2O_3 \bullet Na_2O \bullet P_2O_5$ system. *Journal of Raman Spectroscopy*. 2013;44(8):1187–1194. https://doi.org/10.1002/jrs.4330

23. Takebe H, Suzuki Y, Uemura T. Effect of B2O3 and Al2O3 additions on the structure of phosphate glasses. 2014;55(5):207–210. https://doi.org/10.1115/1.4024145

24. Christensen R, Olson G, Martin SW. Structural Studies of Mixed Glass Former $0.35Na_2O + 0.65[x B_2O_3 + (1 - x)P_2O_5]$ Glasses by Raman and ^{11}B and ^{31}P Magic Angle Spinning Nuclear Magnetic R. *The Journal of Physical Chemistry B*. 2013;117(7):2169–2179. https://doi.org/10.1021/jp308494a

25. Bunker BC, Tallant DR, Kirkpatrick RJ, Turner GL. Multinuclear nuclear magnetic resonance and Raman investigation of sodium borosilicate glass structures. *Physics and Chemistry of Glasses*. 1990;31:30–41.

26. Ducel JF, Videau JJ. Structural study of borophosphate glasses by Raman and infrared spectroscopy. *Physics and Chemistry of Glasses*. 1993;34(5):212–218.

27. Tischendorf B, Otaigbe JU, Wiench JW, Pruski M, Sales BC. A study of short and intermediate range order in zinc phosphate glasses. *Journal of Non-Crystalline Solids*. 2001;282(2–3):147–158. https://doi.org/10.1016/S0022-3093(01)00350-7

28. Koudelka L, Mošner P. Study of the structure and properties of Pb–Zn borophosphate glasses. *Journal of Non-Crystalline Solids*. 2001;293–295:635–641. https://doi.org/10.1016/S0022-3093(01)00765-7

29. Saranti A, Koutselas I, Karakassides MA. Bioactive glasses in the system CaO-B2O3-P2O5: Preparation, structural study and in vitro evaluation. *Journal of Non-Crystalline Solids*. 2006;352(5):390–398. https://doi.org/10.1016/j.jnoncrysol.2006.01.042

30. Walter G, Hoppe U, Vogel J, Carl G, Hartmann P. The structure of zinc polyphosphate glass studied by diffraction methods and 31P NMR. *Journal of Non-Crystalline Solids*. 2010;356(43):252–262. https://doi.org/10.1016/j.jnoncrysol.2003.12.054

31. G. Walter, U. Hoppe, T. Baade, R. Kranold, D. Stachel. Intermediate range order in MeO-P2O5 glasses. *Journal of Non-Crystalline Solids*. 1997;217:299–307. https://doi.org/10.1016/S0022-3093(97)00220-2

32. Matsubara E, Waseda Y, Ashizuka M, Ishida E. Structural study of binary phosphate glasses with MgO, ZnO, and CaO by x-ray diffraction. *Journal of Non-Crystalline Solids*. 1988;103(1):117–124. https://doi.org/10.1016/0022-3093(88)90423-1

33. Rao KJ. Structural Chemistry of Glasses. 1st ed. Oxford: elsevier Science, Ltd.; 2002

II. CHARACTERIZATION OF $20Na_2O•30((1-x)CaO•xSrO)•50P_2O_5$ GLASSES FOR A RESORBABLE OPTICAL FIBER APPLICATION

Parker Freudenberger[1], Akira Saitoh[2], Hikaru Ikeda[3], Md Shihab Adnan[4], Hiromichi Takebe[2], Shingo Nakane[3], Chang-Soo Kim[4], Richard K. Brow[1]

[1] Department of Materials Science and Engineering, Missouri University of Science and Technology, Straumanis-James Hall, 1400 N. Bishop Ave, Rolla 65409, MO, USA

[2] Graduate School of Science and Engineering, Ehime University, 3 Bunkyo-cho, Matsuyama, Ehime 790-8577, Japan

[3] Nippon Electric Glass Co., Ltd., Project Planning Department, Otsu city, Shiga 520-8639 Japan

[4] Department of Electrical Engineering, Missouri University of Science and Technology, Straumanis-James Hall, 1400 N, Bishop Ave, Rolla 65409, MO, USA

ABSTRACT

Resorbable glasses with nominal molar compositions of $20Na_2O·30[(1-x)CaO·xSrO]·50P_2O_5$, where x = 0, 0.25, 0.50, 0.75, and 1, were prepared and characterized. With the replacement of CaO by SrO, the molar volume, refractive index, and CTE increased, and the glass transition temperature, crystallization temperature, and viscosity decreased. The replacement of CaO by SrO decreased the dissolution rate in 37°C water by nearly an order of magnitude. Resorbable glass fibers drawn from melts of the $20Na_2O·30CaO·50P_2O_5$ glass exhibited decreasing transmission of laser light (632 nm) in a predictable way as the fiber dissolved in a phosphate buffer solution. This demonstrated that these glasses could be used to produce resorbable fibers for temporary biosensing or therapeutic applications.

1. INTRODUCTION

Phosphate glasses have been used for different optical devices, including waveguides and optical amplifiers.[1] However, phosphate glasses generally have poor chemical durability, compared to silicate glasses, and this has limited their use in many conventional applications.[2] On the other hand, the reactivity of a glass in an aqueous environment can be viewed as an advantage in the development of resorbable materials.

Phosphate glasses containing alkali and alkaline-earth oxides have been investigated as candidates for biomedical applications. Knowles *et al.* studied property and structure trends for a wide range of glasses from the Na-Ca-phosphate system, and reported that compositions with better chemical durability tended to contribute to bone cell growth.[3–6] These findings were confirmed by Uo *et al*., who found that cytotoxicity and dissolution rates both decrease with increasing alkali and alkaline-earth contents.[7] Strontium additions to bioactive glasses have been shown to promote bone growth.[8, 9] In addition to having a relatively large glass forming region, the solubility and biocompatibility of phosphate glasses can be controlled by composition so that materials specifically tailored for biological applications can be developed.[3–6]

There are increasing demands for resorbable implanted devices for temporary, interventional medical procedures.[10, 11] Previously, a resorbable solid-state electronic device based on a borate glass material was designed to be fully functional during an intended operational lifetime followed by rapid structural degradation, eliminating the need for the removal of the device in a subsequent surgery procedure.[12] In parallel, the concept of resorbable optical waveguiding devices is also emerging for biosensing,

phototherapeutic and optogenetic tools, providing a means to deliver localized light to deep-seated areas otherwise impossible due to the light attenuation through tissue.[13]

Although various resorbable polymers are available, these materials are less ideal than their inorganic counterparts particularly for optical application. Most polymers exhibit bulk hydration that gradually changes the optical properties after implantation. Inorganic glasses are superior in this respect since the hydrolysis starts at the surface, allowing the retention of bulk properties until the device is nearly consumed. The glass-based optical technology is mature for communication and sensing applications. Accordingly, various sensor-integrated resorbable optical probes are feasible, which may provide an unprecedented advantage for such applications. Phosphate glasses have been proposed as candidates for resorbable optical fibers.[14–16] The dissolution rate of optical fibers made with glasses from the Na-Ca-Sr-borophosphate system was shown to be dependant on the borate content and the change in transmission power could be used to track the dissolution of the fibers.[14]

Glasses suitable for use as cores and claddings for optical fibers must have different refractive indices and compatible thermal properties, including viscosity and coefficient of thermal expansion. The compositions studied in the present paper were based on the Na-Ca-metaphosphate glasses developed for biomedical applications by Knowles *et al*.[3–6] To modify the refractive index, SrO systematically replaces CaO and the effects of these changes on thermal properties and dissolution rates have been determined, with the goal of identifying compositions that could be used for resorbable optical fibers.

2. EXPERIMENTAL

2.1. GLASS FORMATION

Na-Ca-Sr-metaphosphate glasses were prepared by batching appropriate amounts of $NaPO_3$ (99.99% - Hakushin Kagaku), $Ca(PO_3)_2$ (99.99% - Hakushin Kagaku), and $Sr(PO_3)_2$ (99.99% - Hakushin Kagaku) to produce either 10 g, 20 g, or 200 g of glass with the nominal molar compositions $20Na_2O{\cdot}30[(1\text{-}x)CaO{\cdot}xSrO]{\cdot}50P_2O_5$, where x = 0, 0.25, 0.50, 0.75, and 1. Batch materials were thoroughly mixed either by mortar and pestle or by a Turbula System Type T2F mixer for 10 minutes for the small-scale and the large-scale samples, respectively. The batch materials were then held for one or four hours at 350°C, depending on batch size, to evolve water from the raw materials. Small-scale (10 g and 20 g) samples were melted in platinum crucibles at 1200°C for 60 and 80 min, respectively. The large-scale (200 g) samples were melted at 1000°C in platinum lined crucibles for two hours and were stirred twice at 30 min intervals during melting. Glasses were quenched by pouring melts into pre-heated carbon molds, and then annealed at 350°C for one hour.

2.2. GLASS PROPERTIES AND STRUCTURE

Densities were measured using the Archimedes Method, with kerosene as the buoyancy fluid for the small-scale samples and ethanol for the large-scale samples. At least three samples from every melt were characterized. Molar volume was calculated from the densities and the analyzed compositions. Energy dispersive spectroscopy (EDS, JSM-6510 Jeol Scanning Electron Microscope) was used to determine the compositions

of the small-scale glasses, and the compositions of the large-scale glasses were determined using X-ray fluorescence spectrometry (XRF, Rigaku ZSX Primus II).

Glass dissolution rates in deionized water were determined using procedures similar to the MCC-1 dissolution method.[17] Samples with final dimensions of 10 mm x 10 mm x 3 mm were polished with 800 and 1200 grit SiC paper, followed by a cerium oxide slurry to yield a mirror finish, and these were suspended by Teflon thread in 200 mL of distilled water contained in covered Teflon beakers and placed in an oven at 37°C. Weight loss and solution pH measurements were made after 24, 48, 96, 192, 382, and 504 hrs. A covered Teflon beaker filled with only distilled water was used as a blank reference for the pH measurements. Weight losses are normalized to the initial sample surface areas and reported as averages for at least three samples from each composition.

Thermal properties, including glass transition temperature (T_g), crystallization temperature (T_c), and crystal melting temperature (T_m) were obtained using a ThermoPlus Evo TG8120 Rigaku DTA for the small-scale glasses, and a ThermoPlus TMA 8310 was used to determine the coefficient of thermal expansion (CTE). The DTA tests for small-scale samples were performed using 30 mg powdered samples with a heating rate of 10°C/min up to 850°C in air, with alumina as a reference material. Each characteristic temperature was determined using the onset method for the respective transition. Low temperature viscosity measurements were collected by the penetration method, using a ThermoPlus TMA 8310 with a 1 mm silica pin. For the small-scale samples, TMA experiments were done on samples (4 mm x 4 mm x 15 mm) that were heated at a rate of 10°C/min, and with an applied load of 98 mN. CTE calculations were made over the 100-300°C temperature range.

The CTE of large-scale glasses (20 mm x φ5 mm) were measured using a Netzsch TD 5000 SE at a heating rate of 3°C/min, and with applied load of 30gf. The DTA tests for large-scale samples were performed (Rigaku TG8110 DTA) using 350 mg powdered samples (< 75 μm particle size) with a heating rate of 10°C/min up to 1000°C in air, with alumina as a reference material. Low temperature viscosity measurements for the large-scale glasses were acquired using the fiber elongation method.[18] Fibers 0.65 ± 0.05 mm in diameter and either 230 ± 2 mm or 430 ± 2 mm in length were used to obtain the softening temperature or annealing temperature and strain point, respectively. For softening temperature measurements, the fiber was heated at 5°C/min until it deformed under its own weight. Fiber samples for annealing temperature and strain point measurements were cooled from 380 °C at a rate of 4°C/min with a 1 kg weight attached to the bottom of the fiber. Annealing temperature and strain point are defined at predetermined deformation rates.[18] At least two measurements were taken at each viscosity, and the reported isokom temperatures were found to be within ±1°C. High temperature viscosities of the large-scale samples were measured using the platinum sphere pull-up method.[19, 20]

The refractive indices of both the small-scale and large-scale samples were obtained using the v-block method. Small-scale samples with mirror-polished surfaces were analyzed using a Precision Refractometer Model KPR – 30V II Shimadzu. Unpolished large-scale samples were analyzed with a Kalnew KPR-2000 Precision Refractometer. Reported values are averages of at least two measurements on every sample. Abbe numbers were calculated from analyzed refractive index values at standard wavelengths of 587.56 nm (n_d), 486.13nm (n_F), and 656.27 nm (n_C).[21]

Transmittance curves for large scale samples were obtained using a Jasco V-670 Spectrophotometer over a range of 200-800 nm, at a resolution of 0.1 nm, and 200 nm/min scan speed. A background scan was recorded and subtracted from all recorded spectra.

A PANalytical X'Pert Materials Research Diffractometer equipped with an x-ray mirror was used to identify the reaction layers after dissolution. The x-ray source was copper and had a weighted average wavelength of 0.15418 nm. All scans were run with a fixed incident angle of 1 degree. XRD measurements were performed over the 2θ angular range of 6-80 degrees with a step size of 0.03 degrees and a time per step of 2 seconds.

Raman spectra for all samples were collected from polished glass samples (1± 0.02 mm thickness) using an integrated near-field spectrometer (JASCO, NFS-230HKG) with a 532 nm laser as excitation source. A Perkin Elmer Spectrum GX FT-IR system was used to collect infrared reflectance spectra for large-scale samples over a 370-7800 cm^{-1} range, using 1 ± 0.02 mm thick, polished samples. A background scan was recorded prior to sample measurement and was subtracted from all recorded spectra.

2.3. FIBER CHARACTERIZATION

For a proof-of-concept demonstration of resorbable fiber behavior, glass fibers about 200 microns in diameter were drawn by hand from melts of the $20Na_2O{\cdot}30CaO{\cdot}50P_2O_5$ (mole%) glass held at about 1100 °C in a platinum crucible. Fiber sections about 15 cm long were used to determine the propagation loss (in dB/m). Fibers were cut using an optical slicer and propagation losses were measured using a 632 nm laser source (0.5 mW He-Ne polarized, Edmund Optics) and a power meter (Model 2935C, Newport). This wavelength is used for common photosensitizers (e.g. porphyrin) for tumor

phototheraphy.[22] Both ends of the fiber were interfaced with a free-space optical setup with lenses to receive light from the laser and deliver the light to the power meter, respectively. Afterward, about 25 mm of fiber from the power meter end was repeatedly cut and the transmitted power was measured to determine propagation loss.

The change of power transmission along the fibers was also observed during dissolution experiments. Transmission measurements were made at various times through 7 cm fiber segments that were enclosed in a dark chamber containing 300 mL of a room temperature phosphate buffer solution (PBS, pH 7.4, Sigma Aldrich). Two ends of the fiber (1.5 cm for each side) were outside the chamber to be interfaced with the same free-space optics as the transmission loss measurements. The PBS was kept at a temperature of 21°C. The dissolution experiments were repeated with three fiber samples and the power of the transmitted light as a function of submersion time is reported.

3. RESULTS

3.1. GLASS PROPERTIES

Glass compositions, obtained by scanning electron microscopy with energy dispersive spectrometry (SEM-EDS, at Ehime University) or x-ray fluorescence (XRF, at NEG) are reported Table 1. The small-scale samples have systematically lower concentrations of Na_2O (and greater P_2O_5 contents) than the large-scale glasses, and both sets of glasses retained the expected CaO-to-SrO ratios. Overall, the analyzed compositions are within 2 mol% of the as-batched compositions. Also included in Table 1 are the water contents of the samples, obtained from infrared absorption measurements using the

methods developed by Ebendorf-Heidepriem.[23, 24] There is no systematic compositional dependence of the water contents, but the glasses prepared in smaller batches at Ehime University have about 30% more water than those prepared in larger batches at NEG.

Table 1. The as-batched and analyzed compositions, and estimated water contents, of the glasses from large-scale and small-scale melts with the nominal molar composition $20Na_2O{\cdot}30[(1\text{-}x)CaO{\cdot}xSrO]{\cdot}50P_2O_5$.

	Sample (x)	Batch Composition (mol %)				Analyzed Composition (mol %)				O/P	OH Content (ppm)
		Na_2O	*CaO*	*SrO*	*P_2O_5*	*Na_2O*	*CaO*	*SrO*	*P_2O_5*		
Large-scale	0	20	30	0	50	19.6	30.6	0	49.8	3.00	370
	0.25	20	22.5	7.5	50	19.9	23.8	6.9	49.3	3.01	500
	0.5	20	15	15	50	19.2	15.5	15.7	49.6	3.01	360
	0.75	20	7.5	22.5	50	19.7	7.9	22.5	50	3.00	540
	1	20	0	30	50	20.3	0	29.8	49.9	3.00	410
Small-scale	0	20	30	0	50	18.5 ± 0.2	30.2 ± 1.3	0 ± 0.0	51.2 ± 1.2	2.98	536
	0.25	20	22.5	7.5	50	18.5 ± 0.5	22.6 ± 0.6	7.2 ± 0.3	51.6 ± 0.5	2.97	505
	0.5	20	15	15	50	18.4 ± 0.2	15.6 ± 0.2	14.2 ± 0.2	51.7 ± 0.7	2.97	444
	0.75	20	7.5	22.5	50	18.2 ± 0.1	7.5 ± 0.3	22.5 ± 0.2	51.7 ± 0.0	2.97	677
	1	20	0	30	50	18.7 ± 0.3	0 ± 0.0	29.7 ± 0.4	51.6 ± 0.1	2.97	613

The compositional dependences of the densities (ρ) and molar volumes (V_m) are given in Figure 1 and show that both properties increase systematically as CaO is replaced by SrO. The trend in density is consistent with the greater molar weight of SrO compared to CaO, and the trend in molar volume reflects the greater size and lower field strength of Sr^{2+} ions compared to Ca^{2+}. The 1-2% differences in molar volume between

the two sets of samples are due to the small differences in their analyzed compositions (Table 1).

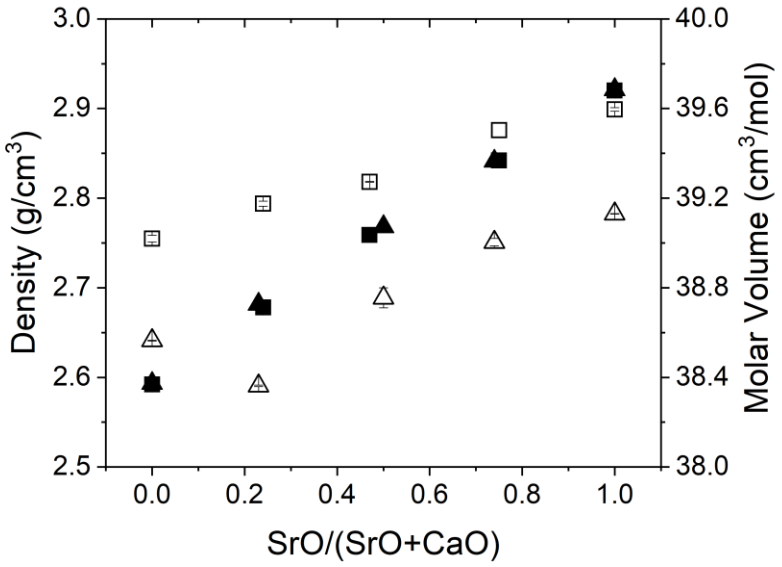

Figure 1. Density (solid symbols) and molar volume (open symbols) for glasses with increasing SrO contents. Data for small-scale samples are represented by squares, and large-scale sample data is represented by triangles. Error bars may be smaller than the symbol.

Table 2 shows the compositional dependences of the thermal properties for both sets of glasses. In general, T_g decreases and CTE increases when SrO replaces CaO. Each sample was found to have one crystallization transition (T_x) in the DTA scans and two melting transitions (T_m), indicating the formation of two different crystalline phases within the same temperature range. The glass with equal concentrations of SrO and CaO had the greatest crystallization temperature, and the greatest difference between T_x and T_g.

Table 2. Thermal properties of the glasses from fits to the viscosity data (MYEGA model[25]) and from thermal transitions analyzed by DTA or DSC. Here, x is the SrO/(SrO+CaO) ratio of an as-batched composition. The characteristic temperatures are reproducible to ± 6°C.

Sample	MYEGA Fit			DTA/DSC/TMA							
	Log Infinite Temp. Visc.	*Frag. Param.*	*Glass Trans. Temp.* [°C]	*Large-scale Samples*				*Small-scale Samples*			
x	η∞	m	T_g	T_g °C	T_x °C	T_m °C	CTE 10^{-7}/°C	T_g °C	T_x °C	T_m °C	CTE 10^{-7}/°C
0	-3.5	28.9	376	383	484	735 761	151	380	502	735 758	149
0.25	-4.6	26.1	372	378	503	728 754	154	370	509	723 747	152
0.5	-3.9	27.3	370	378	518	718 750	158	369	516	707 739	152
0.75	-4.2	26.5	364	372	521	691 744	162	370	500	713 746	163
1	-1.7	34.8	368	373	484	-- 762	163	374	491	698 755	164

Figure 2 shows the temperature dependence of viscosity of the glass melts. The symbols are the measured values of the large scale samples and the lines are fits of that data using the MYEGA model.[25] The viscosity data gathered from the small scale samples are in good agreement with the large scale data. The inset shows the MYEGA fits for viscosity around the fiber working range.[25, 26] For example, at a log viscosity of

6.5 dPa*s, there is a ΔT of 15°C among all samples. The fragility parameter (m) found using the MYEGA model increases from 28.9 to 34.8 with increasing SrO content (Table 2), and these trends are consistent with those reported for other alkali/alkaline earth phosphate glasses.[27, 28]

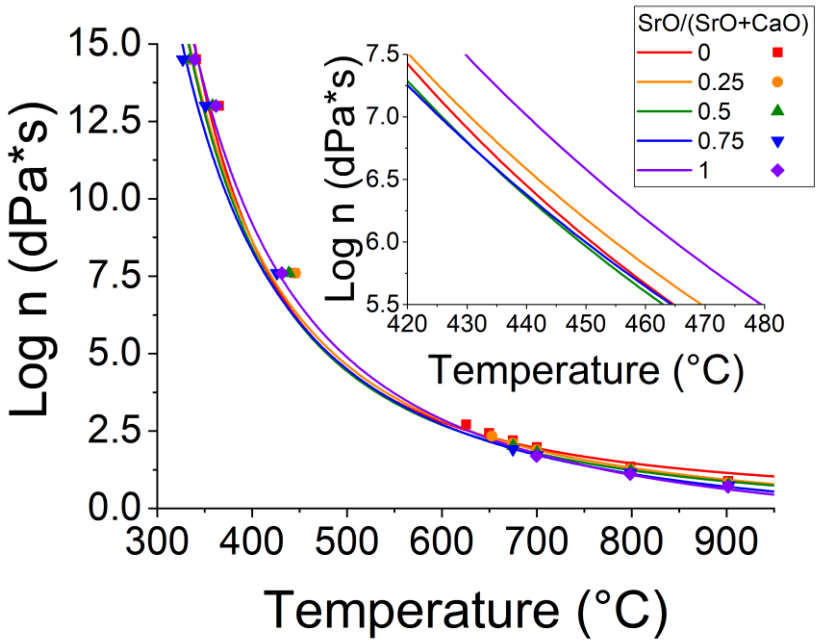

Figure 2. Viscosity data gathered from large-scale samples. The symbols are measured values and the lines are fits using the MYEGA model.[25] The inset compares the viscosities around the working range temperatures.

Figure 3 shows the refractive indices of the large-scale glasses (left) and the Abbe numbers of both sets of glasses (right). As was found for the densities, the refractive indices increase systematically when SrO replaces CaO in the glass composition. There are no significant changes in Abbe number with composition, and the values for

refractive index and Abbe number are similar to those reported for other alkaline earth metaphosphate glasses.[28]

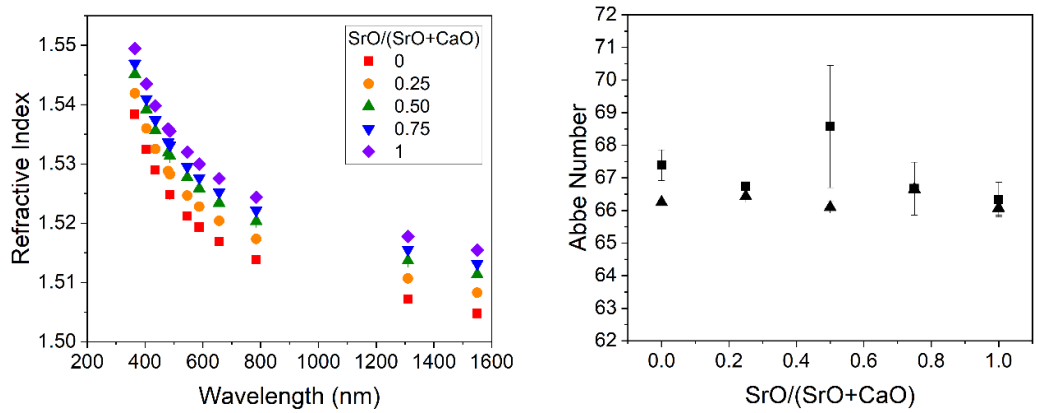

Figure 3. Refractive indices measured from the large-scale glasses (left) and Abbe numbers for both small-scale (square) and large-scale (triangle) glasses (right).

UV-visible transmission spectra for the large scale samples are shown in Figure 4. The absorbance peaks near 250 nm are due to iron contamination in the $Ca(PO_3)_2$ raw materials;[29] no such peaks were noted in the spectra from the small-scale samples (not shown).

Aqueous dissolution rate information for the small-scale samples is expressed by the weight loss data reported in Figure 5. In general, weight loss increases linearly with time, and the slopes of these trends were used to calculate the dissolution rates shown in

Table 3. These rates decreased significantly when SrO replaced CaO in the glass composition, and are similar to values found by Takebe *et al.*[30] Also shown in Figure 5 is the dependence of solution pH on dissolution time. The solutions became slightly more

acidic, relative to the blank sample, with no significant differences between compositions.

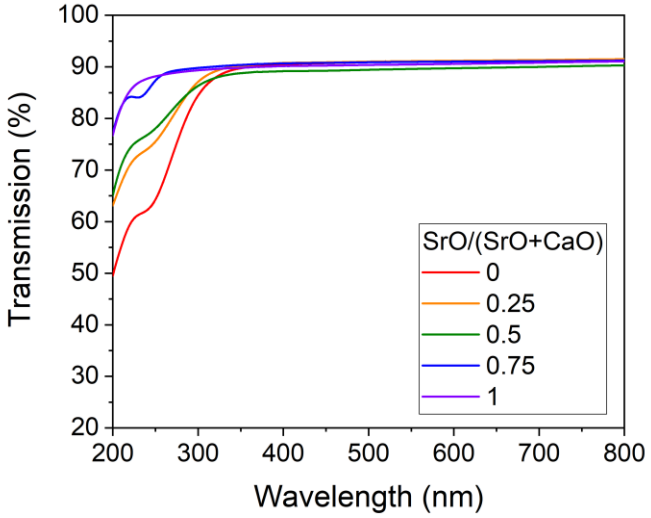

Figure 4. UV-Vis transmission spectra from large-scale glasses.

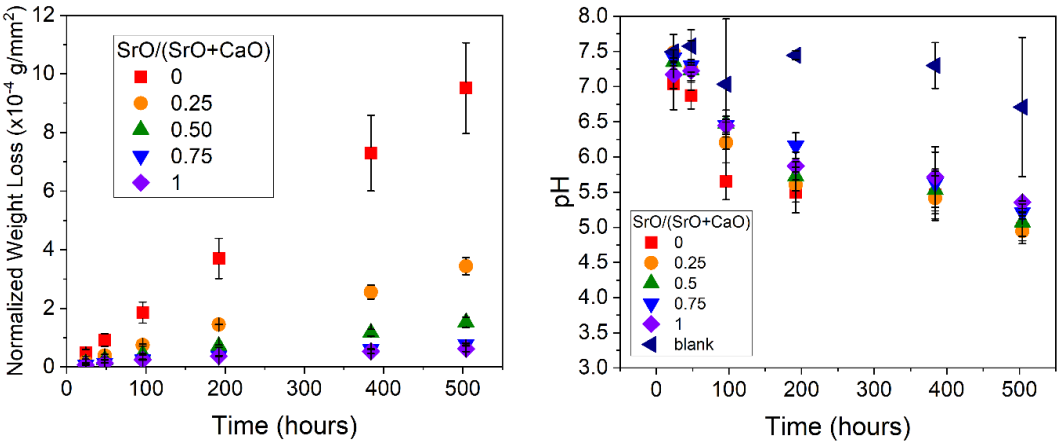

Figure 5. Normalized weight losses of the small-scale samples in deionized water at 37°C (left), and changes in the solution pH with time (right).

Table 3. Dissolution rates in 37°C deionized water for the small-scale samples.

Composition [SrO/(SrO+CaO)]	**Dissolution Rate** [x 10^{-14} kg·mm^{-2}·s^{-1}]
0	53 ± 4.2
0.25	19 ± 0.7
0.50	8.6 ± 0.5
0.75	4.4 ± 0.0
1	3.9 ± 0.2

Figure 6 shows optical micrographs of different glass samples after different times in 37°C water. A visible reaction product has formed on the pure SrO glass after 24 hrs of immersion, whereas the other glasses remain relatively clear at least through 96 hrs of immersion. Takebe described two types of reaction layers that form when phosphate glasses react in water.[30, 31] Type I glasses, like the x=1 composition, develop an opaque white gel on the surface of the glass. The surfaces of Type II glasses, including the alkali/alkaline earth metaphosphate glasses, remain transparent even after 96 hrs in 70°C water.

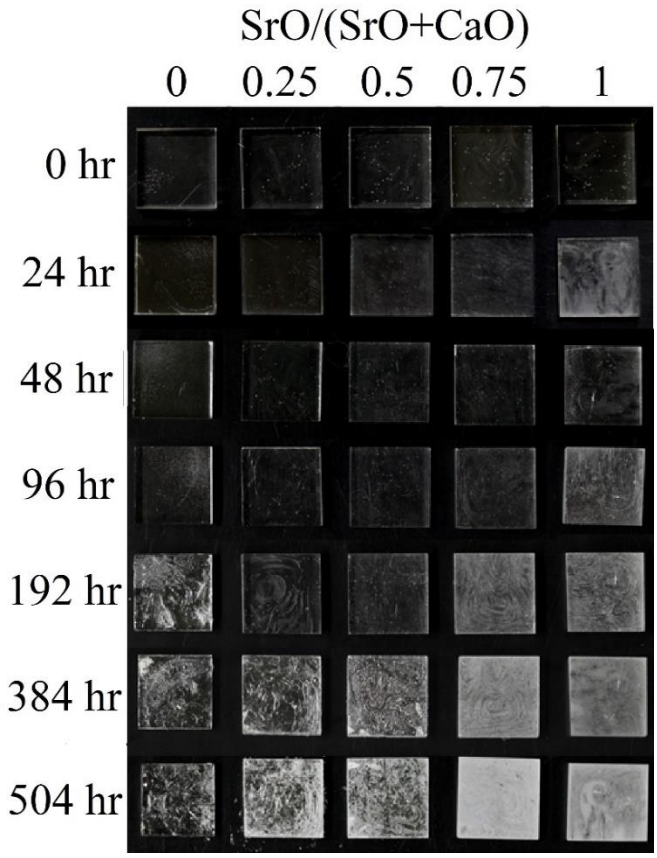

Figure 6. Optical images of the surfaces of dissolution samples (10x10mm) taken after the indicated weight measurements. The formation of a reaction layer can be noted in the SrO-rich glasses after 24 hours and the CaO-rich samples after 192 hours.

X-ray diffraction analyses of samples at the conclusion of the dissolution study, shown in Figure 7, indicate the formation of $Sr(H_2PO_4)_2 \cdot 2H_2O$ (ICCD # 00-044-0796) on the CaO free sample and $CaHPO_4 \cdot 2H_2O$ (ICCD # 01-071-0656) on the SrO-free sample. Mixtures of these two phases, along with the possible presence of $SrHPO_4$ (ICCD # 00-044-0797), were detected on the corroded surfaces of the glasses with both CaO and SrO. Massera *et al.* reported that a Ca-phosphate crystallite layer could be detected on the surfaces of Na-Ca-borophosphate glass fibers exposed to simulated body fluid at 37°C for 72 hours.[14]

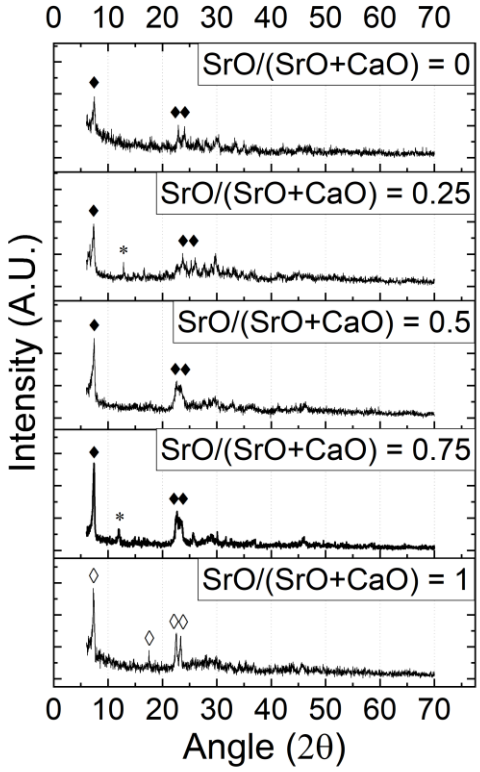

Figure 7. Thin film XRD analyses of the surfaces of dissolution samples after immersion in deionized water at 37°C for 504 hours. $Sr(H_2PO_4)_2 \cdot 2H_2O$ (ICCD # 00-044-0796) is noted by open diamonds, $CaHPO_4 \cdot 2H_2O$ (ICCD # 01-071-0656) is marked by solid diamonds, and $SrHPO_4$ (ICCD # 00-044-0797) peaks are indicated by asterisks.

3.2. GLASS STRUCTURE

Raman scattering and FT-IR reflectance spectra for the large-scale compositions are shown in Figure 8. These spectra are consistent with spectra previously reported for metaphosphate glasses,[32–36] and significant Raman and IR peak assignments are given in Table 4. The Raman spectra are dominated by two peaks, one near 690 cm^{-1}, assigned to symmetric stretching modes associated with bridging oxygens between neighboring Q^2 tetrahedra ($\nu(POP)_{sym}$), and one near 1170 cm^{-1}, assigned to symmetric stretching modes for the nonbridging oxygens on a Q^2 tetrahedron ($\nu(PO_2)_{sym}$). (The Q^x terminology refers

to the number of bridging oxygens associated with a P-tetrahedron.[2]) The low intensity peak near 1260 cm^{-1} is assigned to asymmetric stretching modes for the nonbridging oxygens on a Q^2 tetrahedron ($\nu(PO_2)_{asym}$). There are small but systematic changes in the positions of the Raman peaks to lower frequencies as SrO replaces CaO. Similar changes were observed when magnesium was replaced by calcium in another Raman study of metaphosphate glasses.[37]

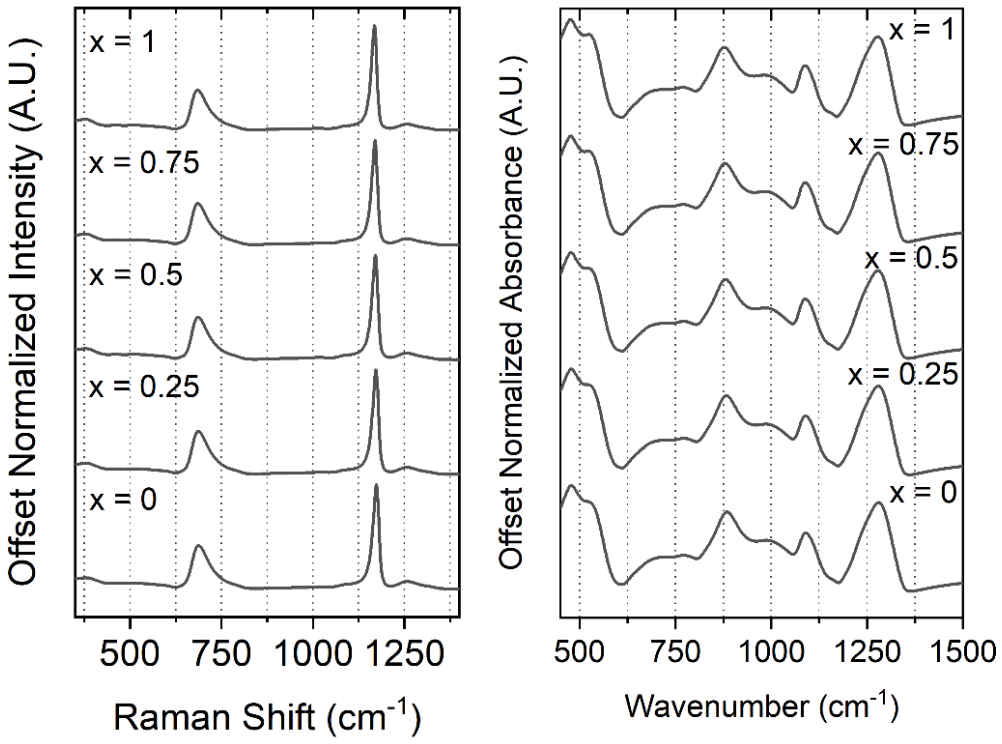

Figure 8. Raman (left) and FT-IR (right) spectra from the large-scale glasses; x is the ratio SrO/(SrO+CaO).

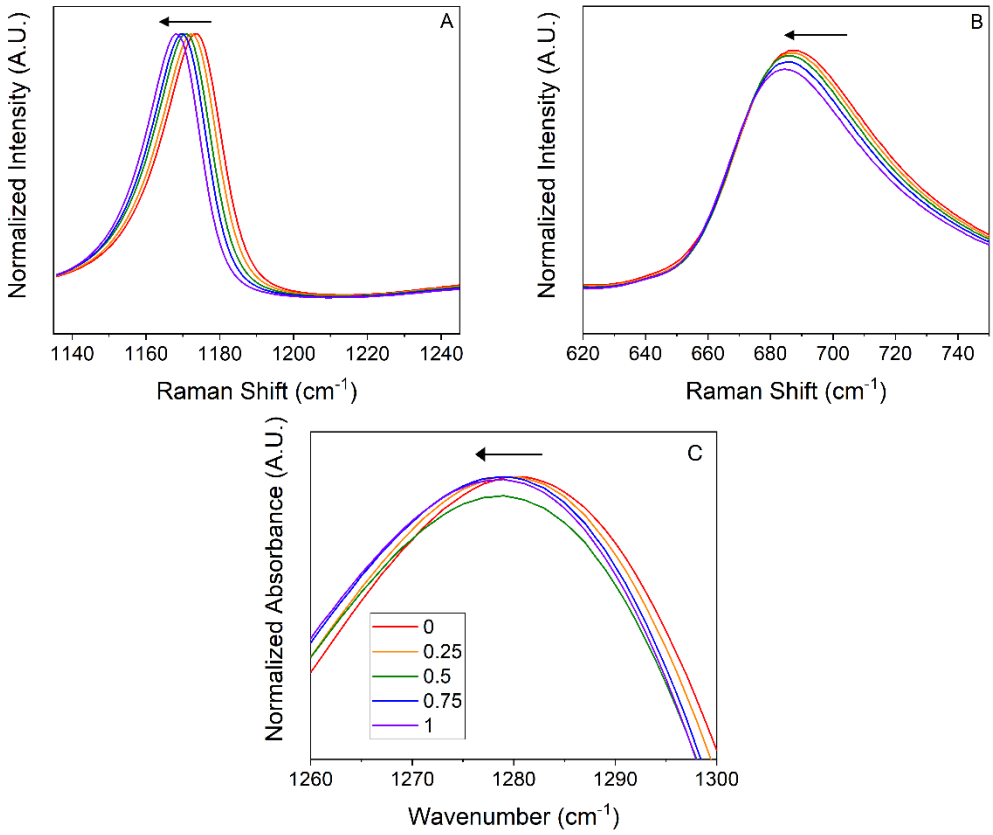

Figure 9. Expanded Raman (A,B) and IR (C) spectra from Figure 8. The Raman spectral intensities from each glass were normalized at the peak near 1170 cm^{-1} (A) to show the systematic decrease in the relative intensity of the peak near 680 cm^{-1} (B) with increasing SrO-content. The IR spectral intensities were normalized to the largest peak at 490 cm^{-1}, and the decrease in relative intensity of the peak is observed at 1280 cm^{-1} (C). Arrows show shifts in frequencies for each set of peaks with increasing SrO content.

For the IR spectra, the major absorption bands are located at 500 cm^{-1}, 700-770 cm^{-1}, 880 cm^{-1}, and 1260 cm^{-1}, and these and their shoulders can all be attributed to the interactions between phosphorus and oxygen. The band around 500 cm^{-1} is assigned to general deformation of P-O bonds.[38] The two peaks found between 700 and 770 cm^{-1} are the stretching modes of bridging oxygens in metaphosphate chains ($\nu(POP)_{sym}$).[37–39] The asymmetric stretching modes of these bridging oxygens ($\nu(POP)_{asym}$) are characterized by

the peak at 880 cm^{-1} [38-40]. The peak at 1260 cm^{-1} and its shoulder at 1154 cm^{-1} are assigned to the asymmetric ($\nu(PO_2)_{asym}$) and symmetric ($\nu(PO_2)_{sym}$) stretching modes of the non-bonding oxygens on a Q^2 tetrahedron, respectively. [37–39]

Table 4. Raman and IR spectral peak assignments.

Raman Shift (cm^{-1})	**IR wavenumber** (cm^{-1})	**Assignment**	**References**
1260	1260	$(PO_2)_{asym}$, NBO, Q^2	26, 28, 30, 32
1170	1150, shoulder	$(PO_2)_{sym}$, NBO, Q^2	26, 28, 30, 32
1048	1085	$(PO_3)_{sym}$, NBO, Q^1	29, 32
1014	880	$(POP)_{asym}$, BO, Q^2	26, 30, 32
680	700, 775	$(POP)_{sym}$, BO, Q^2	26, 28, 30, 32

4. DISCUSSION

4.1. OXYGEN BONDS AND REFRACTIVE INDEX

The structures of glasses with metaphosphate compositions, like those in this study, are based on long chains (or rings) of Q^2 phosphate tetrahedra, tetrahedra that link to their neighboring P-tetrahedra through two bridging oxygens. The remaining two nonbridging oxygens (NBO) provide the coordination environments for the metal cations which then link neighboring P-anions through the more ionic NBO-metal-NBO bonds.[2] Compositional trends for the properties of the metaphosphate glasses prepared in the present study can be related to systematic changes in the nature of the phosphate bonds,

including bond symmetry, bond length, and oxygen polarizability, as SrO replaces CaO. These structural changes are reflected in the compositional dependence of the positions and intensities of the Raman and IR peaks shown in Figure 8. Specifically, the Raman frequencies of the PO_2 symmetric stretching ($\nu(POP)_{sym}$, near 1170 cm^{-1}) and P-O-P symmetric stretching modes ($\nu(POP)_{sym}$, near 690 cm^{-1}), and the IR frequencies of the PO_2 asymmetric stretching modes ($\nu(PO_2)_{asym}$, near 1260 cm^{-1}), all decrease systematically when SrO replaces CaO (Figure 9). In addition, the Raman peak intensity ratio $I(\nu(POP)_{asym})/I(\nu(PO_2)_{sym})$ decreases when SrO replaces CaO.

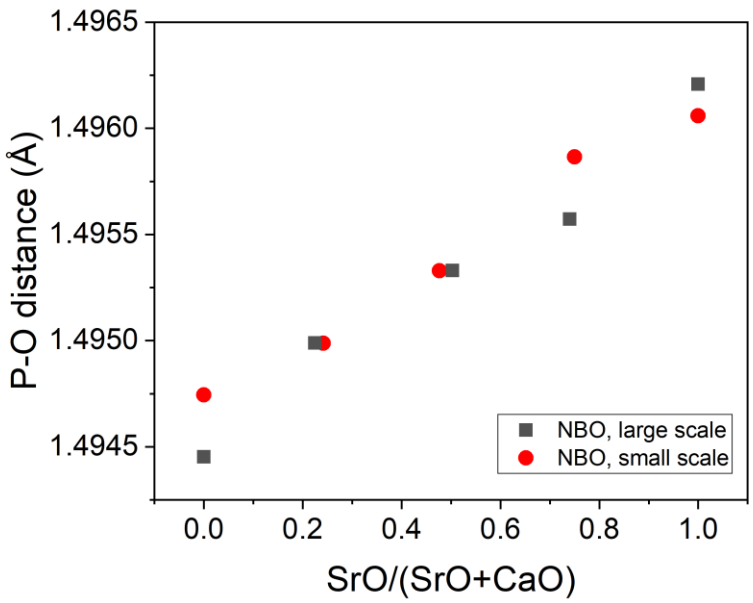

Figure 10. P-NBO bond lengths in Q^2 units, determined from the frequency of the respective $\nu(PO_2)_{sym}$ Raman peaks of both sets of glasses, using Equation 1. The P-NBO bond length increases with increasing SrO content.

The field strength of the larger Sr^{2+} ion is less than that of the smaller Ca^{2+} ion and so the substitution of the former for the latter decreases the average force constant of the metal-NBO bonds that link neighboring P-anions. In their Raman studies of metaphosphate glasses, Rouse *et al.*[33] noted that metal cations (M) with lower field strengths (or lower electronegativities) produced more ionic NBO-M bonds and consequently, less ionic and generally longer P-NBO bonds. Lower P-NBO ionicity was associated with both a decrease in the frequency of the $\nu(POP)_{sym}$ stretching modes and an increase in the peak intensity ratio $I(\nu(POP)_{asym})/I(\nu(PO_2)_{sym})$.[30] Popovic *et al.*[38] proposed an empirical relationship between the Raman peak positions (v, cm^{-1}) and P-O bond lengths (R, Å) for a wide range of crystalline phosphates:

$$v = 6.3 \times 10^3 - (3.43 \times 10^3)R \qquad [1]$$

Figure 10 shows the effect of composition on the P-NBO bond length, calculated from Equation 1 using the $\nu(PO_2)_{sym}$ Raman peak frequencies for both series of glasses. The P-NBO bond lengths increase systematically when SrO replaces CaO.

There have been many attempts to relate ion polarizability to the optical properties of glass,[39–41] often through the Lorentz-Lorenz equation, which relates molar refractivity (R_m) to the refractive index (n) and molar volume (V_m) of a glass.[40, 41]

$$R_m = \frac{(n^2 - 1)}{(n^2 + 2)} V_m \qquad [2]$$

In the present work, the refractive index at 656 nm and the molar volumes, based on the respective densities and analyzed compositions, were used to calculate R_m for each glass. Because glasses are isotropic, R_m can then be related to the molar polarizability α_m (in Å^3) of an Avogadro's Number (N_A) of ions:[42]

$$R_m = \frac{4\pi}{3} N_A \alpha_m = 2.52\alpha_m \qquad [3]$$

Assuming that both R_m and α_m are additive quantities, the average oxygen polarizability can then be calculated from:[42]

$$\alpha_{O2-} = \frac{\left(\frac{V_m}{2.52}\right)\left(\frac{n^2 - 1}{n^2 + 2}\right) - \sum \alpha_i}{N_{O2}} \qquad [4]$$

where $\sum \alpha_i$ is the total molar cation polarizability, calculated from the atom fraction of each cation and its individual ionic polarizability, and N_{O2} is the fraction of oxygen ions in the glass. Using values of α_i for Na^+, Ca^{2+}, Sr^{2+}, and P^{5+} from Dimitrov and Komatsu[43] along with their respective analyzed atom fractions (Table 1), values of α_{O2-}

were calculated for each composition and are reported in Table 5. The average oxygen polarizability was then used to calculate optical basicity (Λ)[43] and the optical interaction parameter (A),[44] according to:

$$\Lambda = 1.67\ (1 - \frac{1}{\alpha_{O2-}}) \qquad [5]$$

$$A = \sum \frac{X_{M_pO_q}(\alpha_f^- - \alpha_{O2-})}{2(\alpha_{f(M)}^+ + \alpha_f^-)(\alpha_{f(M)}^+ + \alpha_{O2-})} \qquad [6]$$

In Equation 6, α_f^- is the electronic polarizability of the free oxide ion (Pauling's value of 3.921 $Å^3$ used here), and $\alpha_{f(M)}^+$ is the electronic polarizability of cation M. Values of $\alpha_{f(M)}^+$ for Na^+, Ca^{2+}, Sr^{2+}, and P^{5+} were obtained from Dimitrov *et al.*[45] Table also lists these optical parameters for each glass.

Optical basicity is a measure of the average electron donor power of the oxygen species in a non-protonic, non-aqueous system such as glasses, oxides, alloys, slags, etc.[43] The interaction parameter is a way to express the average polarizability difference between an oxygen in a glass structure and an oxygen ion in free space.[44, 45] The interaction parameter thus describes the electronic overlap between an oxygen and its neighboring cations, and as the interaction parameter decreases, the average ionic character of those bonds increases.

Table 5. Optical parameters of glasses, calculated from analyzed compositions and molar volumes, and using the refractive index at 656 nm; α_{O2-} is the average oxygen polarizability (Eq. 4), Λ is the optical basicity (Eq. 4.5), and A is the optical interaction parameter (Eq. 4.6).

	SrO/(SrO+CaO)	$\mathbf{n_{656}}$	α_{O2-} (Å^3)	**Λ**	**A**
Large-scale	0	1.5169	1.469	0.533	0.183
	0.22	1.5204	1.469	0.534	0.180
	0.50	1.5234	1.476	0.539	0.176
	0.74	1.5252	1.476	0.538	0.175
	1	1.5275	1.478	0.540	0.172
Small-scale	0	1.5176	1.465	0.529	0.184
	0.24	1.5206	1.460	0.526	0.183
	0.47	1.5233	1.459	0.525	0.181
	0.75	1.5259	1.466	0.531	0.177
	1	1.5282	1.468	0.532	0.174

The glasses in this study are typical of what Dimitrov and Komatsu[43] characterized as Second Group compositions, glasses formed by acidic glass formers and basic oxide modifiers, with medium range refractive indices (1.5-1.9), low oxide polarizability (1.3-1.9), low optical basicity (0.4-0.85), and a large interaction parameter (0.24-0.10 Å), relative to other glasses. For the present series, when SrO replaces CaO, the oxide polarizability term generally increases, as does the optical basicity, whereas the interaction parameter decreases (Table). These trends are consistent with the formation of

a glass network with longer, more ionic bonds, indicated by the trends in the vibrational spectra described above.

4.2. DISSOLUTION BEHAVIOR

Understanding the aqueous dissolution behavior of the Na-Ca-Sr-metaphosphate glasses is a necessary first step for designing resorbable glass fibers. As noted above, metaphosphate glasses consist of long P-anions that are linked together through more ionic bonds between the nonbridging oxygens on a P-tetrahedron and the metal cations. Under neutral conditions, like those in the present study, the hydration rates of the metal-NBO bonds are significantly faster than the hydrolysis rates of the bridging oxygens between tetrahedra, so when the glasses react in water, the phosphate anions are released along with the metal cations, causing the glasses to dissolve congruently.[46, 47] The weight losses shown in Figure 6 are linear with time, consistent with other dissolution studies of metaphosphate glasses,[30, 36, 47] and the dissolution rates decrease with the substitution of SrO for CaO (Figure 5 and Table 3).[48]

Takebe *et al.* have reported an interesting correlation between the symmetry of the electronic charge distributed on an average phosphate tetrahedron and the dissolution rate of a phosphate glass.[31] They used the ratio of the Raman intensities of the asymmetric and symmetric PO_2 stretching modes, $I(\nu(PO_2)_{asym})/I(\nu(PO_2)_{sym})$ as a measure of the asymmetry of the electronic charge associated with an average Q^2 tetrahedron, and found that glasses with greater asymmetry had faster dissolution rates. As shown in Figure 11, this same relationship holds for the glasses in the present study. Takebe *et al.* proposed in their work that greater electronic asymmetry makes the NBO-metal bonds

more reactive with water,[30, 31] and that the faster hydration rates then lead to faster dissolution rates, consistent with an earlier proposal by Thilo and Wieker.[49] In the present study, then, the replacement of CaO by SrO reduces the electronic asymmetry associated with the NBOs, making the glasses more resistant to hydration.

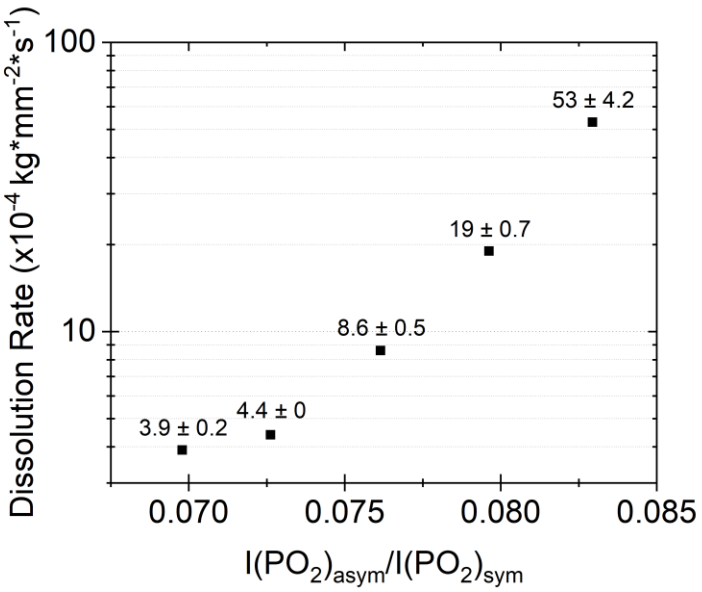

Figure 11. Dissolution rates of the bulk glasses suspended in static deionized water at 37°C plotted as a log function of the ratio of asymmetric to symmetric peak intensities. The dissolution rate increases with increasing asymmetry in the P-NBO in a Q^2 unit.

It should be noted that the development of the corrosion films on the surfaces of these glasses (Figure 6) did not change the linear weight loss rates over the course of these experiments, and the formation of these films may affect the overall change in sample weight shown in Figure 5.

4.3. PROOF-OF-CONCEPT FOR A RESORBABLE FIBER

The Na-Ca-Sr-metaphosphate glasses prepared for this study have the thermal properties required to fabricate both the core and cladding materials for optical fibers. Glass transition temperatures gradually decrease and the CTE increases as SrO replaces CaO (Table 1). These property trends are consistent with weaker bonds between the larger Sr^{2+} ions and nonbridging oxygens on the P-anions. The thermal expansion difference between the SrO-free (151 x 10^{-7}/°C) and CaO-free (164 x 10^{-7}/°C) glass is within acceptable limits for typical rod-in-tube optical fiber processing,[50] as are the small changes in viscosity when CaO replaces SrO (Figure 3).

In addition to having useful thermal properties, the range of refractive indices of the glasses from this compositional series are appropriate to produce optical fiber core and cladding materials. Two important metrics for optical fibers are the numerical aperture and the critical angle that can be calculated from the refractive indices of the core and cladding materials to represent the range of angles at which light is received by a fiber and the angle for total internal reflection, respectively. For example, an optical fiber with a CaO-free core and an SrO-free cladding would have a critical angle of 83.2° and a numerical aperture value of 0.18 at a wavelength of 632 nm (estimated using a Sellmeier Fit); these values are comparable to current optical fibers.[51]

The time-dependence of the transmitted power was simulated using the Finite Difference Eigenmode (FDE) solver function in the Mode Solution by Lumerical software [Vancouver, British Columbia], using the measured refractive indices of the glass and the PBS (1.3369 ± 0.0029) as constants, and the estimated fiber diameter over time. Equivalent time for decreasing fiber diameter was calculated from a separately

measured dissolution rate of the glass composition. The simulation setup assumed two ports placed at the two ends of the fiber and the transmitted power was calculated using the scattering parameter S21. Mode solution refers to available optical modes contained within a fiber by imposing the boundary conditions of total internal reflection. The optical mode is a solution of Maxwell's equation satisfying the boundary condition. The Eigensolver finds these modes by solving Maxwell's equations on a cross-sectional mesh of the optical fiber wherein the finite difference algorithm is used for meshing the fiber geometry. The final solution from Eigensolver reports modal profiles, power loss and transmitted power.

Average propagation loss measured with 10 cm fibers (n = 3) was 14.37 ± 0.36 dB/m at 632 nm wavelength. This loss is significantly high compared to those of conventional silica-based fibers (typically less than 10 dB/km) used in telecommunication.[52] Since the required length of biomedical implantation is, however, only approximately one foot at the deepest location, this loss is not a critical problem for biomedical applications.

Figure 12 compares the measured and simulated power transmitted through a fiber as it dissolves in PBS. Also shown is the change in fiber diameter with dissolution time. Assuming linear dissolution, the fiber dissolves at a rate of 22 x 10^{-14} $kg \cdot mm^{-2} \cdot s^{-1}$ in 21°C PBS, in reasonable agreement with the dissolution rate of 53 x 10^{-14} $kg \cdot mm^{-2} \cdot s^{-1}$ measured in 37°C deionized water (Table 3).

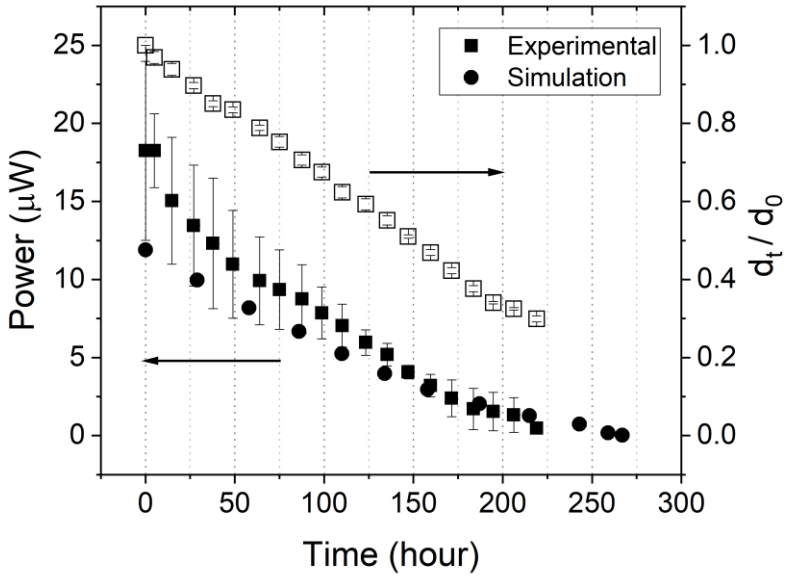

Figure 12. Loss of transmitted power through a metaphosphate fiber exposed to 21°C phosphate buffer solution; closed squares are measured values and closed circles are the calculate values based on the decreasing fiber diameter (open squares).

Both the simulation and experimental values in Figure 12 show the decrease in transmission power principally due to decreasing diameter of the fiber and increasing evanescent losses to the surrounding PBS as the fibers dissolve. The experimental values shows lower transmitted power than the simulation. This can be due to the surface roughness of the fiber, which creates more evanescent loss compared to null surface roughness in simulation.[53] Additionally, the local refractive index change of the PBS solution as the fiber dissolves is not accounted for in the simulation. If dissolution rates are known for a particular resorbable glass, then these losses can be compensated for, and a fiber with an intended operational lifetime can be fabricated for that specific biomedical application.

5. CONCLUSION

Five compositions of glasses from the $20Na_2O{\cdot}30[(1\text{-}x)CaO{\cdot}xSrO]{\cdot}50P_2O_5$ system were characterized and the links between changes in structure and properties have been established. As SrO replaces CaO in the glass, evidence for an increase in length of various phosphorus-oxygen bonds and a decrease in asymmetry of these bonds was obtained from the Raman and FT-IR spectra. These changes were consistent with the compositional trends in optical basicity, interaction parameter, and ion polarization, determined from trends in the refractive index. Weaker bonds between nonbridging oxygens and the metal cations contribute to increases in the molar volume and CTE and decreases in the characteristic temperatures and viscosity, as SrO replaces CaO. The linear dissolution rates in water decrease by over an order of magnitude when SrO replaces CaO and can be related to the electronic asymmetry of the P-O bonds. Fibers drawn from melts of the $20Na_2O{\cdot}30CaO{\cdot}50P_2O_5$ glass were used to transmit 632 nm light when submerged in phosphate buffer solution. The loss of transmission as a function of time was related to the systematic decrease in fiber diameter as predicted by a simulation study. These results demonstrate that theses glasses could be used for implantable, resorbable fibers designed with an intended operational lifetime. Such resorbable fibers are anticipated to enable a variety of temporary niche interventional sensing and therapeutic procedures.

ACKNOWLEDGEMENTS

This research would not have been possible without the assistance and hospitality of the Materials Processing Engineering Lab at Ehime University and the Project Planning Department team at Nippon Electric Glass Co., Ltd., in addition to the funding provided by the National Science Foundation Grant DMR-1207520 and support from the International Materials Institute for New Functionality in Glass at Lehigh University (NSF DMR-0844014).

REFERENCES

1. Kriedl N, Weyl W. Phosphates in ceramic ware: IV, Phosphate glasses. J Am Ceram Soc. 1941;24:372-78.

2. Brow R. Review: the structure of simple phosphate glasses. J Non Cryst Solids. 2000;263-264:1-28.

3. Ahmed I, Lewis M, Olsen I, Knowles J. Phosphate glasses for tissue engineering: Part 1. Processing and characterisation of a ternary-based P_2O_5-CaO-Na_2O glass system. Biomaterials. 2004;25:491-99.

4. Ahmed I, Lewis M, Olsen I, Knowles J. Phosphate glasses for tissue engineering: Part 2. Processing and characterisation of a ternary-based P_2O_5–CaO–Na_2O glass fibre system. Biomaterials. 2004;25:501–7.

5. Franks K, Abrahams I, Knowles J. Development of soluble glasses for biomedical use part I: In vitro solubility measurement. J Mater Sci Mater Med. 2000;11:609–14.

6. Salih V, Franks K, James M, Hastings G, Knowles J, Olsen I. Development of soluble glasses for biomedical use part II: The biological response of human osteoblast cell lines to phosphate-based soluble glasses. J Mater Sci Mater Med. 2000;11:615–20.

7. Uo M, Mizuno M, Kuboki Y, Makishima A, Watari F. Properties and cytotoxicity of water soluble Na_2O-CaO-P_2O_5 glasses. Biomaterials. 1998;19:2277–84.

8. O'Donnell M, Hill R. Influence of strontium and the importance of glass chemistry and structure when designing bioactive glasses for bone regeneration. Acta Biomater. 2010;6:2382–85.

9. Hurtel-Lemaire A, Mentaverri R, Caudrillier A, Cournarie F, Wattel A, Kamel S, et al. The calcium-sensing receptor is involved in strontium ranelate-induced osteoclast apoptosis new insights into the associated signaling pathways. J. Biol. Chem. 2009;284:575–84.

10. Fu K, Wang Z, Dai J, Carter M, Hu L. Transient Electronics: Materials and Devices. *Chem Mater*. 2016;28:3527-39.

11. Hwang S, Park G, Cheng H, Song J, Kang S, Yin L, et al. 25th Anniversary Article: Materials for High Performance Biodegradable Semiconductor Devices. Adv Mater. 2014;26:1992-2000.

12. Adnan M, Lee K, Ghasr M, O'Keefe M, Day D, Kim C. Water-soluble glass substrate as a platform for biosorbable solid-state devices. IEEE J Electron Devi. 2016;4:490-4.

13. Nazempour R, Zhang Q, Fu R, Sheng X. Biocompatible and implantable optical fibers and waveguides for biomedicine. *Materials*. 2018;11:1283.

14. Massera J, Ahmed I, Petit L, Aallos V, Hupa L. Phosphate-based glass fiber vs. bulk glass: Change in fiber optical response to probe in vitro glass reactivity. Mater Sci Eng C. 2014;37:251–57.

15. Massera J, Shpotyuk Y, Sabatier F, Jouan T, Boussard-Plédel C, Roiland C, et al. Processing and characterization of novel borophosphate glasses and fibers for medical applications. J Non-cryst Solids. 2015;425:52–60.

16. Ceci-Ginistrelli E, Pugliese D, Boetti N, Novajra G, Ambrosone A, Lousteau J, et al. Novel biocompatible and resorbable UV-transparent phosphate glass based optical fiber. Opt Mater Express. 2016;6:2040-51.

17. Strachan D, Turcotte R, Barnes B. MCC-1: a standard leach test for nuclear waste forms. 1981.

18. ASTM C598-93 [Internet]. West Conshohocken (PA): ASTM International; 2013. Standard Test Method for Annealing Point and Strain Point of Glass by Beam Bending; 1-5. Available from: https://doi.org/10.1520/C0598-93R13.

19. Imoto F, Hirao M. The viscosity of high-lead borosilicate glasses. J Ceram Assoc Jpn. 1959;67:381–5.

20. Takahashi K, Tanioka M. Studies on the drawing sphere viscometer. Oyo Buturi. 1966;35:786–96.

21. ASTM C1648-12 [Internet]; West Conshohocken (PA): ASTM International; 2018. Standard Guide for Choosing a Method for Determining the Index of Refraction and Dispersion of Glass; 1-15. Available from: https://doi.org/10.1520/C1648-12R18.

22. O'Connor A, Gallagher W, Byrne A. Porphyrin and Nonporphyrin Photosensitizers in Oncology: Preclinical and Clinical Advances in Photodynamic Therapy. Photochemistry and Photobiology. 2009;85:1043-127.

23. Ebendorff-Heidepriem H, Seeber W, Ehrt D. Dehydration of phosphate glasses. J Non-cryst Solids. 1993;163:74–80.

24. Arriagada J, Burckhardt W, Feltz A. The influence of the water content on absorption and dispersion behaviour of calcium metaphosphate glasses. J Non-cryst Solids. 1987;91:375–85.

25. Mauro J, Yue Y, Ellison A, Gupta P, Allan D. Viscosity of glass-forming liquids, Proc Natl Acad Sci USA. 2009;106:19780-4.

26. Shelby J. Introduction to Glass Science and Technology. 2nd Ed. Cambridge: The Royal Sociaety of Chemistry: 2005. 111-7.

27. Konidakis I, Varsamis P, Kamitsos E, Möncke D, Ehrt D. Structure and Properties of Mixed Strontium−Manganese Metaphosphate Glasses. J Phys Chem C. 2010;114:9125–38.

28. Muñoz-Senovilla L, Muñoz F. Behavior of viscosity in metaphosphate glasses. J Non-cryst Solids. 2014;385:9-16.

29. Sharmin N, Parsons A, Rudd C, Ahmed I. Effect of boron oxide addition on fibre drawing, mechanical properties and dissolution behavior of phosphate-based glass fibres with a fixed 40, 45, and 50 mol% P_2O_5. J Biomater Appl. 2014;29:639-653.

30. Abo-Naf S, El-Amiry M, Abdel-Khalek A. FT-IR and UV-Vis optical absorption spectra of gamma-irradiated calcium phosphate glasses doped with Cr_2O_3, V_2O_5 and Fe_2O_3. Opt Mater (Amst). 2008;30:900-909.

31. Takebe H, Baba Y, Kuwabara M. Compositional Dependence of Water Durability in Phosphate Glasses. Proceedings of the XXIst International Conference of Glass; 2007.

32. Takebe H, Baba Y, Kuwabara M. Dissolution behavior of $ZnO-P_2O_5$ glasses in water. J Non-cryst Solids.2006;352:3088-94.

33. Pemberton J, Latifzadeh L, Fletcher J, Risbud S. Raman spectroscopy of calcium phosphate glasses with varying CaO modifier concentrations. Chem Mater. 1991;3:195–200.

34. Rouse G, Miller P, Risen W. Mixed alkali glass spectra and structure. J Non-cryst Solids. 1978;28:193–207.

35. Ducel J, Videau J. Structural study of borophosphate glasses by Raman and infrared spectroscopy. Phys Chem Glass. 1993;34:212–8.

36. Carta D, Qiu D, Guerry P, Ahmed I, Abou Neel E, Knowles J, et al. The effect of compositions on the structure of sodium borophosphate glasses. J Non-cryst Solids. 2008;354:3671-7.

37. Massera J, Petit L, Cardinal T, Videau J, Hupa M, Hupa L. Thermal properties and surface refractivity in simulated body fluid of new strontium ion-containing phosphate glasses. J Mater Sci: Mater Med. 2013;24:1407-16.

38. Lee I, Shin S, Foroutan F, Lakhkar N, Gong M, Knowles J. Effects of magnesium content on the physical, chemical and degradation properties in a MgO-CaO-$Na_2O-P_2O_5$ glass system. J Non-cryst Solids. 2013;363:57-63.

39. Popović L, de Waal D, Boeyens J. Correlation between Raman wavenumbers and P-O bond lengths in crystalline inorganic phosphates, J Raman Spectrosc. 2005;36:2-11.

40. Kordes E. Physikalisch-chemische untersuchungen über den feinbau von gläsern. I. mitteilung. die molrefraktion binärer phosphat-, silikat- und boratgläser. Z Anorg Allg Chem. 1939;241:1-38.

41. Fajans K, Kreidl N. Stability of lead glasses and polarization of ions. J Am Ceram Soc. 1948;31:105-14.

42. Weyl W, Marboe E. The Constitution of Glasses. New York: Wiley: 1962.

43. Dimitrov V, Komatsu T. Classification of oxide glasses: A polarizability approach. J of Solid State Chem. 2005;178:831-46.

44. Duffy J. Optical basicity: A practical acid-base theory for oxides and oxyanions. J of Chem Edu. 1996;73:1138-42.

45. Dimitrov V, Komatsu T. Effect of interionic interaction on the electronic polarizability, optical basicity and binding energy of simple oxides. J Ceram Soc Jpn. 1999;107:1012-8.

46. Dimitrov V, Komatsu T. Interionic interactions, electronic polarizability and optical basicity of oxide glasses. J Ceram Soc Jpn. 2000;108:330-8.

47. Bunker B, Arnold G, Wilder J. Phosphate glass dissolution in aqueous solutions, J Non-cryst Solids. 1984;64:291–316.

48. Ma L, Brow R, Schlesinger M. Dissolution behavior of Na-Ca-polyphosphate glasses. Phys Chem Glasses B. 2018;59:205-12.

49. Abou Neel E, Chrzanowski W, Pickup D, O'Dell L, Mordan N, Newport R, et al. Structure and properties of strontium doped phosphate-based glasses. J R Soc Interface 2008;6:435-46.

50. Thilo E, Wieker W. Study of degradation of polyphosphates in aqueous solution. J Polym Sci Part A. 1961;53:55-9.

51. Gannon J, inventor; Corning Glass Works, assignee. Optical Fiber Formed of MgO-Al_2O_3-SiO_2. United States Patent 4664473. 1987, Apr 1.

52. Allison S, Boatner L, Sales B, inventor; Lockheed Martin Energy Systems Inc, assignee. Very High Numerical Aperture Light Transmitting Device. United States Patent 5812729. 1998, Sep 22.

53. National Bureau of Standards [Internet]. Gaithersburg (MD): National Institute of Standards and Technology; 1983. Optical Fiber Characterization, Report No. 637.

III. NETWORK STRUCTURES AND THE PROPERTIES OF Na-Ca-Sr-BOROPHOSPHATE GLASSES

Parker T. Freudenberger[1], Rebekah L. Blatt[1], Randall E. Youngman[2], and Richard K. Brow[1]

[1]Department of Materials Science and Engineering, Missouri University of Science and Technology, Rolla, Missouri

[2]Science & Technology Division, Corning Incorporated, Corning, New York

ABSTRACT

Borophosphate glasses were prepared with the nominal molar compositions $16Na_2O$-(24-y)CaO-ySrO-xB_2O_3-(60-x)P_2O_5 (mol%), where $0 \leq x \leq 60$ and y=0, 12, and 24. Information about the compositional dependence of borate and phosphate site speciation and next nearest neighbor linkages was obtained by ^{11}B and ^{31}P MAS NMR and Raman spectroscopies, and by high pressure liquid chromatography (HPLC). With the initial replacement of P_2O_5 by B_2O_3, tetrahedral borate sites linked to four phosphate anions, $B(ØP)_4$, are created in the glass structure, and the average phosphate anion becomes smaller as bridging PØP bonds are replaced by bridging PØB bonds. With further increases in the B_2O_3 content, borate units, including B-triangles, replace phosphate units linked to the B-tetrahedra. Compositional trends for the glass transition temperature (T_g) and molar volume are explained by considering the number and types of bridging oxygens per glass former, consistent with topological models reported elsewhere.

1. INTRODUCTION

Borophosphate glasses have been developed for a wide variety of applications, including their use in biomedical, optical, and energy storage devices.[1–7] Small additions of borate to phosphate glass increase thermal stability,[3, 8, 9] reduce a tendency towards devitrification[3, 5] and decrease dissolution rates in aqueous solutions.[1, 2, 5] The ionic conductivity of alkali borophosphate glasses has a nonlinear dependence on composition when borate replaces phosphate, and this behavior has been called the "mixed glass-former effect".[4, 10]

The structures of the borophosphate glasses have been studied by a variety of techniques, including several different nuclear magnetic resonance (NMR) experiments; e.g., magic angle spinning (MAS), multiple quantum magic angle spinning (MQMAS), heteronuclear correlation (HETCOR), and rotational echo double resonance (REDOR).[4, 10–13] These studies have shown that heteroatomic linkages are preferred in the structures of borophosphate glasses to maximize the number of B-O-P linkages per boron.[9–13] $^{31}P\{^{11}B\}$ and $^{11}B\{^{31}P\}$ rotational echo double resonance (REDOR) curves collected from alkali borophosphate glasses indicate a preference for phosphate species linked to two borate groups and another phosphate group.[12] Overall, these NMR studies reveal that for alkali borophosphate glasses, the anionic moieties that form with the systematic replacement of phosphate by borate occur in the order $B^4 > P^2 > P^1 > P^0 > B^2 > B^1 > B^0$, where the superscript indicates the number of bridging oxygens associated with the respective B- and P-sites.[11, 14]

Hermansen *et al.* [14, 15] used information from similar structural studies with assumptions including the borate avoidance principal[16] to develop a topological model to predict the compositional dependences of the relative concentrations of the B- and P-sites that constitute the structures of phosphate and borophosphate glasses, and used this model to explain compositional trends in physical properties, including glass transition temperature (T_g), Vicker's hardness, melt fragility, and the isobaric heat capacity jump at T_g. The model was evaluated using information collected on borophosphate glasses with a variety of modifying oxides, including sodium, lithium, potassium, cesium, and calcium. The model considered the effects of glass formers and modifiers on network topology, although some modifications were required to account for the compositional dependence of the thermal properties of calcium borophosphate glasses.[14]

Sodium calcium phosphate and borophosphate glasses have been developed for biomedical applications.[3, 7, 17–21] Strontium and calcium have similar physiological effects as they are both absorbed in the gastrointestinal tract, concentrated in bone, and excreted primarily in urine.[22] *In vivo* studies have shown that the substitution of strontium for calcium in different bioactive silicate-based glasses and ceramics stimulated osteoblasts to generate new bone and osteoclasts were prevented from resorbing bone, responses similar to those induced by strontium ranelate, a drug approved for the treatment and prevention of osteoporosis.[23–25] The substitution of strontium for calcium in sodium metaphosphate glasses decreased dissolution rates in water by over an order of magnitude and increased the refractive index while maintaining an acceptable difference in the coefficient of thermal expansion, properties designed to produce core-clad fibers with potential biomedical applications.[26]

Many studies of the compositional dependence of the properties and structures of borophosphate glasses have been done on series where variations in the modifier contents affected the borate and phosphate site speciation.[8, 9, 11, 12, 27, 28] In the present study, the modifier to glass former ratio is kept constant so that the effects of the systematic substitution of borate for phosphate on the structures and properties of Na-Ca-Sr-borophosphate glasses could be characterized using ^{11}B and ^{31}P MAS NMR, Raman spectroscopy, and high pressure liquid chromatography (HPLC). The structural information was analyzed using a modified version of the topological model proposed by Hermansen *et al.*[14] to explain the compositional trends in glass transition temperature and density. The effects of the composition and structure on the dissolution behavior of these glasses in water and in simulated body fluids are described in a separate paper.[29]

2. EXPERIMENTAL PROCEDURE

Borophosphate glasses with the nominal molar compositions $16Na_2O$-(24-y)CaO-ySrO-xB_2O_3-(60-x)P_2O_5, where $0 \leq x \leq 60$ and y=0, 12, and 24, were prepared in 50g batches using $NaPO_3$ (Shanghai Muhong Industrial Co., Ltd., Optical Grade), $Ca(PO_3)_2$ (Shanghai Muhong Industrial Co., Ltd., Optical Grade), H_3BO_3 (Fisher, ≥99.5%), Na_2CO_3 (Alfa Aesar, 99.5%), $CaCO_3$ (Fisher, >98.0%), $SrCO_3$ (Alfa Aesar, 97.5%) and H_3PO_4, 85% (Fisher, ACS Cert.) as raw materials. Powders were combined in a 150 mL Nalgene bottle and thoroughly shaken by hand before adding to a platinum crucible. When phosphoric acid was used as a raw material, it was added to the well-mixed dry components in the platinum crucible. Each batch was calcined at 300°C for four to twelve

hours, depending on the composition, to evolve water from the batch materials. The batch was then melted at 1000-1200°C for one hour, stirred with a platinum rod after 30 minutes to promote homogeneity, and then cast into preheated graphite molds. The resulting glasses were annealed for one hour at 350°C before cooling to room temperature and then stored in a vacuum desiccator. Glasses were confirmed to be fully amorphous by x-ray diffraction (XRD), using a PANalytical X'Pert Multipurpose diffractometer with a Cu Kα source and a PIXcel detector, and XRD was used to identify crystalline phases in melts that crystallized on quenching.

To determine glass compositions, 50mg of powders (<250μm) were dissolved in 50mL of 3% HNO_3 for up to one week. These solutions were then diluted to obtain three separate solutions having 1-50 ppm of the target ion concentrations, and these solutions were analyzed using inductively coupled plasma optical emission spectrometry (Perkin-Elmer Avio 200) to provide the average oxide compositions. Glasses are described throughout this manuscript using the analyzed B_2O_3-content.

Densities were measured using Archimedes' method, with deionized water as the buoyancy liquid. At least three bubble-free samples from each glass were characterized and those densities were used with the analyzed molar compositions to calculate the respective molar volumes.

Differential thermal analysis was performed either with a Perkin Elmer Differential Thermal Analyzer 7 using the Pyris Series - DTA 7 software or with a TA Instruments Q600 SDT using the TA Instrument Explorer software. 50mg samples (250-500μm) were heated in a platinum crucible at a rate of 10°C/min to 900°C under a

nitrogen atmosphere, and at least two tests were performed on each sample to verify reproducibility.

Raman spectra were collected using a Horiba Jobin Yvon LabRAM ARAMIS micro-Raman spectrometer with a HeNe (632.8 nm) 17 mW laser or a diode (785 nm) 100 mW laser, depending on composition, and a 1200 grating at 10x magnification. Fluorescence in the spectra above 1000cm^{-1} required the use of the diode source for the x = 30, 35, and 40 compositions in all three series. At least twenty 10 s scans were collected on each sample, and the respective average spectra are reported. For those spectra taken with the diode source, the Smooth (Adjacent-Averaging, ≤25 Points of Window) function of OriginPro (Massachusetts, USA), was used to reduce noise.

High pressure liquid chromatography (HPLC) was performed with a Dionex GP50-2 pump, an Ionpack AS7 4x250 mm analytical ion exchange column, and an AD25 absorbance detector. Glass samples were ground to less than 125μm particle size, dissolved overnight in a solution of 5 mM EDTA and 0.22 M NaCl (pH=10), and analyzed within 24 h. Three chromatographs were collected for each sample, using a linear solution gradient from 0.053 M NaCl to 0.5 M NaCl, both with 5 mM EDTA. The procedure was based on methods described by Sales *et al.*[30] to characterize the distributions of anion chain lengths in phosphate glasses.

Both ^{11}B and ^{31}P magic angle spinning nuclear magnetic resonance (MAS NMR) spectroscopy was performed using an Agilent DD2 spectrometer and Agilent 700/54 Premium Shielded superconducting magnet (16.4 T). Powdered glass was packed into 3.2mm zirconia rotors and were spun at a rate of 20 kHz. For the ^{11}B measurements, at a resonance frequency of 224.52 MHz, the radio-frequency pulse lengths were 0.6 μs,

corresponding to a π/12 tip angle, and a 5 s recycle delay occurred between acquisitions. ^{11}B MAS NMR spectra were collected by signal averaging 160 to 2000 scans depending on boron content of the glass, and the data were processed without any additional line broadening (apodization) using commercial software. ^{11}B MAS NMR spectra were referenced to a secondary shift standard of aqueous boric acid (19.6 ppm relative to BF_3-etherate). Spectra were fitted using DMfit Software[31], incorporating 2nd-order quadrupolar lineshapes for the trigonal boron resonances and a mixture of Gaussian and Lorentzian peaks for the tetrahedral boron resonances. A small correction to the BO_4 peak intensity was made by fitting the first set of satellite transition spinning sidebands and incorporating a similar peak under the central transition resonances.[32]

The radio-frequency pulse length for ^{31}P experiments (283.27 MHz resonance frequency) was 1 μs, corresponding to a π/6 tip angle, and a 180 sec recycle delay was used between acquisitions. ^{31}P MAS NMR spectra were collected by signal averaging of 54 to 400 scans, and the data were processed without any additional line broadening (apodization) using commercial software. ^{31}P MAS NMR spectra were referenced to an 85% H_3PO_4 solution at 0.0 ppm. All central peaks and their spinning sidebands were fitted with Gaussian lineshapes to determine peak areas.

3. RESULTS

X-ray amorphous, visually homogeneous glasses were produced from melts from the $16Na_2O$-(24-y)CaO-ySrO-xB_2O_3-(60-x)P_2O_5 series for all compositions in increments of $10B_2O_3$ except at x=50.

Table 1. As-batched and analyzed molar compositions for glasses in the series $16Na_2O$-(24-y)CaO-ySrO-xB_2O_3-(60-x)P_2O_5. ICP-OES analyses of glasses were done in triplicate and are reported as averages with one standard deviation. Asterisks indicate compositions that crystallized and were not measured in triplicate.

Sample		**Analyzed by ICP-OES (mol %)**				
x	*y*	*Na_2O*	*CaO*	*SrO*	*B_2O_3*	*P_2O_5*
0	0	14.2±0.1	25.5±0.1	--	0.0±0.3	60.4±0.5
10		13.9±0.1	25.3±0.1	--	10.8±0.1	50.0±0.2
20		13.7±0.1	25.0±0.2	--	20.3±0.1	41.0±0.3
23.3		12.8±0.2	24.4±0.3	--	23.7±0.3	39.0±0.1
30		13.9±0.1	24.5±0.3	--	30.0±0.4	31.6±0.2
35		13.0±0.1	24.4±0.1	--	35.9±0.5	26.7±0.3
40		14.1±0.1	24.2±0.2	--	40.6±0.2	21.2±0.1
43*		15.0	25.8	--	44.1	15.1
50*		14.9	25.3	--	52.3	7.5
56*		14.6	23.2	--	58.3	3.9
60		15.2±0.1	24.3±0.2	--	60.5±0.2	0.0±0.0
0	12	13.4±0.7	12.6±0.6	12.7±0.5	0.0±0.1	61.4±1.8
10		13.3±0.5	12.6±0.3	13.5±1.5	10.4±0.2	50.2±0.6
20		13.2±0.3	12.6±0.2	12.2±0.2	20.6±0.2	41.4±0.3
30		13.7±0.3	12.6±0.1	11.0±0.1	31.3±0.1	31.5±0.4
40		13.3±0.3	12.1±0.1	12.5±0.0	41.6±0.6	20.5±0.2
60		13.2±0.2	12.4±0.1	14.0±0.1	60.4±0.2	0.0±0.1
0	24	15.0±0.2	--	28.8±0.4	0.0±0.0	56.3±0.4
10		13.0±0.1	--	25.3±0.2	10.5±0.1	51.2±0.1
20		12.8±0.1	--	25.3±0.2	20.0±0.1	42.0±0.2
30		12.8±0.2	--	25.2±0.2	30.9±0.5	31.2±0.2
40		13.0±0.0	--	24.8±0.2	41.0±0.2	21.2±0.2
60		13.7±0.1	--	25.2±0.1	61.0±0.1	0.0±0.0

For the y = 0 series, several additional compositions were also produced and characterized, including ones to determine the crystallization range, which extended from x = 43 to x = 56. The crystalline phases identified by XRD include a calcium borate phosphate phase ($Ca_{9.93}(P_{5.84}B_{0.16}O_{24})(B_{0.67}O_{1.79})$, ICCD # 01-080-0537) at x = 43 and a sodium calcium phosphate phase ($Na_3Ca_6(PO_4)_5$, ICCD # 00-011-0236) at x = 50 and 56. The compositions analyzed by ICP-OES are shown in Table 1. There are minor, non-systematic deviations in the analyzed compositions (±2.0 mol %) from the as-batched compositions, including the crystallized samples. Throughout this paper, trends in structures and properties are reported in terms of the analyzed B_2O_3 content (Table 1).

3.1. RAMAN SPECTROSCOPY

Figure 1 shows representative Raman spectra collected from the SrO-free series (y=0) of the Na-(Ca,Sr)-borophosphate glasses; similar spectra were collected from the SrO-containing glasses and are shown in the appendix. It is worth noting that fluorescence in the spectra above 1000cm^{-1} required a change of excitation source for the x = 30, 35, and 40 compositions in all three series, as noted above.

Table 2 lists the assignments for the dominant peaks, which fall into three ranges: 1. Stretching modes for P-O nonbridging oxygens (NBO) are assigned to peaks in the 1000-1300 cm^{-1} range, and nonbridging oxygens on B-triangles account for the broad peak near 1400-1500 cm^{-1}; 2. Stretching modes associated with bridging oxygens between phosphate and/or borate sites are assigned to peaks in the 600-1000 cm^{-1} range; 3. Bending modes associated with P- and B-polyhedra, and vibrational modes associated with alkali and alkaline earth ions, are assigned to peaks below about 500 cm^{-1}.

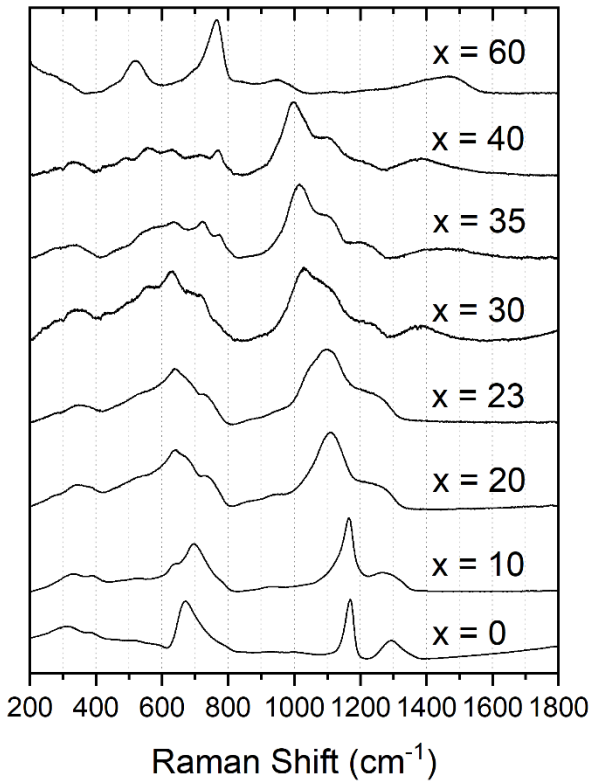

Figure 1. Raman spectra from glasses in the SrO-free (y=0) nominal molar compositional series $16Na_2O$-$24CaO$-xB_2O_3-$(60-x)P_2O_5$. The intensity of each spectrum was normalized to the most intense peak in that spectrum for visual comparison.

The spectrum from the borate-free (x=0) glass is similar to that reported for other ultraphosphate glasses with similar O/P ratios.[39] The intense peak at 1160 cm^{-1} is due to the symmetric stretching modes of nonbridging oxygens on Q^2 phosphate tetrahedra, and the broader, asymmetric peak centered near 1300 cm^{-1} is due to overlapping bands assigned to the asymmetric P-NBO stretching modes on Q^2 tetrahedra and the symmetric stretching modes of terminal oxygens on Q^3 tetrahedra. Here, the Q^i terminology is used to describe P-tetrahedra with "i" bridging oxygens.[40] The asymmetric peak centered near

700cm^{-1} is due to the symmetric stretching modes of bridging oxygens that link neighboring P-tetrahedra.

Table 2. Assignments to the peaks in the Raman spectra collected from the $16Na_2O$-(24-y)CaO-ySrO-xB_2O_3-(60-x)P_2O_5 glasses.

Raman Shift (cm^{-1})	**Assignment**	**Ref.**
300	alkali/alkaline earth vibrational modes	33
520	B-O-B bending	11, 34–36
550	P-O-P bending	21, 33
630	P-O-B$_{sym}$ stretch, P_{jB}^{2}	4, 7, 12, 14, 34
700	P-O-P$_{sym}$ stretch, P_{0B}^{2}	4, 7, 34
720	six-membered borate ring with at least two BO_4^- units	4, 12, 37
750, 770	P-O-B stretching modes	34
770	six-membered borate ring with at least one BO_4^- unit	4, 12, 21, 34, 37
1160	$(PO_2)_{sym}$ stretch (NBO), P_{jB}^{2} units	4, 7, 12
1050-1220	$(PO_3)_{sym}$ stretch, P_{jB}^{1} units	12, 34, 38
1250	$(PO_2)_{asym}$ stretch (NBO), P_{jB}^{2} units	4, 7, 12
1300	P=O$_{sym}$ stretch, P_{jB}^{3} units	4, 7, 12
1300-1450	BO_3 in various borate rings	34
1450-1500	B_{jP}^{2} vibrational modes	4

The Raman spectrum of the phosphate-free (x=60) glass is similar to those reported for other alkali-rich borate glasses.[35, 36] The intense peak at 770 cm^{-1} has been assigned to the symmetric breathing modes associated with six-membered rings (three

borons and three bridging oxygens) that include one or two B-tetrahedra.[35] These rings have been associated with several different borate superstructural units, including pentaborates, tetraborates, and diborates. The lower intensity peak near 520 cm^{-1} has been assigned to the vibrational modes of B-tetrahedra that are not associated with one of the ring units. [11, 34–36] The broad peak that extends from about 1300 to 1550 cm^{-1} has been assigned to the vibrational modes associated with nonbridging oxygens on trigonal borate sites. [11, 34–36]

There are systematic changes in the Raman spectra as borate replaces phosphate in the glass composition. With the initial addition of borate (x=10), new peaks appear at 630 cm^{-1}, 750 cm^{-1}, and 770 cm^{-1} and steadily increase in relative intensity with increasing borate content. All three of these peaks have been assigned to vibrational modes associated with various borophosphate linkages.[4, 7, 12, 34] The peak at 720cm^{-1} in the spectrum of the x = 35 glass is assigned to a six membered borate ring, similar to what is found in the phosphate-free composition. [4, 7, 12, 34] The shift in the frequency of this peak to 770 cm^{-1} with increasing borate content may indicate that the dominant borate ring changes from one with one trigonal borate unit to one with two trigonal borate units.[4, 12, 21, 34, 37]

The transition from a phosphate to a borophosphate to a distinctly borate network with increasing borate content is also reflected in the evolution of the Raman peaks in the 1000-1300 cm^{-1} range. For example, the peak at 1160 cm^{-1}, associated with the P-NBO stretching modes on Q^2 tetrahedra, decreases in frequency and broadens with increasing borate contents. Both trends indicate that one or both of the bridging P-O-P bonds on those Q^2 tetrahedra are being replaced either by a bridging oxygen to a borate site or by

another nonbridging oxygen. [11, 34, 38] The spectra of glasses with B_2O_3 contents from 23 to 40 have three distinct peaks centered roughly around 1000, 1100, and 1200 cm^{-1}, with the intensity of the 1000 cm^{-1} peak becoming dominant in the borate-rich glass. Ducel *et al*.[31] explained similar compositionally-dependent changes in Raman spectra by the formation of isolated phosphate tetrahedra, ones that link to no other phosphate tetrahedra, in the structures of their borophosphate glasses.

Broad bands centered near 1400 cm^{-1} appear in the spectra from glasses with x > 30, indicating the presence of trigonal borate species in the glass structure. Some of these triangles may be associated with borate rings that produce the sharp peaks in the 600-1000 cm^{-1} range of spectra from the same glasses.[29-30] The spectra of the borophosphate glasses in this frequency range are much more complex than either the borate-free or phosphate free end members, indicating structures with a variety of phosphate, borophosphate, and borate linkages. With increasing borate content, the broad band around 1400 cm^{-1} shifts to a higher frequency, around 1450 cm^{-1}, indicating the presence of B^2 species in the borate compositions.

3.2. HIGH PRESSURE LIQUID CHROMATOGRAPHY

Figure 2 shows examples of chromatographs collected from the Na-(Ca,Sr)-borophosphate glasses. Peaks in the chromatographs with increasing retention time represent phosphate anions with increasing numbers of phosphate tetrahedra. For example, peaks near three minutes represent isolated, monophosphate anions (PO_4^{3-}), those near seven minutes represent diphosphate anions ($P_2O_7^{4-}$), those near ten minutes represent triphosphate anions ($P_3O_{10}^{5-}$), etc. A peak labeled 3m, near 17 minutes, is

assigned to a three-membered ring anion ($P_3O_9^{3-}$).[41] The chromatographs collected from the x=0 glasses are not shown here because the networks of those ultraphosphate compositions are partially hydrolyzed during the preparation of the chromatographic solutions[30, 42] and so the resulting anion distributions are not representative of the original glass structure.

With the replacement of phosphate by borate, the dominant phosphate anions become increasingly smaller, until for the x = 40 composition, only isolated monophosphate anions remain. The replacement of CaO for SrO has no obvious effect on the phosphate anion distributions.

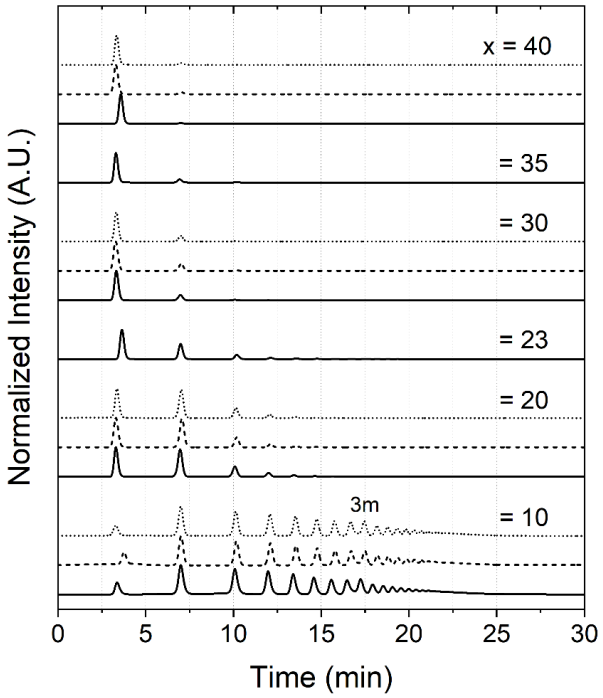

Figure 2. Representative HPLC chromatographs from glasses with the nominal molar composition $16Na_2O$-(24-y)CaO-ySrO-xB_2O_3-(60-x)P_2O_5, where y=0 (solid), y=12 (dashed), and y=24 (dotted). The intensity of each chromatograph is normalized to the most intense peak in that chromatograph for visual comparison.

3.3. NUCLEAR MAGNETIC RESONANCE SPECTROSCOPY

Figure 3A shows representative ^{11}B MAS NMR spectra collected from the borate-containing glasses. Based on previous NMR studies of borophosphate glasses,[11, 12, 14, 43] the peaks in the range 0 to -4 ppm are assigned to tetrahedral borate species, and the broader peak centered around approximately 15 ppm and exhibiting significant 2nd-order quadrupolar line broadening, is assigned to trigonal borate species. With increasing borate content, the tetrahedral peaks split to reveal new peaks at lower frequencies and a systematic decrease in the overall peak frequency. The broad trigonal peak is first detected in the spectrum of the x=23 glass, then increases in relative intensity for glasses with greater borate contents. There are no significant differences in the spectra from the CaO-, CaO/SrO-, and SrO-glasses, in contrast to another study which showed that SrO-containing borophosphate glasses have greater relative concentrations of tetrahedral borate sites than do CaO-containing glasses.[27]

Figure 3B shows representative ^{31}P MAS NMR spectra. Two peaks are apparent in the spectra collected from the three borate-free glasses. The peaks near -28 ppm are assigned to the Q^2 tetrahedra and the lower intensity peaks near -45 ppm are assigned to the Q^3 tetrahedra that constitute the structures of these ultraphosphate glasses.[44] With the addition of borate to each series, the ^{31}P MAS NMR peaks become broader and shift towards lower frequencies, trends seen in the NMR spectra of other borophosphate glasses.[4, 45]

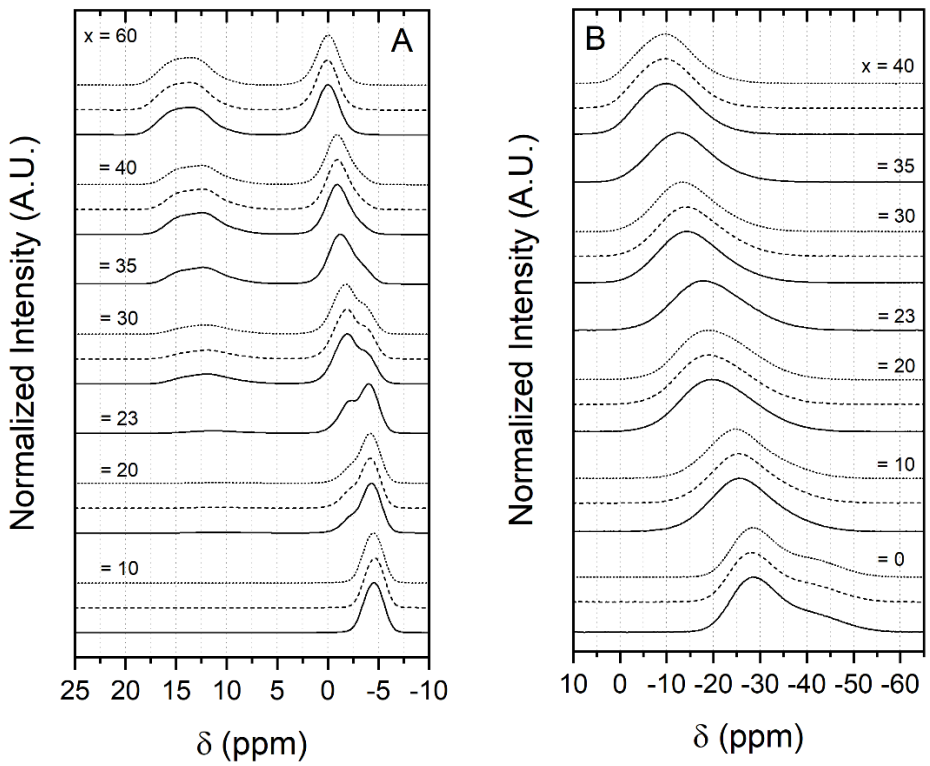

Figure 3. The ^{11}B MAS NMR (A) and ^{31}P MAS NMR (B) spectra from glasses with the nominal molar composition $16Na_2O$-(24-y)CaO-ySrO-xB_2O_3-(60-x)P_2O_5, where y=0 (solid), y=12 (dashed), and y=24 (dotted). The intensity of each spectrum was normalized to the most intense peak in that spectrum for visual comparison.

3.4. GLASS PROPERTIES

The compositional dependences of density (ρ) are shown in Figure 4A. Density increases in the series CaO<(CaO+SrO)<SrO, a consequence of the greater average molar weight of the alkaline earth modifier. Density also goes through a maximum with increasing borate content for each series, near a B_2O_3 content of 23 mole%.

Molar volume (V_m) was calculated from density and the analyzed molar weight of the glass, then normalized to the analyzed atom fraction of oxygen [O] using Equation 1.

$$V_m^O = \frac{MW_{glass}}{\rho \cdot [O]} \quad [1]$$

Figure 4B shows the effects of composition on the normalized molar volumes. In general, the molar volumes of the SrO-glasses are 1-2% greater than those of the respective CaO-glasses, consistent with the larger size of the Sr^{2+} ion, but the type of alkaline earth has a much smaller effect on V_m^O than does the replacement of P_2O_5 by B_2O_3. The break in the molar volume trend near x = 23 indicates some change in the way that the ions pack in the borate-rich glasses.

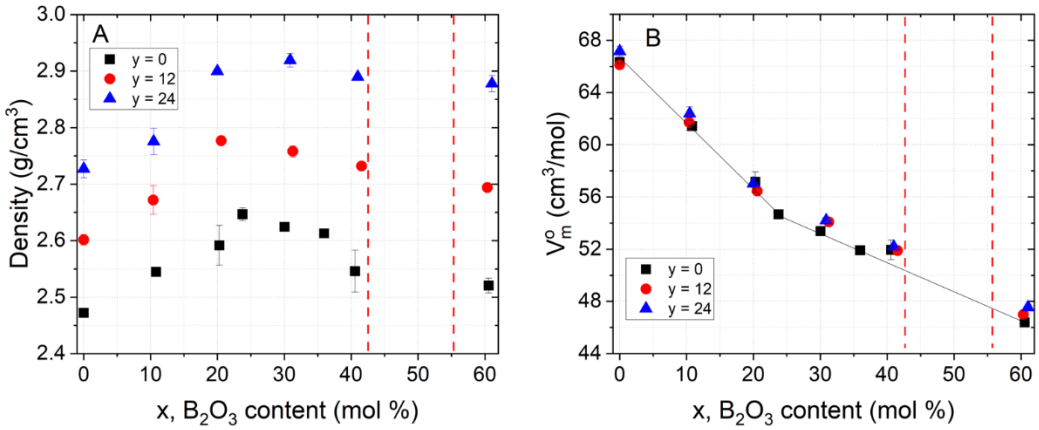

Figure 4. The effects of analyzed borate contents on the density (A) and molar volume normalized to oxygen content (B) of glasses with the nominal molar composition $16Na_2O$-(24-y)CaO-ySrO-xB_2O_3-(60-x)P_2O_5. The dotted vertical lines mark the range of compositions in the y=0 series ($43 \leq x \leq 56$) that crystallized upon quenching. Error bars represent one standard deviation and may be smaller than the symbol.

The glass transition temperatures (T_g) for all three series of glasses are shown in Figure 5. The initial addition of borate to the phosphate base glass, up to x ~ 23, increases

T_g, whereas further additions of borate have less effect. There appears to be no systematic effect of changing the alkaline earth modifier from CaO to SrO on T_g.

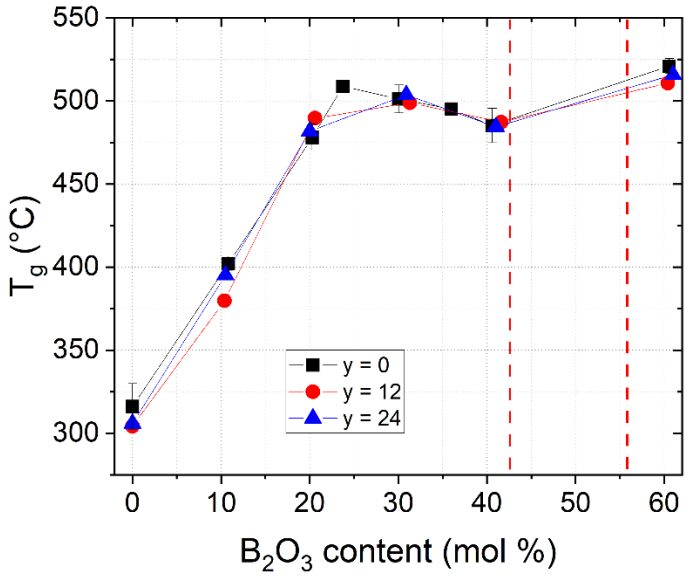

Figure 5. The effects of analyzed borate contents on the glass transition temperatures for the glasses with the nominal molar composition $16Na_2O$-(24-y)CaO-ySrO-xB_2O_3-(60-x)P_2O_5. The dotted vertical lines mark the range of compositions in the y=0 series that crystallized upon quenching.

4. DISCUSSION

The following nomenclature will be used to designate the P- and B-sites that constitute the glass structural networks. Phosphate sites are labeled as P_{jB}^{i}, where the superscript "i" is the total number of bridging oxygens on a phosphate tetrahedron and the subscript "j" is the number of oxygens on that same phosphate tetrahedron that bridge to a borate anion. Similarly, the borate sites that constitute the glass network are labeled

as B_{jP}^{i}, where the superscript "i" is the total number of bridging oxygens on a borate polyhedron (tetrahedron or triangle) and the subscript "j" is the number of oxygens on that same borate polyhedron that bridge to a phosphate anion. For example, the quartz-like structure of BPO_4 is made up of linkages between P_{4B}^{4} and B_{4P}^{4} tetrahedra. A metaphosphate glass will have a network based on P_{0B}^{2} tetrahedra[40] and a diborate glass will be constituted from B_{0P}^{4} and B_{0P}^{3} polyhedra.[16, 36] A borate triangle that has one nonbridging oxygen and two bridging oxygens to other borate polyhedra is designated B_{0P}^{2}.

4.1. QUANTITATIVE MAS NMR ANALYSIS

Representative fitted ^{11}B MAS NMR and ^{31}P MAS NMR spectra are shown in Figure 6A and B, respectively. Two peaks were used to fit the ^{11}B MAS NMR spectral envelope assigned to trigonal borate, one for neutral B_{0P}^{3} sites and a second for anionic B_{0P}^{2}; the latter was identified by its relatively large electric field gradient asymmetry parameter (η_Q>0.5).[11] For the current fits, η_Q was fixed as 0.6 for these B_{0P}^{2} peaks. Charge balance calculations shown in the appendix further support the need for these anionic B_{0P}^{2} units, but only for the borate (x = 60) compositions. Additionally, spectroscopic evidence, aside from high frequency bands in the Raman spectra, will require further analyses to confirm the presence of these units in the borophosphate compositions, and so the entire trigonal boron signal will be assigned to B_{0P}^{3} sites for x = 30, 35, and 40.

The tetrahedral boron satellite transition spinning sidebands under the central peak were accounted for by subtracting the average of the +/-1 sideband integrated intensities from the total integrated intensity of the tetrahedral peaks to obtain an accurate

measure of the tetrahedral borate fraction. This part of the spectral envelope was then decomposed into Gaussian peaks representing different B_{jP}^{i} tetrahedra. The peak positions of the borate tetrahedra with respect to the borate content for all three series are summarized in Figure 7. The shaded horizontal areas in Figure 7 show the range of frequencies assigned to similar borate-species by Carta, *et al*.[9] There is good agreement for the assignments in the present study with those by Carta, *et al*., although they did not identify B_{0P}^{4} sites in their glasses.

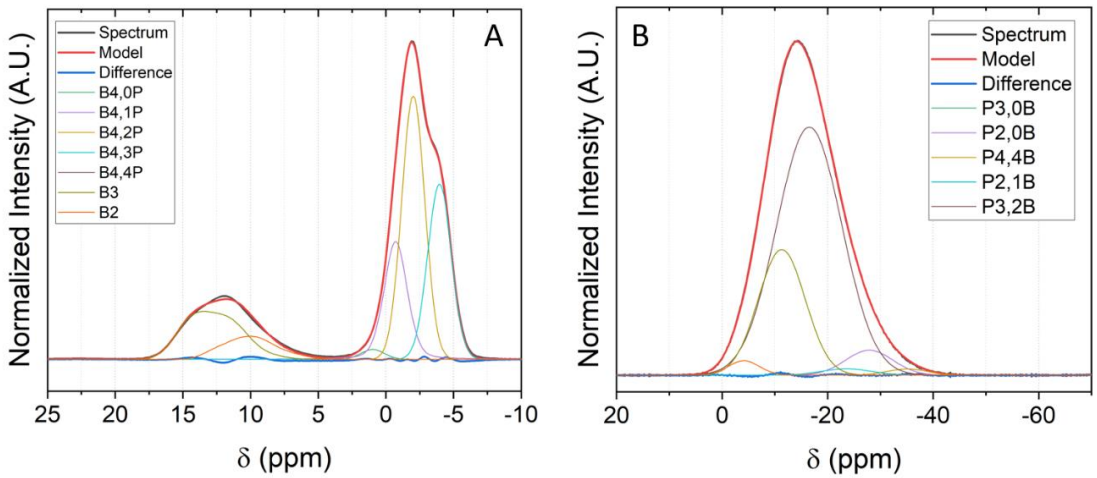

Figure 6. Fitting the (A) ^{11}B MAS NMR spectrum and the (B) ^{31}P MAS NMR spectrum collected from the glass with the nominal molar composition $16Na_2O$-$24CaO$-$30B_2O_3$-$30P_2O_5$.

The phosphate spectra, an example of which is shown in Figure 6B, were fit using Gaussian line-shapes and by constraining peak widths to 13-15ppm for P_{jB}^{3} tetrahedra, 8-10ppm for P_{jB}^{2} tetrahedra and 5-7ppm for P_{jB}^{1} tetrahedra, following the methods of Carta *et al.*[9] Similar P_{jB}^{2} and P_{jB}^{3} units have been assigned to the features of the ^{31}P MAS NMR

spectra collected from other alkali borophosphate glasses.[4, 43] Of note, BPO_4 (P_{4B}^4) units were identified in amounts less than 10% of the total phosphate sites for glasses with compositions in the range 10≤ x≤35, for all three series. The ^{31}P NMR peak positions for each unit were averaged across each series (y = 0, 12, and 24) and are plotted in Figure 7, along with the peak positions of relevant phosphate and borophosphate crystals, listed in Table 3. The shaded boxes represent the respective ranges of similar assignments made by Carta, *et al.*[9]

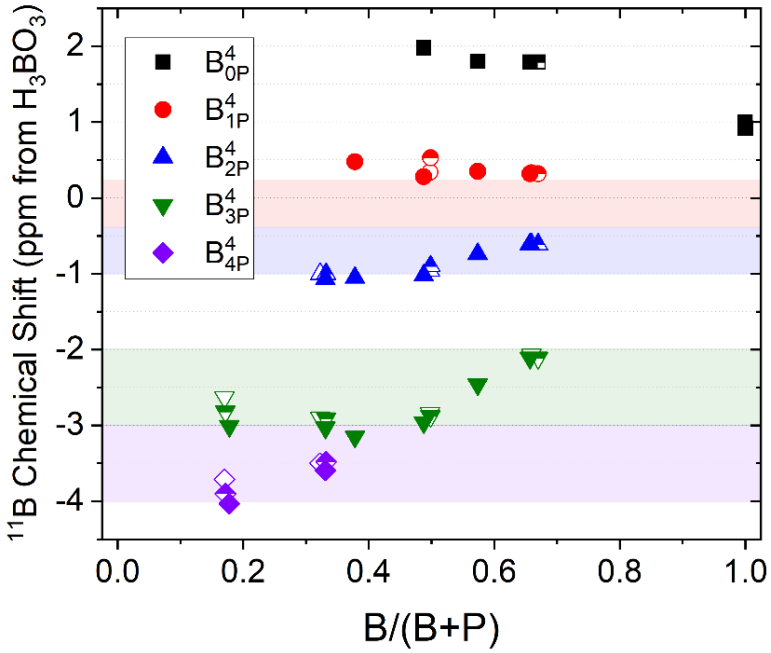

Figure 7. The ^{11}B peak positions of the borate tetrahedra in glasses with the nominal molar composition $16Na_2O$-(24-y)CaO-ySrO-xB_2O_3-(60-x)P_2O_5. The shaded boxes represent the respective ranges for each species, reported by Carta *et al.*[9]

Quantitative fits and peak assignments for the ^{11}B MAS NMR and ^{31}P MAS NMR spectra were made considering anion-to-cation charge balance, the structural information

obtained by both Raman spectroscopy and HPLC, and the assignments made in other NMR studies of borophosphate glasses.[11, 12, 43] Notably, P_{2B}^{3} structures were assumed to be the predominate moiety for P_{jB}^{3} units, and that P_{1B}^{3} and P_{3B}^{3} are not present, as noted by Raskar *et al.*[12] Additionally, it was assumed that neutral B^3 units would form before anionic trigonal species (B^2).

Table 3. The ^{31}P MAS NMR peak shifts (δ_{iso}) reported for the indicated structural units in crystalline phosphates, used to compare with the respective peak assignments for the Na-Ca/Sr-borophosphate glasses in Figure 8.

Structural Unit	**Compound**	**δ_{iso} (ppm)**	**Reference**
P^0	hydroxyapatite	2.9, 3.3	46, 47
P^0	$CaHPO_4 \cdot 2H_2O$	2.0	47
P^0	β-$Ca_3(PO_4)_2$	0.5, 1.9, 5.0	48
P_{0B}^{1}	α-$Ca_2P_2O_7$	-8, -8.9, -10.8	47, 48
P_{0B}^{2}	β-$Ca(PO_3)_2$	-26.8, -29.3, -31.0	47
P_{2B}^{2}	$CaBPO_5$, $SrBPO_5$	-9.1, -11.1	49
P_{4B}^{4}	BPO_4	-29.2, -30.0	13, 47, 49

The relative fractions of borate and phosphate sites were determined using the analyzed compositions (Table 1) and the relative areas of the peaks in the fitted ^{11}B and ^{31}P MAS NMR spectra, and these are shown in Figures 9A and 9B, respectively. B_{jP}^{4} units are the first borate sites to form with the initial replacement of P_2O_5 by B_2O_3 and their relative fractions reach a maximum in compositions with 20-30 mole % B_2O_3, the

compositions at which borate triangles first appear. The relative fractions of these trigonal groups increase systematically with increasing B_2O_3-contents. At the same time, the fraction of P_{jB}^2 units in the network decrease systematically with increasing B_2O_3 content, whereas the fraction of the P_{jB}^3 units remains relatively constant up to about 30mole% B_2O_3. (As noted above, borate units systematically replace the phosphate units as next-nearest neighbors for these P_{jB}^3 moieties with increasing B_2O_3-content.) Small fractions of P_{4B}^4 are detected in the x=10 compositions, and small fractions of P_{jB}^1 and P^0 sites are present in the x=40 glasses.

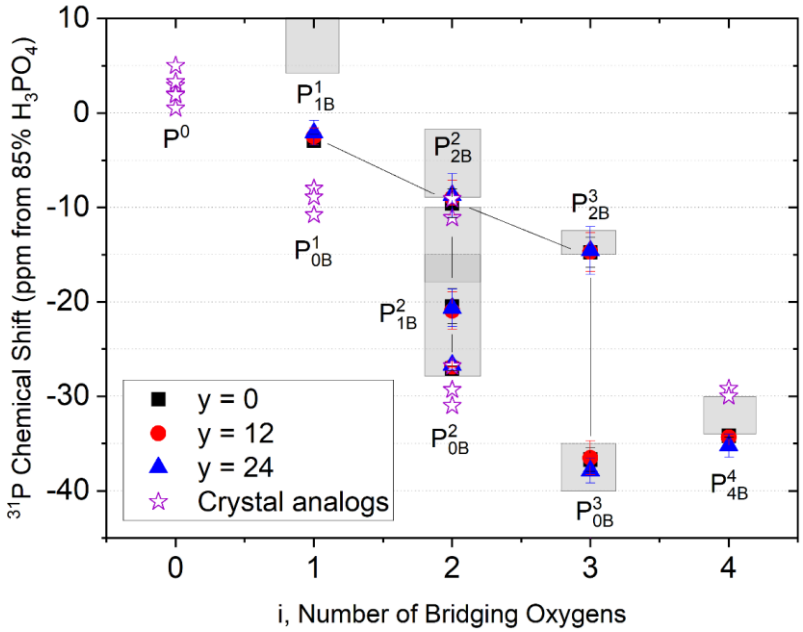

Figure 8. ^{31}P chemical shifts, averaged across each series, for the different phosphate tetrahedra identified in glasses with the nominal molar composition $16Na_2O$-(24-y)CaO-ySrO-xB_2O_3-(60-x)P_2O_5. The shaded boxes represent respective chemical shift ranges, reported by Carta *et al.*[9] The chemical shifts reported for crystalline phosphates (Table 3) are shown as the open stars.

Table 4. Summary of the equations used by Hermansen to determine structural units for the glass compositions shown in Figure 9.[14]

Structural Unit	Set of Equations
$[B^4]$	$= \begin{cases} y, y \leq y^* \\ y^*, y^* < y \end{cases}$
$[B^3]$	$= \begin{cases} y - [B^4], \frac{x}{1-x} \leq y^* + 3 \times (1-y) \\ y - [B^4] - \left(\frac{x}{1-x} - y^* - 3 \times (1-y)\right), y^* + 3 \times (1-y) < \frac{x}{1-x} \end{cases}$
$[B^2]$	$= \begin{cases} 0, \frac{x}{1-x} \leq y^* + 3 \times (1-y) \\ \frac{x}{1-x} - y^* - 3 \times (1-y), y^* + 3 \times (1-y) < \frac{x}{1-x} \end{cases}$
$[P^3]$	$= \begin{cases} (1-y) - \left(\frac{x}{1-x} - [B^4]\right), \frac{x}{1-x} \leq y^* + (1-y) \\ 0, y^* + (1-y) < \frac{x}{1-x} \end{cases}$
$[P^2]$	$= \begin{cases} \frac{x}{1-x} - [B^4], \frac{x}{1-x} \leq y^* + (1-y) \\ 2 \times (1-y) - \left(\frac{x}{1-x} - [B^4]\right), y^* + (1-y) < \frac{x}{1-x} \leq y^* + 2 \times (1-y) \\ 0, y^* + 2 \times (1-y) < \frac{x}{1-x} \end{cases}$
$[P^1]$	$= \begin{cases} 0, \frac{x}{1-x} \leq y^* + (1-y) \\ \left(\frac{x}{1-x} - [B^4]\right) - (1-y), y^* + (1-y) < \frac{x}{1-x} \leq y^* + 2 \times (1-y) \\ 3 \times (1-y) - \left(\frac{x}{1-x} - [B^4]\right), y^* + 2 \times (1-y) < \frac{x}{1-x} \leq y^* + 3 \times (1-y) \\ 0, y^* + 3 \times (1-y) < \frac{x}{1-x} \end{cases}$
$[P^0]$	$= \begin{cases} 0, \frac{x}{1-x} \leq y^* + 2 \times (1-y) \\ \left(\frac{x}{1-x} - [B^4]\right) - 2 \times (1-y), y^* + 2 \times (1-y) < \frac{x}{1-x} \leq y^* + 3 \times (1-y) \\ (1-y), y^* + 3 \times (1-y) < \frac{x}{1-x} \end{cases}$

Topological models of glass structures derived from constraint theories have proved useful for explaining composition-property trends for a variety of glass forming systems.[28, 50–53] Hermansen assumed that borate was first incorporated into a phosphate

network as B^4_{4P} units, and then beyond a critical B-to-P ratio, other anionic sites would emerge, in the order B^4_{jP}>P^2_{jB}>P^1_{jB}>P^0>B^2.[14] Hermansen also assumed that no more than two different phosphate sites (P^i_{jB}) would be present in a borophosphate network and that the anionic charges of the network sites are balanced by the modifying cation charges. Table shows the equations used by Hermansen to describe the compositional dependences of B- and P-sites for glasses with the nominal molar compositions xR'O(1 − x)[yB_2O_3(1 − y)P_2O_5], where R'O represents both alkali and alkaline earth oxides, and these equations are plotted as the solid lines in Figures 9A and 9B.[14]

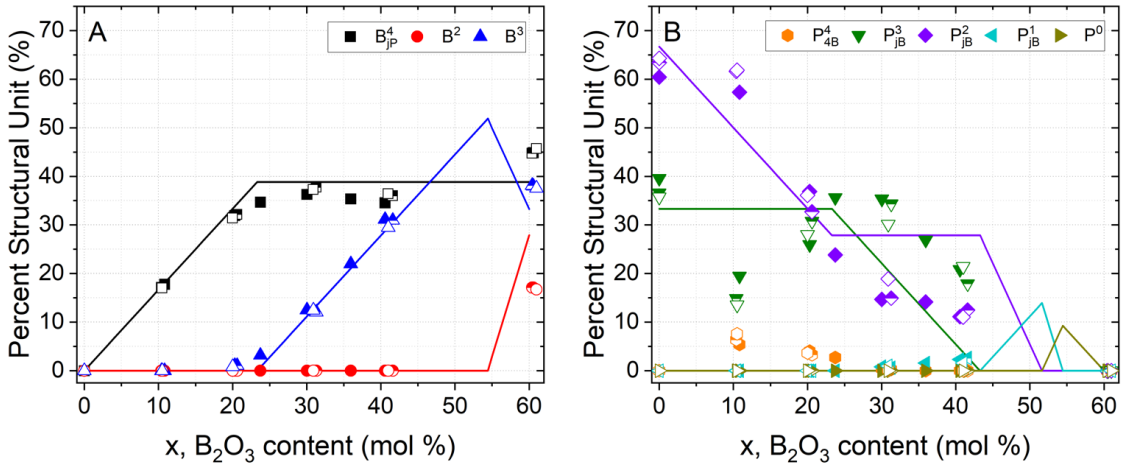

Figure 9. The respective fractions of borate (A) and phosphate (B) sites obtained from the ^{11}B and ^{31}P MAS NMR spectra from glasses with the nominal molar composition $16Na_2O$-(24-y)CaO-ySrO-xB_2O_3-(60-x)P_2O_5, where y = 0 (solid symbols), 12 (half-filled symbols) and 24 (open symbols). The solid lines are the predicted distributions from the model proposed by Hermansen *et al.*.[14]

In general, the compositional dependences of the relative concentrations of the major B- and P-sites derived from the ^{11}B and ^{31}P MAS NMR spectra of the glasses in

the present study are consistent with the predictions of the Hermansen model. In particular, Hermansen predicted that only B_{jP}^{4} sites would be present in glasses with up to 23mole% B_2O_3 and indeed, significant concentrations of trigonal borate units were detected only in glasses with greater borate concentrations (Figure 9A). Hermansen predicted similar breaks in the compositional dependences of the P_{jB}^{3} and P_{jB}^{2} unit concentrations at 23 mole% B_2O_3, although these changes are less obvious in the quantitative NMR data shown in Figure 9B. The disproportionation of P_{jB}^{2} sites to P_{jB}^{3} and P_{jB}^{1} sites has been noted in previous studies of borophosphate glasses modified with higher field strength cations, like Ca^{2+},[14, 54] and similar reactions may account for some of the site-concentration differences between the present measurements and Hermansen's predictions.

There are several other differences between the quantitative site analyses of the glasses in the present study and those predicted by Hermansen. First, the ^{31}P MAS NMR spectra in the present study (Figure 3B) reveal small (<10%) fractions of P_{4B}^{4} sites in glasses with up to 20 mole% B_2O_3; Hermansen assumed that these sites would not form in these glasses. And secondly, the ^{31}P MAS NMR spectra reveal that these borophosphate glasses have more than two distinct P-sites, an interpretation consistent with the complexity of the Raman spectra in the 1000-1300 cm^{-1} range (Figure 1) and with the large number of P-anions detected by HPLC for glasses with a B_2O_3 content less than about 35 mole% (Figure 2).

Despite these differences, the Hermansen model still provides useful insight into the evolution of the borophosphate network with increasing borate contents, insight that will be used below to explain the compositional dependence of the glass properties.

4.2. OXYGEN SPECIATION

The equations in Table 5 summarize those used by Hermansen *et al.* to calculate oxygen speciation based on the borate and phosphate site concentration equations in Table 4.2. In these equations, b is a measure of the allowable B^4-O-B^4 bonds per B_{jP}^4 unit, and Hermansen *et al.* assumed that no tetrahedral borate units were connected to another tetrahedral boron ($b = 0$).

Table 5. Equations used by Hermansen *et al.* to determine oxygen speciation in borophosphate glasses with nominal compositions of $xR'O(1-x)[yB_2O_3(1-y)P_2O_5]$.[14]

Oxygen Speciation	**Set of Equations**
[BØP]	$= \begin{cases} \dfrac{(4-b)\times[B^4]}{\left(x+(1-x)\times\left(3y+5(1-y)\right)\right)/\left(2\times(1-x)\right)}, y \le y^* \\ \dfrac{4\times[P^4]+3\times[P^3]+2\times[P^2]+1\times[P^1]}{\left(x+(1-x)\times\left(3y+5(1-y)\right)\right)/\left(2\times(1-x)\right)}, y^* < y \end{cases}$
[BØB]	$= \begin{cases} \dfrac{\frac{1}{2}\times(3\times[B^3]+2\times[B^2]+1\times[B^1])}{\left(x+(1-x)\times\left(3y+5(1-y)\right)\right)/\left(2\times(1-x)\right)}, y \le y^* \\ \dfrac{\frac{1}{2}\times(4\times[B^4]+3\times[B^3]+2\times[B^2]+1\times[B^1])}{\left(x+(1-x)\times\left(3y+5(1-y)\right)\right)/\left(2\times(1-x)\right)} - \dfrac{1}{2}\times[B\emptyset P], y^* < y \end{cases}$
[PØP]	$= \begin{cases} \dfrac{\frac{1}{2}\times(4\times[P^4]+3\times[P^3]+2\times[P^2]+1\times[P^1])}{\left(x+(1-x)\times\left(3y+5(1-y)\right)\right)/\left(2\times(1-x)\right)} - \dfrac{1}{2}\times[B\emptyset P], y \le y^* \\ 0, y^* < y \end{cases}$
[NBO]	$= \dfrac{1\times[B^2]+2\times([B^1]+[P^2])+3\times([B^0]+[P^1])+4\times[P^0]}{\left(x+(1-x)\times\left(3y+5(1-y)\right)\right)/\left(2\times(1-x)\right)}$

In the present study, the number of bridging oxygens per glass former and non-bridging oxygens per glass former are calculated from the fractions of structural units, $[B_{jP}^{i}]$ and $[P_{jB}^{i}]$, obtained by MAS NMR using Equations 2 and 3:

$$\frac{[\emptyset]}{(B+P)} = \sum\left(\frac{\mathrm{i}}{2}[\mathrm{B}_{\mathrm{jP}}^{\mathrm{i}}]\right) + \sum\left(\frac{\mathrm{i}}{2}[\mathrm{P}_{\mathrm{jB}}^{\mathrm{i}}]\right) \qquad [2]$$

$$\frac{[\mathrm{NBO}]}{(B+P)} = [B^2] + \sum\left((4-i)[\mathrm{P}_{\mathrm{jB}}^{\mathrm{i}}]\right) \qquad [3]$$

For these calculations, the B^3 units are assumed not to have links to phosphate tetrahedra, consistent with the $^{11}B\{^{31}P\}$ REDOR study of alkali borophosphate glasses by Rinke and Eckert.[11] Additionally, the fraction of each type of bridging oxygen to total number of oxygens can also be calculated from the fraction of structural units, $[B_{jP}^{i}]$ and $[P_{jB}^{i}]$, obtained by MAS NMR (summarized in Appendix) using Equations 4, 5, and 6, respectively:

$$[B\emptyset P] = \frac{\sum\left(\frac{j}{2}\,[B_{jP}^{i}]\right) + \sum\left(\frac{j}{2}\,[P_{jB}^{i}]\right)}{\emptyset + NBO} \qquad [4]$$

$$[B\emptyset B] = \frac{\sum\left(\frac{(i-j)}{2}[B_{jP}^{i}]\right)}{\emptyset + NBO} \quad [5]$$

$$[P\emptyset P] = \frac{\sum\left(\frac{(i-j)}{2}[P_{jB}^{i}]\right)}{\emptyset + NBO} \quad [6]$$

The compositional dependences of the fractions of the three bridging oxygen species ([BØP], [BØB], and [PØP]), and non-bridging oxygens associated with borate and phosphate units ([NBO(B)] and [NBO(P)], respectively), are shown in Figure 10. The solid lines are the trends predicted by the Hermansen model. The trends in speciation can be divided into two regions with x = 23 as the pivotal composition. It is worth noting that this composition is the same at which the structural model by Hermansen predicts the maximum fraction of tetrahedral borate units and the onset of the formation of trigonal borate units.

In the compositional range $0 \leq x \leq 23$, an exchange of PØP for BØP linkages occurs as tetrahedral borate units replace phosphate units to form a borophosphate network. At the pivotal composition (x = 23), the maximum in [BØP] marks the point at which the glass structure is a fully interconnected borophosphate network. Above this composition (x>23), the additional borate units are incorporated into a distinctly borate network as BØP linkages are replaced by BØB linkages, including those that link increasing fractions of trigonal borate sites (Figure 9A).

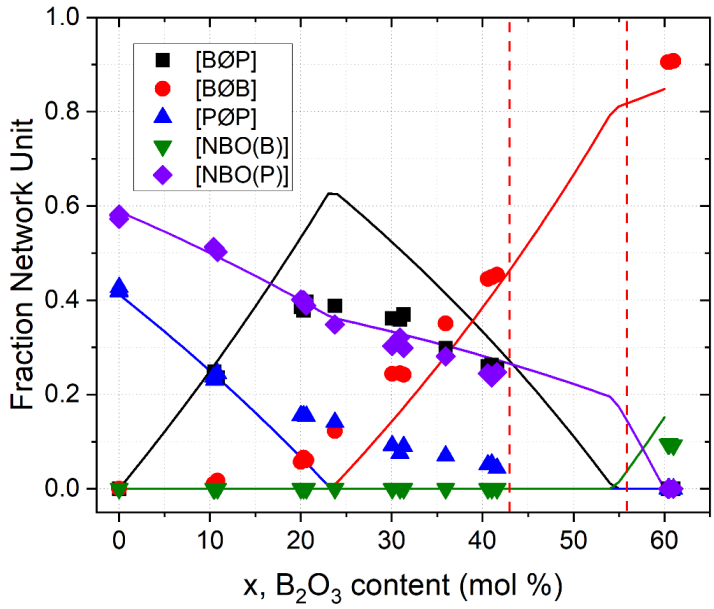

Figure 10. Compositional dependence of the oxygen speciation for glasses with the nominal molar composition $16Na_2O$-(24-y)CaO-ySrO-xB_2O_3-(60-x)P_2O_5, where y=0, y=12, and y=24. Solid lines are the predictions from Hermansen's structural model. The dotted lines mark the range where the compositions crystallize upon quenching.

The primary assumption made by Hermansen *et al.* that differs from the results of this analysis is that the borate units first form heteroatomic linkages with phosphate units before they form homoatomic linkages to other borate units. There is clear evidence in the ^{11}B MAS NMR spectra for a greater fraction of homoatomic BØB bonds in the structures of glasses in the compositional range $20 \leq B_2O_3 \leq 40$ (mol %), and in the ^{31}P MAS NMR spectra and the chromatographs for the presence for greater fractions of homoatomic PØP linkages in in the same glasses leading to smaller fractions of heteroatomic BØP than are predicted by Hermansen's structural model. There is good agreement between the compositional dependences of the nonbridging oxygens fractions, ([NBO(B)] and [NBO(P)], and Hermansen's predictions.

Figure 11 plots the compositional dependence of the number of bridging oxygens per glass former for the three series of CaO/SrO borophosphate glasses. This metric will be used below to explain the compositional dependence of the glass transition temperatures.

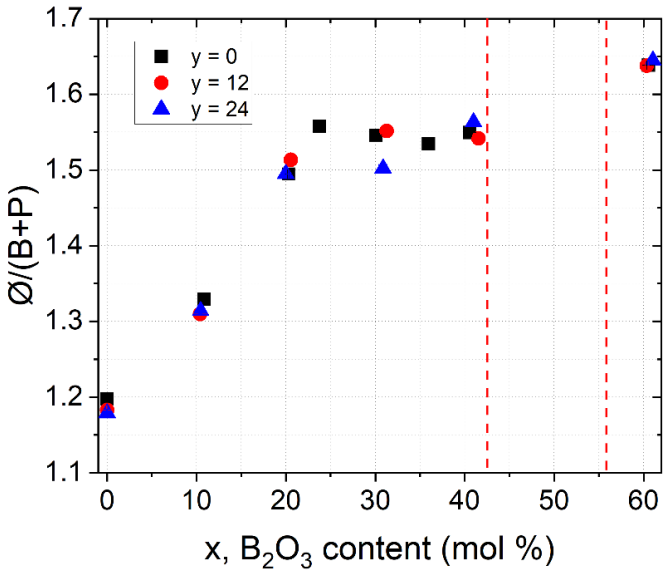

Figure 11. Compositional dependence of the number of bridging oxygens per glass former (Ø/(B+P)) for glasses with the nominal molar composition $16Na_2O$-(24-y)CaO-ySrO-xB_2O_3-(60-x)P_2O_5. The vertical dotted lines mark the range where the compositions crystallize upon quenching.

The Raman spectra in Figure 1 show an evolution in the network structures of these glasses from phosphate to borophosphate to borate as B_2O_3 replaces P_2O_5, consistent with the interpretations of the MAS NMR and HPLC data. The intense peak centered near 1160 cm^{-1} in the spectrum of the borate-free compositions broadens and shifts to lower frequencies with increasing B_2O_3 content. This peak is assigned to the

symmetric stretching modes of nonbridging oxygens on Q^2 phosphate tetrahedra, and the shift to lower frequencies is an indication of the replacement of a phosphate by a borate as the next nearest neighbors; viz., the conversion of P_{0B}^2 to P_{1B}^2.[4, 14] The development of these PØB linkages is further indicated by the increase in the intensity of the Raman peak at 1050 cm^{-1} with increasing borate content. The relative intensity of this peak is maximized for the glass where x = 30. In the Raman spectra from the high-borate compositions, where x > 35, peaks near 720 and 750cm^{-1} assigned to borate vibrational modes become apparent. These features are consistent with the appearance of the trigonal borate sites in the ^{11}B MAS NMR spectra (Figure 3).

4.3. PHOSPHATE ANION DISTRIBUTIONS

When phosphate glasses are dissolved under the conditions used to prepare the HPLC solutions, ionic bonds that link the phosphate anions through the modifying cations are hydrated, releasing those anions to be separated by the chromatography column and then analyzed. The hydrolysis of the bridging oxygen bonds (PØP) that link the neighboring P-tetrahedra that constitute those anions is relatively slow and so the distribution of anions recorded by HPLC is assumed to represent that found in the original glass.[30] However, when ultraphosphate glasses react in aqueous solutions, the P_{0B}^3 units hydrolyze to release smaller P-anions and so the distributions of those anions in solution are different from those in the original glass.[42, 55, 56] Therefore, quantitative structural information for phosphate glasses from HPLC is limited to the polyphosphate (O/P>3) compositions.[57–60]

In the preparation of the HPLC samples from the borophosphate glasses in the present study, the oxygens that bridge borate and phosphate units (BØP) are assumed to hydrolyze much faster than the bridging PØP bonds. Protonated tetrahedral borates which initially form when borates are hydrated are unstable and immediately convert to more stable protonated trigonal borates,[61, 62] leading to the hydrolysis of the bridging BØB bonds and the release of borate species to solution.[63] Similar reactions are assumed to occur with the borophosphate bonds, leading to the separate release of phosphate anions and boric acid.

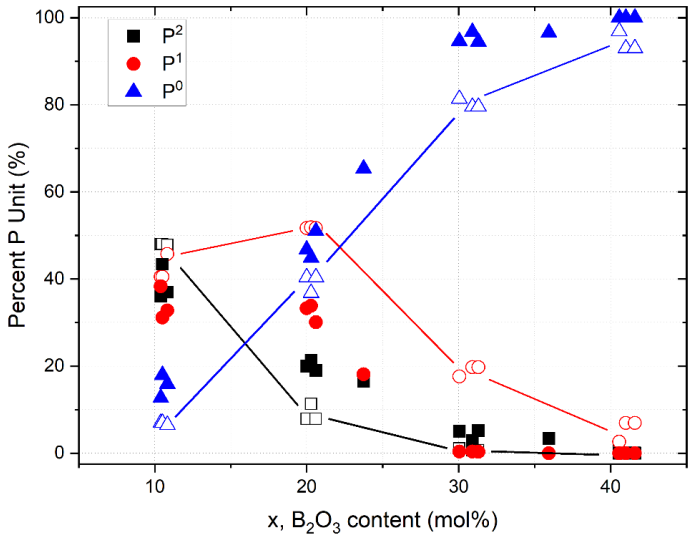

Figure 12. Fractions of P^0, P^1, and P^2 units for glasses with the nominal molar composition $16Na_2O$-(24-y)CaO-ySrO-xB_2O_3-(60-x)P_2O_5 as measured by ^{31}P MAS NMR (closed symbols) and HPLC (open symbols). The lines are meant as guides for the eye.

Figure 12 compares the quantitative P-speciation results from the HPLC data with those from the ^{31}P MAS NMR spectra. Here, the different P_{jB}^{i} units identified in the

NMR spectra are combined to their respective values of "i" and compared to the fractions of P^i sites obtained directly from the associated chromatographs. In this analysis, it was assumed that [42, 55, 56]every P_{2B}^3 unit identified in the NMR data was hydrolyzed to form a P^0 anion in the HPLC solutions, leading to reasonably good agreement between the two data sets.

The average P-anion size ($\bar{n}$) in a polyphosphate glass can be predicted from its composition using Equation 7:[40, 64]

$$\bar{n} = \frac{1}{([O]/[P]) - 3} \qquad [7]$$

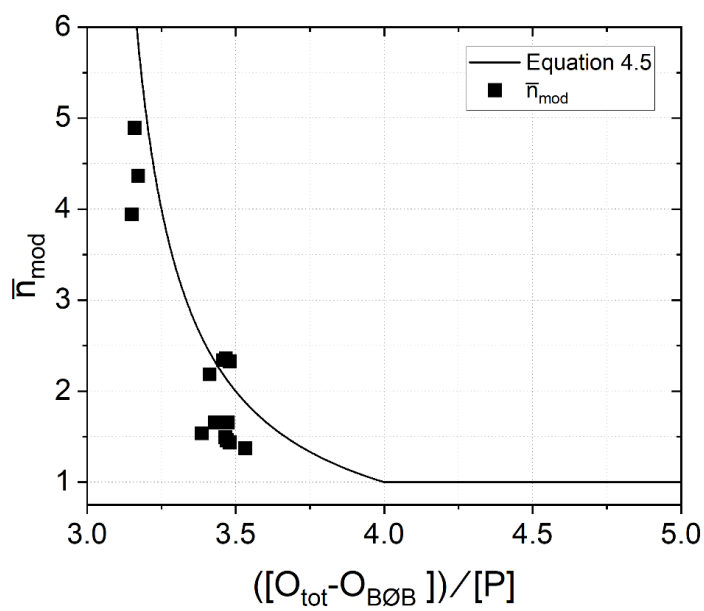

Figure 13. Average phosphate chain length determined by ^{31}P MAS NMR ($\bar{\mathbf{n}}_{mod}$) compared to what is expected from the modified O/P ratio (($[O_{tot}-O_{BØB}]/[P]$), which excludes oxygens sequestered in BØB linkages.

Here, it is assumed that all oxygens in the glass structure are linked to a phosphate unit. In the present borophosphate glasses, some fraction of oxygens bridge neighboring borate units as BØB bonds and so do not modify the phosphate linkages. However, if these oxygens are subtracted from the total oxygen content, then, as shown in Figure 13, the average P-anion size measured by NMR is in good agreement with that predicted by the following modified version of Eq. 7:

$$\bar{n}_{mod} = \frac{1}{\left(\left([O_{tot} - O_{B\emptyset B}]\right)/_{[P]}\right) - 3} \qquad [8]$$

4.4. GLASS PROPERTIES

Topological structural models, like the one proposed by Hermansen, *et al*. for borophosphate glasses, have proved to be useful for predicting properties that are sensitive to the nature of the glass-forming network.[14] In the present study, the similarity in the compositional dependence of the glass transition temperature (Figure 5) and the number of bridging oxygens per glass-forming cation (Figure 11) indicates that the former directly depends on the latter. Indeed, Figure 14 shows a systematic increase in T_g with increasing numbers of Ø/(B+P). Rinke *et al.* observed a similar correlation between glass transformation temperatures and the network former connectivity for Na-borophosphate glasses.[11]

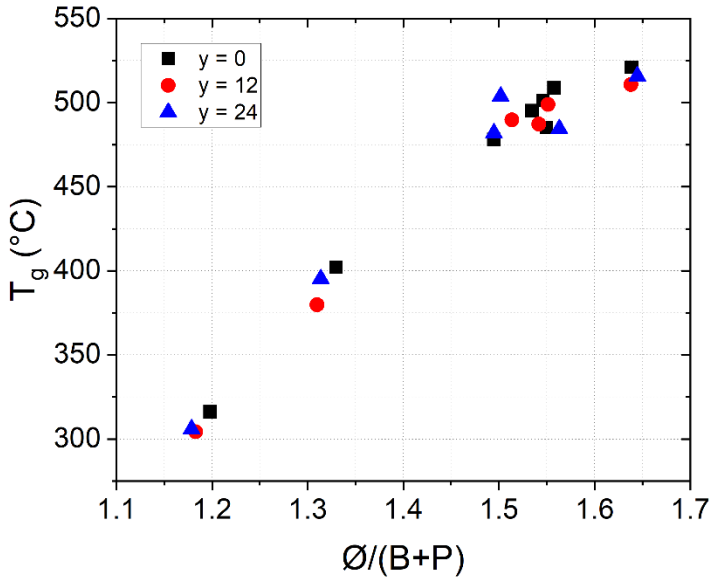

Figure 14. The dependence of glass transition temperature on the number of bridging oxygens per glass former (Ø/(B+P)) for glasses with the nominal molar composition $16Na_2O$-(24-y)CaO-ySrO-xB_2O_3-(60-x)P_2O_5.

The dependence of T_g on average number of network crosslinks shown in Figure 10 can be used to explain the compositional dependence of T_g (Figure 5) and to highlight the significance of the glasses with 23 mole% B_2O_3. The initial replacement of P_2O_5 by B_2O_3 creates highly cross-linked B_{4P}^{4} network sites that replace less-crosslinked P_{0B}^{3} and P_{0B}^{2} units that constitute the structure of the ultraphosphate (x=0) glasses. Indeed, the average Ø/(B+P) ratio increases from 1.22 to 1.55 when the B_2O_3 content increases from 0 to 23 mole%. Further replacement of P_2O_5 by B_2O_3 ($23 \leq x \leq 40$) creates lower dimensional trigonal borates and depolymerized phosphate sites, causing T_g to decrease. The phosphate-free compositions (x=60) have the highest glass transition temperatures and the greatest Ø/(B+P) ratios. This analysis indicates that the type of bridging oxygen

bond (PØP, BØP, BØB) has less influence on the glass transition temperature than the total number of bridging oxygens per network former.

The effects of composition on molar volume (Figure 4B) are more subtle, but the break in the trend near 23 mole% B_2O_3 can also be explained by the transition in the structural motif at this composition. The initial replacement of P_2O_5 by B_2O_3 results in the replacement of PØP bonds by BØP bonds, with the relative fraction of the latter reaching a maximum at 23 mole% B_2O_3 (Figure 11). Above this composition, BØB bonds become increasingly dominant in the glass structures. Qiu *et al.* studied the structures of Na-borophosphate glasses using high-energy X-ray diffraction and found that the distances between network formers across bridging oxygens decreased in the order PØP (2.88Å)>BØP (2.73Å)>BØB (2.63Å).[65] The trend towards shorter average bond distances is consistent with the overall decrease in V_m^O with increasing B_2O_3 content (Figure 4B), and the steeper slope in the V_m^O trend below 23 mole% is consistent with the greater difference between the PØP and BØP bond distances. At compositions above x > 23, BØP linkages are exchanging for BØB linkages, which are closer in bond length, leading to a less negative change in molar volume per oxygen.

5. SUMMARY

Borate and phosphate site speciation in the structures of three series of glasses with the nominal molar composition $16Na_2O$-(24-y)CaO-ySrO-xB_2O_3-(60-x)P_2O_5 (mol%), where $0 \leq x \leq 60$ and y=0, 12, and 24, were quantified by ^{11}B and ^{31}P MAS NMR and found to be in good agreement with the structural information obtained by HPLC and

Raman spectroscopy. The initial addition of B_2O_3 creates tetrahedral borophosphate units (B_{jP}^4) that reduce the average size of the P-anions that constitute the glass structures. Trigonal borates are present in glasses with greater B_2O_3 contents, and become more significant as the overall compositions and structures evolve from borophosphates to borates.

The evolution of these structures is in general agreement with the topological model proposed by Hermansen, et al., and indicate that a local maximum in network cross-link density is reached at 23 mole% B_2O_3, where a maximum in the fraction of BØP bonds is expected. Above this composition BØB bonds associated with tetrahedral and trigonal B-sites become dominant. Changes in the compositional dependences of the glass transition temperature and the molar volume occur at 23 mole% B_2O_3, and are consistent with the changes in the molecular-level structures of these glasses.

ACKNOWLEDGEMENTS

This work was supported by the Graduate Assistance in Areas of National Need (GAANN) fellowship from the US Department of Education. The authors would like to thank Alana Buznego for her assistance with glass preparation and Dr. Eric Bohannan for his assistance with the X-ray diffraction analyses.

REFERENCES

1. Lim JW, Schmitt ML, Brow RK, Yung SW. Properties and structures of tin borophosphate glasses. *Journal of Non-Crystalline Solids*. 2010;356(28–30):1379–1384. https://doi.org/10.1016/j.jnoncrysol.2010.02.019

2. Massera J, Ahmed I, Petit L, Aallos V, Hupa L. Phosphate-based glass fiber vs. bulk glass: Change in fiber optical response to probe in vitro glass reactivity. *Materials Science and Engineering: C*. 2014;37:251–257. https://doi.org/10.1016/j.msec.2014.01.021

3. Massera J, Shpotyuk Y, Sabatier F, *et al.* Processing and characterization of novel borophosphate glasses and fibers for medical applications. *Journal of Non-Crystalline Solids*. 2015;425:52–60. https://doi.org/10.1016/j.jnoncrysol.2015.05.028

4. Christensen R, Olson G, Martin SW. Structural Studies of Mixed Glass Former $0.35Na_2O+0.65[xB_2O_3+(1–x)P_2O_5]$ Glasses by Raman and ^{11}B and ^{31}P Magic Angle Spinning Nuclear Magnetic Resonance Spectroscopies. *The Journal of Physical Chemistry B*. 2013;117(7):2169–2179. https://doi.org/10.1021/jp308494a

5. Sharmin N, Parsons a. J, Rudd CD, Ahmed I. Effect of boron oxide addition on fibre drawing, mechanical properties and dissolution behaviour of phosphate-based glass fibres with fixed 40, 45 and 50 mol% P_2O_5. *Journal of Biomaterials Applications*. 2014;29(5):639–653. https://doi.org/10.1177/0885328214539824

6. Takebe H, Suzuki Y, Uemura T. Effect of B_2O_3 and Al_2O_3 additions on the structure of phosphate glasses. 2014;55(5):207–210. https://doi.org/10.1115/1.4024145

7. Hidi IJ, Melinte G, Stefan R, Bindea M, Baia L. The study of the structure and bioactivity of the $B_2O_3 \bullet Na_2O \bullet P_2O_5$ system. *Journal of Raman Spectroscopy*. 2013;44(8):1187–1194. https://doi.org/10.1002/jrs.4330

8. Sharmin N, Hasan MS, Parsons AJ, *et al.* Effect of boron addition on the thermal, degradation, and cytocompatibility properties of phosphate-based glasses. *BioMed Research International*. 2013;2013. https://doi.org/10.1155/2013/902427

9. Carta D, Qiu D, Guerry P, *et al.* The effect of composition on the structure of sodium borophosphate glasses. *Journal of Non-Crystalline Solids*. 2008;354(31):3671–3677. https://doi.org/10.1016/j.jnoncrysol.2008.04.009

10. Larink D, Eckert H, Reichert M, Martin SW. Mixed network former effect in ion-conducting alkali borophosphate glasses: Structure/property correlations in the system $[M_2O]_{1/3}[(B_2O_3)_x(P_2O_5)_{1-x}]_{2/3}$(M = Li, K, Cs). *Journal of Physical Chemistry C*. 2012;116(50):26162–26176. https://doi.org/10.1021/jp307085t

11. Rinke MT, Eckert H. The mixed network former effect in glasses: Solid state NMR and XPS structural studies of the glass system $(Na_2O)_x(BPO_4)_{1-x}$. *Physical Chemistry Chemical Physics*. 2011;13(14):6552–6565. https://doi.org/10.1039/c0cp01590c

12. Raskar D, Rinke MT, Eckert H. The Mixed-Network Former Effect in Phosphate Glasses: NMR and XPS Structural Studies of the Connectivity Distribution in the Glass System $(NaPO_3)_{1-x}(B_2O_3)_x$. *The Journal of Physical Chemistry C*. 2008;112:12530–12539. https://doi.org/10.1039/c0cp01590c

13. Zeyer-Düsterer M, Montagne L, Palavit G, Jäger C. Combined ^{17}O NMR and ^{11}B–^{31}P double resonance NMR studies of sodium borophosphate glasses. *Solid State Nuclear Magnetic Resonance*. 2005;27(1–2):50–64. https://doi.org/10.1016/J.SSNMR.2004.06.009

14. Hermansen C, Youngman RE, Wang J, Yue Y. Structural and topological aspects of borophosphate glasses and their relation to physical properties. *Journal of Chemical Physics*. 2015;142(18). https://doi.org/10.1063/1.4919798

15. Hermansen C, Mauro JC, Yue Y. A model for phosphate glass topology considering the modifying ion sub-network. *Journal of Chemical Physics*. 2014;140(15). https://doi.org/10.1063/1.4870764

16. Wright AC. Borate structures: crystalline and vitreous. *Physics and Chemistry of Glasses - European Journal of Glass Science and Technology Part B*. 2010;51(1):1–39.

17. Ahmed I, Lewis M, Olsen I, Knowles JC. Phosphate glasses for tissue engineering: Part 1. Processing and characterisation of a ternary-based P_2O_5-CaO-Na_2O glass system. *Biomaterials*. 2004;25(3):501–507. https://doi.org/10.1016/S0142-9612(03)00547-7

18. Ahmed I, Lewis M, Olsen I, Knowles JC. Phosphate glasses for tissue engineering: Part 2. Processing and characterisation of a ternary-based P_2O_5–CaO–Na_2O glass fibre system. *Biomaterials*. 2004;25(3):501–507. https://doi.org/10.1016/S0142-9612(03)00547-7

19. Islam MT, Felfel RM, Abou Neel EA, Grant DM, Ahmed I, Hossain KMZ. Bioactive calcium phosphate–based glasses and ceramics and their biomedical applications: A review. *Journal of Tissue Engineering*. 2017;8:1 –16. https://doi.org/10.1177/2041731417719170

20. Abo-Naf SM, Khalil ESM, El-Sayed ESM, Zayed HA, Youness RA. In vitro bioactivity evaluation, mechanical properties and microstructural characterization of Na_2O-CaO-B_2O_3-P_2O_5 glasses. *Spectrochimica Acta - Part A: Molecular and Biomolecular Spectroscopy*. 2015;144:88–98. https://doi.org/10.1016/j.saa.2015.02.076

21. Saranti A, Koutselas I, Karakassides MA. Bioactive glasses in the system CaO-B_2O_3-P_2O_5: Preparation, structural study and in vitro evaluation. *Journal of Non-Crystalline Solids*. 2006;352(5):390–398. https://doi.org/10.1016/j.jnoncrysol.2006.01.042

22. Wren A, Boyd D, Towler MR. The processing, mechanical properties and bioactivity of strontium based glass polyalkenoate cements. *Journal of Materials Science: Materials in Medicine*. 2008;19(4):1737–1743. https://doi.org/10.1007/s10856-007-3287-z

23. Gentleman E, Fredholm YC, Jell G, *et al.* The effects of strontium-substituted bioactive glasses on osteoblasts and osteoclasts in vitro. *Biomaterials*. 2010;31(14):3949–3956. https://doi.org/10.1016/j.biomaterials.2010.01.121

24. Wu C, Ramaswamy Y, Kwik D, Zreiqat H. The effect of strontium incorporation into $CaSiO_3$ ceramics on their physical and biological properties. *Biomaterials*. 2007;28(21):3171–3181. https://doi.org/10.1016/J.BIOMATERIALS.2007.04.002

25. Lao J, Jallot E, Nedelec JM. Strontium-delivering glasses with enhanced bioactivity: A new biomaterial for antiosteoporotic applications? *Chemistry of Materials*. 2008;20(15):4969–4973. https://doi.org/10.1021/cm800993s

26. Freudenberger PT, Saitoh A, Ikeda H, *et al.* Characterization of $20Na_2O \cdot 30((1-x)CaO \cdot xSrO) \cdot 50P_2O_5$ glasses for a resorbable optical fiber application. *International Journal of Applied Glass Science*. 2019;10(3). https://doi.org/10.1111/ijag.13106

27. Jin T, Bernard GM, Miskolzie M, Terskikh V v., Michaelis VK. A ^{11}B and ^{31}P MAS NMR study of the impact of Ca^{2+} and Sr^{2+} network modifying cations on the structure of borate and borophosphate glasses. *Physics and Chemistry of Glasses: European Journal of Glass Science and Technology Part B*. 2018;59(4):174–180. https://doi.org/10.13036/17533562.59.4.048

28. Jiang Q, Zeng H, Liu Z, *et al.* Glass transition temperature and topological constraints of sodium borophosphate glass-forming liquids. *J Chem Phys*. 2013;139:124502. https://doi.org/10.1063/1.4821617

29. Freudenberger PT, Blatt RL, Youngman RE, Brow RK. Dissolution Behavior of Borophosphate Glasses in Deionized Water and Simulated Body Fluid. *in preparation*. 2021.

30. Sales BC, Boatner LA, Ramey JO. Chromatographic studies of the structures of amorphous phosphates: a review. *Journal of Non-Crystalline Solids*. 2000;263–264:155–166. https://doi.org/10.1016/S0022-3093(99)00644-4

31. Massiot D, Fayon F, Capron M, *et al.* Modelling one and two-dimensional solid-state NMR spectra. *Magnetic Resonance in Chemistry*. 2002;40:70–76.

32. Massiot D, Bessada C, Coutures J, Taulelle F. A quantitative study of ^{27}Al MAS NMR in crystalline YAG. *Journal of Magnetic Resonance (1969)*. 1990;90(2):231–242.

33. Hudgens JJ, Martin SW. Glass Transition and Infrared Spectra of Low-Alkali, Anhydrous Lithium Phosphate Glasses. *Journal of the American Ceramic Society*. 1993;76(7):1691–1696. https://doi.org/10.1111/j.1151-2916.1993.tb06636.x

34. Ducel JF, Videau JJ. Structural study of borophosphate glasses by Raman and infrared spectroscopy. *Physics and Chemistry of Glasses*. 1993;34(5):212–218.

35. Kamitsos EI, Chryssikos GD. Borate glass structure by Raman and infrared spectroscopies. *Journal of Molecular Structure*. 1991;247:1–16. https://doi.org/https://doi.org/10.1016/0022-2860(91)87058-P

36. Konijnendijk WL, Stevels JM. The Structure of Borate Glasses Studied by Raman Scattering. *Journal of Non-Crystalline Solids*. 1975;18:307–331.

37. Maniua D, Iliescu T, Ardelean I, Cinta-Pinzaru S, Tarcea N, Kiefer W. Raman study on B_2O_3-CaO glasses. *Journal of Molecular Structure*. Vols. 651–653. Elsevier; 2003:485–488. https://doi.org/10.1016/S0022-2860(03)00129-7

38. Scagliotti M, Villa M, Chiodelli G. Short range order in the network of the borophosphate glasses: Raman results. *Journal of Non-Crystalline Solids*. 1987;93(2–3):350–360. https://doi.org/10.1016/S0022-3093(87)80180-1

39. Hudgens JJ, Brow RK, Tallant DR, Martin SW. Raman spectroscopy study of the structure of lithium and sodium ultraphosphate glasses. *Journal of Non-Crystalline Solids*. 1998;223(1–2):21–31. https://doi.org/10.1016/S0022-3093(97)00347-5

40. Brow RK. Review: the structure of simple phosphate glasses. *Journal of Non-Crystalline Solids*. 2000;263–264:1–28. https://doi.org/10.1016/S0022-3093(99)00620-1

41. Sales BC, Ramsey RS, Bates JB, Boatner LA. Investigation of the Structural Properties of Lead-Iron Phosphate Glasses Using Liquid Chromatography and Raman Scattering Spectroscopy. *Journal of Non-Crystalline Solids*. 1986;87:137–158.

42. Strauss UP, Treitler TL. Degradation of Polyphosphates in Solution. I. Kinetics and Mechanism of the Hydrolysis at Branching Points in Polyphosphate Chains. *J Am Chem Soc*. 1956;78(15):3553–3557. https://doi.org/10.1039/j3970000x001

43. Muñoz-Senovilla L, Tricot G, Muñoz F. Kinetic fragility and structure of lithium borophosphate glasses analysed by 1D/2D NMR. *Physical Chemistry Chemical Physics*. 2017;19(34):22777–22784. https://doi.org/10.1039/c7cp04171c

44. Brow RK, Click CA, Alam TM. Modifier coordination and phosphate glass networks. *Journal of Non-Crystalline Solids*. 2000;274:9–16.

45. Villa M, Scagliotti M, Chiodelli G. Short range order in the network of the borophosphate glasses: A ^{31}P NMR-MAS (Magic Angle Spinning) study. *Journal of Non-Crystalline Solids*. 1987;94(1):101–121. https://doi.org/10.1016/S0022-3093(87)80264-8

46. Miquel JL, Facchini L, Legrand AP, Rey C, Lemaitre J. Solid state NMR to study calcium phosphate ceramics. *Colloids and Surfaces*. 1990;45(C):427–433. https://doi.org/10.1016/0166-6622(90)80041-2

47. Hayakawa S, Tsuru K, Iida H, Ohtsuki C, Osaka A. ^{31}P MAS-NMR studies of phosphate salts formation on calcium-containing oxide glasses in a simulated body fluid. *Journal of the Ceramic Society of Japan*. 1996;104(11):1000–1003. https://doi.org/10.2109/jcersj.104.1000

48. Jakeman RJB, Cheetham AK, Clayden NJ, Dobson CM. A magic angle spinning NMR study of the phase diagram Ca3-xZnx(PO4)2. *Journal of Solid State Chemistry*. 1989;78(1):23–34. https://doi.org/10.1016/0022-4596(89)90124-2

49. Grimmer AR, Müller D, Gözel G, Kniep R. Multinuclear (^{11}B, ^{31}P) MAS NMR spectroscopy of borophosphates. *Fresenius' Journal of Analytical Chemistry*. 1997;357(5):485–488. https://doi.org/10.1007/s002160050197

50. Smedskjaer MM. Structural and Topological Basis of Glass Properties and Diffusion. Aalborg University; 2011

51. Smedskjaer MM, Mauro JC, Youngman RE, Hogue CL, Potuzak M, Yue Y. Topological Principles of Borosilicate Glass Chemistry. *J Phys Chem B*. 2011;115:12930–12946. https://doi.org/10.1021/jp208796b

52. Wilkinson CJ, Zheng Q, Huang L, Mauro JC. Topological constraint model for the elasticity of glass-forming systems. *Journal of Non-Crystalline Solids: X*. 2019;2:100019. https://doi.org/10.1016/J.NOCX.2019.100019

53. Hermansen C, Guo X, Youngman RE, Mauro JC, Smedskjaer MM, Yue Y. Structure-topology-property correlations of sodium phosphosilicate glasses. *Journal of Chemical Physics*. 2015;143(6). https://doi.org/10.1063/1.4928330

54. Elbers S, Strojek W, Koudelka L, Eckert H. Site connectivities in silver borophosphate glasses: New results from $^{11}B\{^{31}P\}$ and $^{31}P\{^{11}B$ rotational echo double resonance NMR spectroscopy. *Solid State Nuclear Magnetic Resonance*. 2005;27(1–2):65–76. https://doi.org/10.1016/j.ssnmr.2004.08.007

55. Tischendorf B, Otaigbe JU, Wiench JW, Pruski M, Sales BC. A study of short and intermediate range order in zinc phosphate glasses. *Journal of Non-Crystalline Solids*. 2001;282(2–3):147–158. https://doi.org/10.1016/S0022-3093(01)00350-7

56. Döhler F, Mandlule A, van Wüllen L, Friedrich M, Brauer DS. 31P NMR characterisation of phosphate fragments during dissolution of calcium sodium phosphate glasses. *Journal of Materials Chemistry B*. 2015;3(6):1125–1134. https://doi.org/10.1039/c4tb01757a

57. Ma L, Brow RK. Structural study of Na_2O–FeO–Fe_2O_3–P_2O_5 glasses by high-pressure liquid chromatography. *Journal of Non-Crystalline Solids*. 2014;387:16–20. https://doi.org/10.1016/j.jnoncrysol.2013.12.011

58. Ma L, Brow K, Schlesinger ME. Dissolution behaviour of sodium calcium polyphosphate glasses. 2018;59(5):205–212. https://doi.org/10.13036/17533562.59.5.018

59. Sales BC, Otaigbe JU, Beall GH, Boatner LA, Ramey JO. Structure of zinc polyphosphate glasses. *Journal of Non-Crystalline Solids*. 1998;226(3):287–293. https://doi.org/10.1016/S0022-3093(98)00415-3

60. Wang B, Kwak BS, Sales BC, Bates JB. Ionic conductivities and structure of lithium phosphorus oxynitride glasses. *Journal of Non-Crystalline Solids*. 1995;183(3):297–306. https://doi.org/10.1016/0022-3093(94)00665-2

61. Zapol P, He H, Kwon KD, Criscenti LJ. First-principles study of hydrolysis reaction barriers in a sodium borosilicate glass. *International Journal of Applied Glass Science*. 2013;4(4):395–407. https://doi.org/10.1111/ijag.12052

62. Geneste G, Bouyer F, Gin S. Hydrogen-sodium interdiffusion in borosilicate glasses investigated from first principles. *Journal of Non-Crystalline Solids*. 2006;352(28–29):3147–3152. https://doi.org/10.1016/j.jnoncrysol.2006.04.023

63. Goetschius KL, Beuerlein MA, Bischo CM, Brow RK. Dissolution behavior of ternary alkali-alkaline earth-borate glasses in water. *Journal of Non-Crystalline Solids*. 2018;487:12–18. https://doi.org/10.1016/j.jnoncrysol.2018.02.011

64. Van Wazer JR. Phosphorus and its Compounds. New York, NY: Interscience; 1958

65. Qiu D, Guerry P, Ahmed I, *et al.* A high-energy X-ray diffraction, ^{31}P and ^{11}B solid-state NMR study of the structure of aged sodium borophosphate glasses. *Materials Chemistry and Physics*. 2008;111(2–3):455–462. https://doi.org/10.1016/j.matchemphys.2008.04.045

IV. DISSOLUTION RATES OF BOROPHOSPHATE GLASSES IN DEIONIZED WATER AND IN SIMULATED BODY FLUID

Parker T. Freudenberger, Rebekah L. Blatt, and Richard K. Brow

[1]Department of Materials Science and Engineering, Missouri University of Science and Technology, Rolla, Missouri

ABSTRACT

Particles of borophosphate glasses with the nominal molar compositions $16Na_2O$-(24-y)CaO-ySrO-xB_2O_3-(60-x)P_2O_5 (mol%), where $0 \leq x \leq 60$ and y=0, 12, and 24 were reacted in deionized water and in simulated body fluid (SBF) at 37°C. For the dissolution experiments in water, the pH of the solution at the conclusion of the experiments increased systematically, from 2.1 to 9.5, for y=0 glasses when 'x' increased from 0 to 60. The reaction rates over the first 8-24 hours of dissolution in both SBF and deionized water followed linear kinetics, with reaction rates dependent on glass composition. For glass particles in SBF, replacing P_2O_5 with up to 20 mole% B_2O_3 decreased the dissolution rate (fraction dissolved) by two orders of magnitude, from 7.0×10^{-3} hr^{-1} for x=0 to 2.0×10^{-5} hr^{-1} for x=20. Further replacement of P_2O_5 by B_2O_3 increased dissolution rates by three orders of magnitude, to 2.3×10^{-2} hr^{-1} at x = 60. The compositional dependence of the dissolution rates is explained by changes in the glass structure, with the most durable glasses possessing the greatest fraction of tetrahedral borophosphate sites in the glass network. Crystalline brushite was detected on Ca-glasses with 35 and 40 mole% B_2O_3, but the dominant material on both the Ca- and Sr-glasses is an amorphous combination of orthophosphate and pyrophosphate species.

1. INTRODUCTION

Phosphate-based glasses have been developed for the delivery of antibacterial ions [1] and phosphate glass fibers have been used to promote muscle and nerve regeneration [2,3]. The dissolution of phosphate glasses in aqueous environments occurs by the penetration of water into the glass surface and then the hydration of the bonds between modifying cations and the nonbridging oxygens on the phosphate anions that constitute the phosphate glass structure [4]. Na-Ca-phosphate glasses form more acidic solutions when they dissolve, particularly glasses with greater phosphate contents [4-6].

Modifying cations with greater field strengths generally have slower hydration rates and so decrease the overall phosphate glass dissolution rates [4,7,8] but contribute to the hydrolysis of phosphate anions in solution by polarizing P-O bonds [9,10]. In addition, the hydration rates of the cation bonds to smaller, more negatively charged phosphate anions are generally slower [4,11,12]. SrO-containing glasses are of interest because they can promote bone formation and prevent osteoporosis [13,14]. Additionally, it has been shown that the systematic replacement of CaO by SrO decreased the dissolution rate by by nearly an order of magnitude in metaphosphate glasses [15].

Replacing silica with B_2O_3 generally increases the dissolution rate of bioactive silicate glasses, [16,17] and so borate-based glasses have been developed for potential soft-tissue medical applications [18-19,20]. Borate-based glasses generally dissolve congruently in aqueous solutions and the dissolution rates depend on the concomitant hydrolysis of the borate network and the hydration of modifying cations that charge balance the borate network anions [21]. Increasing the fraction of tetrahedral network borate sites decreases the glass dissolution rates [21-23]. When dissolved in aqueous

solutions, Na-Ca-borate glasses increase pH, with greater values of pH resulting from the dissolution of glasses with greater Na- and Ca-contents [21,22].

Calcium-containing borate glasses react in phosphate solutions to precipitate calcium phosphate phases, including hydroxyapatite (HA), on the glass surface [24,25]. Changes in the local pH affect the type of calcium phosphate (CP) materials that initially form on the surface of bioactive glasses and ceramics [26], including brushite (pH=2.0-6.0), amorphous calcium phosphate (pH=5.0-12.0), and hydroxyapatite (pH=9.5-12). The form and stoichiometry of the CP phases affect how those materials react in the physiological environment. For example, hollow hydroxyapatite (HA) microspheres have been shown to encourage bone regeneration, and their properties can be tailored by reacting the borate glass spheres in phosphate solutions with different values of pH [27,39].

The addition of borate to a phosphate glass composition can stabilize the glass against crystallization and will decrease dissolution rates in aqueous solutions [28-30]. There have been many systematic studies of the substitution of borate for phosphate on the properties of borophosphate glasses [31-37], but few have considered how the composition of borophosphate glasses affect their dissolution rates in aqueous solutions or how those reactions alter local pH. The latter point is important because pH control is important for specific biomedical applications [38-40]. For example, endothelial cell viability increases in the presence of pH neutral borophosphate glasses, relative to more alkaline borate-based glasses [38], but antibacterial activity is generally increased in the presence of more alkaline glasses [19,39].

The goal of this paper is to relate the dissolution properties of a series of Na-Ca-Sr-borophosphate glasses, including ion release rates, changes in solution pH, and the nature of any precipitating phases, to the glass composition and network structure. In an earlier paper, we describe a quantitative composition-structure model that shows that physical properties depend on the number of network crosslinks between phosphate and borate polyhedral [40], and that model will be used in the present paper to explain the dependence of glass dissolution rates and resulting solution pH in water and in simulated body fluids on glass composition.

2. EXPERIMENTAL PROCEDURE

X-ray amorphous, visually homogeneous glasses with the nominal molar compositions $16Na_2O$-(24-y)CaO-ySrO-xB_2O_3-(60-x)P_2O_5 could be prepared for each alkaline earth series (y = 0, 12 and 24) in increments of $10B_2O_3$ except at x=50, where melts from each series crystallized upon quenching. In the y = 0 series, two additional compositions at x = 23.3 and 35 were prepared. Details about glass formation and characterization are described elsewhere [41]. The analyzed components are within ±2.0 mol % (absolute) of the as-batched compositions and those analyzed compositions will be used to describe the property trends in this paper.

Two series of dissolution experiments were performed. In the first test, 150 mg of glass powder (75-150 μm particle size) from the SrO-free (y=0) glasses were sealed in porous (45 μm openings) nylon mesh bags which were then immersed into HDPE centrifuge tubes filled with 50 mL of 37°C deionized water, and these samples were then

reacted in a heated shaker bath for up to 192 hours. In the second test, 300mg of glass powder (250-500 μm particle size, y= 0, 12, and 24) were added to similar mesh bags and then immersed in HDPE centrifuge tubes that were filled with 50 mL of 37°C simulated body fluid (SBF), prepared according to Kokubo *et al.* [41], then reacted in the shaker bath for up to 168 hours. The solution pH and sample weight losses were recorded at each time point, the latter after drying the samples in air for at least 8 hours at 90°C. After each time point, the glass particles and the respective solutions were retained for analyses. Every experiment was done in triplicate.

Ion concentrations in the dissolution solutions were analyzed using Inductively Coupled Plasma – Optical Emission Spectroscopy (ICP-OES), using a Perkin-Elmer Avio 200. Solutions were diluted using 1% HNO_3 to prepare samples with ion concentrations in the 1-50 ppm range. Due to the high concentrations of calcium, sodium, and phosphate in SBF, only boron concentrations were measured in the solutions from those experiments.

Glass particles, before and after the dissolution experiments in SBF, were analyzed by x-ray diffraction using a PANalytical X'Pert Multipurpose diffractometer with a Cu Kα source and a PIXcel detector. Raman spectra were collected from reacted particles after rinsing with ethanol and drying using a Horiba Jobin Yvon LabRAM ARAMIS micro-Raman spectrometer with a HeNe (632.8 nm) 17 mW or a diode (785 nm) 100 mW laser and a 1200 grating at 10x magnification. At least twenty 10 s scans were collected on each sample, and the respective average spectra are reported.

3. RESULTS

3.1. GLASS DISSOLUTION IN DEIONIZED WATER

The time-dependence of the solution pH values for the glass powders (y=0) reacted in 37°C deionized water are shown in Figure 1. There was an immediate increase in the pH, to a value of 9.5, for the solution containing the phosphate-free (x=60) glass and a slower decrease in the pH, to a value of 2.2, for the solution containing the borate-free (x=0) glass. For the other glasses, the solution pH after 192 hours on test increased systematically as borate replaced phosphate in the glass composition.

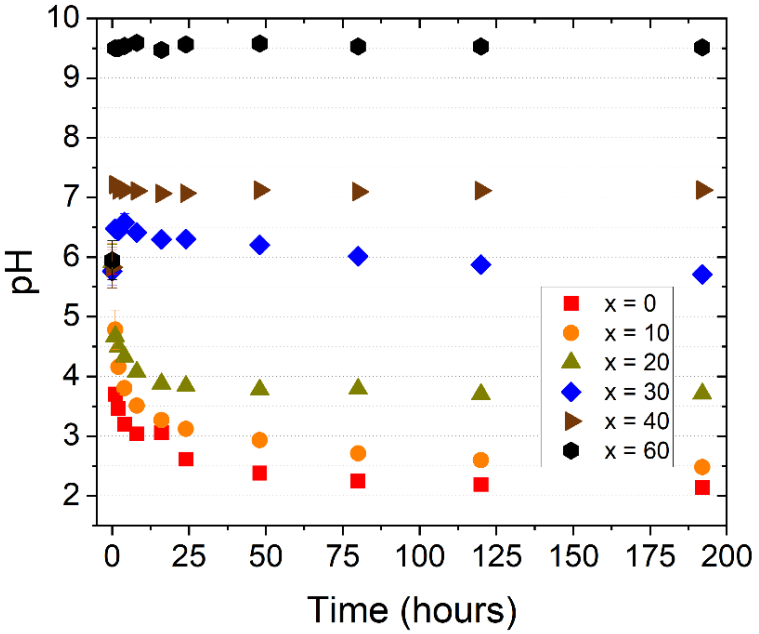

Figure 1. Solution pH over time for the 150 mg samples (75-150 µm particles) in deionized water for the $16Na_2O$-$24CaO$-xB_2O_3-$(60-x)P_2O_5$ compositional series (y = 0). All experiments were carried out in a shaker bath set to 37°C. Error bars may be smaller than the symbol.

The normalized ion release (NIR) rates for the glass powders (y = 0) dissolved in deionized water are shown in Figure 2 and were determined using the equation:

$$NIR = \frac{c_i \times V}{f_i \times m} \qquad [1]$$

Where c_i is the measured (ICP-OES) concentration (ppm) of element i in solution, V is the sample volume (L), f_i is the mass fraction of element i in the original glass, m is the original mass of the powdered sample (mg). This normalizes the concentrations of the ions in solution to the respective concentrations of those ions in the glass.

Similar NIR values for each ion, for example, for the x=0, 10, 20, and 60 glasses, indicate congruent dissolution. For the x=30 and 40 glasses, B and Na are released at similar rates whereas the normalized Ca and P contents of the solution were significantly lower. The x=60 glass was completely dissolved and the x=0 glass was nearly completely dissolved (94% wt. loss) after 192 hours on test, and the Na and B contents of the x=40 glass were completely released after about 48 hours.

X-ray diffraction analyses (not shown) showed that the reacted x=40 particles had converted to crystalline brushite ($CaHPO_4 \cdot 2H_2O$, ICCD # 01-071-0656), whereas the reacted x=10, 20 and 30 particles were x-ray amorphous. The x=0 and x=60 particles were completely dissolved after 192 hours on test.

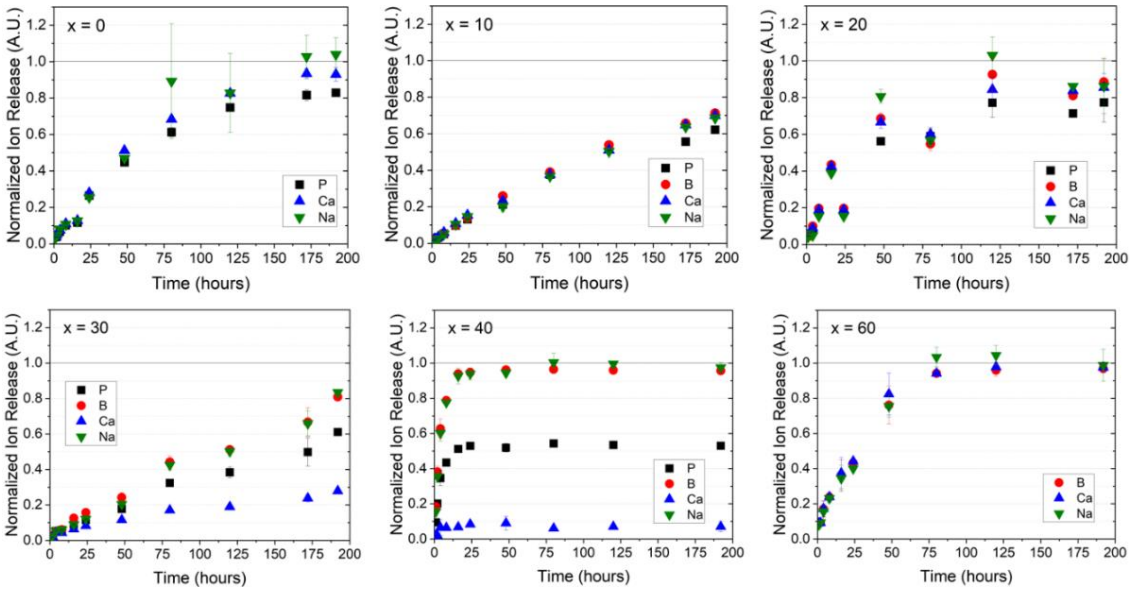

Figure 2. Normalized ion release (NIR) of the $16Na_2O$-$24CaO$-xB_2O_3-$(60-x)P_2O_5$ compositional series when 150mg of 75-150μm particles are reacted in deionized water at 37°C in a shaker bath. The horizontal lines indicate full dissolution (NIR = 1.0).

3.2. GLASS DISSOLUTION IN SIMULATED BODY FLUID

Figure 3 shows weight loss data, presented as the fraction of the initial weight lost (α), for all three series (y = 0, 12, 24) of glass particles reacted in 37°C SBF. Over the course of the experiments, the phosphate-free compositions were fully dissolved (α=1.0) by 60 hours. The fraction of weight lost from the three versions of x=40 plateaued around α=0.50-0.60. The remaining borate-free (x=0) and borophosphate glasses (x = 10, 20, 23, and 30) all dissolved more slowly.

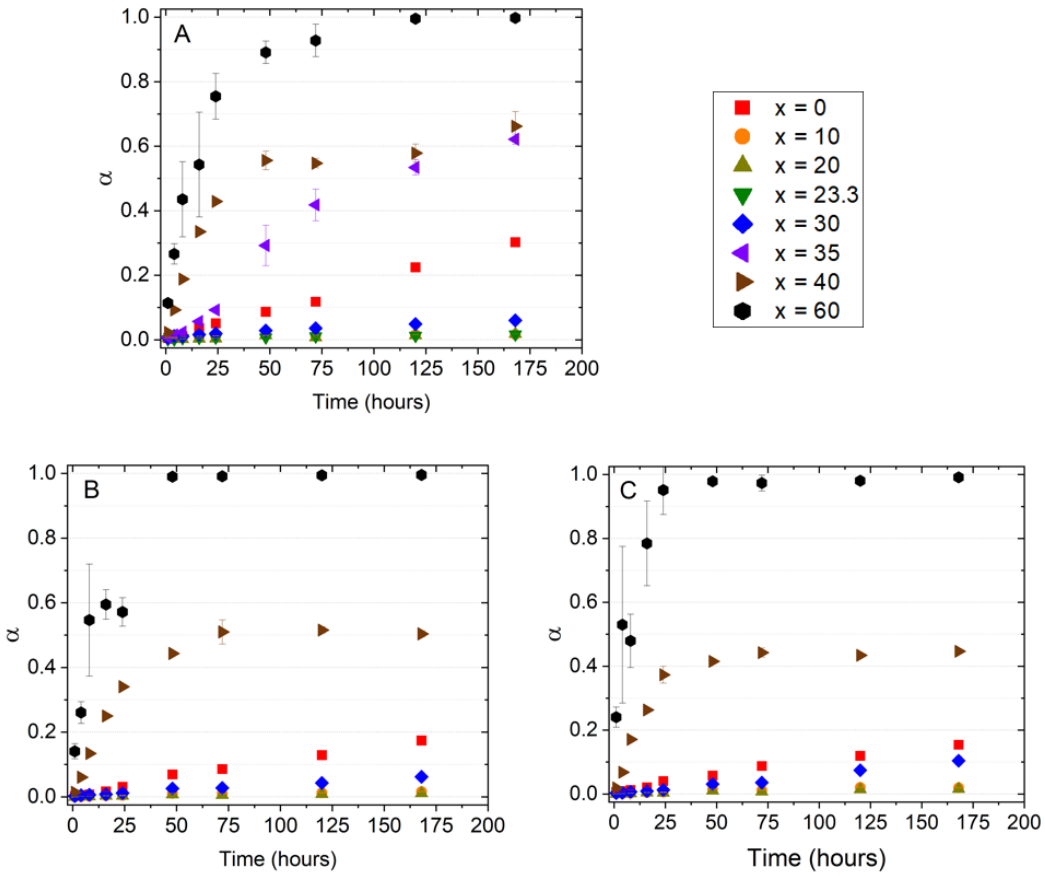

Figure 3. The fraction weight loss (α), over time for the 300mg samples (250-500µm) reacted in SBF of the $16Na_2O$-(24-y)CaO-ySrO-xB_2O_3-(60-x)P_2O_5 compositional series, where y = 0 (A), 12 (B) and 24 (C). All experiments were carried out in a shaker bath set to 37°C.

Figure 4 shows the normalized boron release rates from the glass particles in SBF (Equation 1). As was found for the experiments done in water, boron was fully released from the x = 40 and 60 glasses after about 48 hours, whereas B-release from the x = 10, 20, 23, and 30 glasses was much slower.

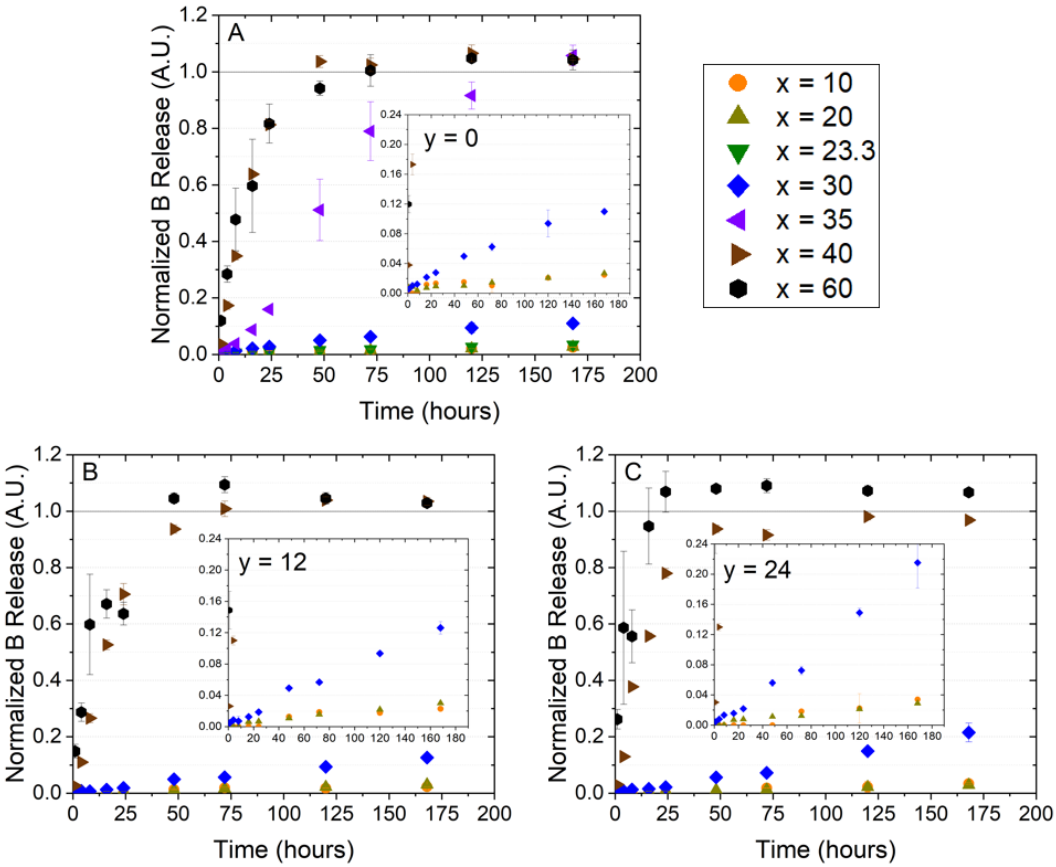

Figure 4. Normalized boron release (NBR) for the 300mg samples (250-500µm particle size) with an insert to provide a view of the x = 10, 20, 23, and 30 compositions of the $16Na_2O$-(24-y)CaO-ySrO-xB_2O_3-(60-x)P_2O_5 compositional series, where y = 0 (A), 12 (B), and 24 (C), in SBF at 37°C in a shaker bath. The horizontal lines indicate full dissolution (NBR = 1.0).

Figure 5 shows how the pH values of the SBF changed with time over the course of the dissolution experiments. There was a significant increase in pH, from about 7.4 to 8.7, with the dissolution of the three series of phosphate-free (x=60) glasses. The pH of the SBF solutions in which the three series of x=40 glasses were reacted dropped to values near 7.0 and the pH of the solution from the x=35/y=0 experiment dropped to 6.5. The pH values of the solutions from the other experiments generally varied between 7.4

and 7.7, although the borate-free (x=0) particles did reduce the solution pH values at longer times.

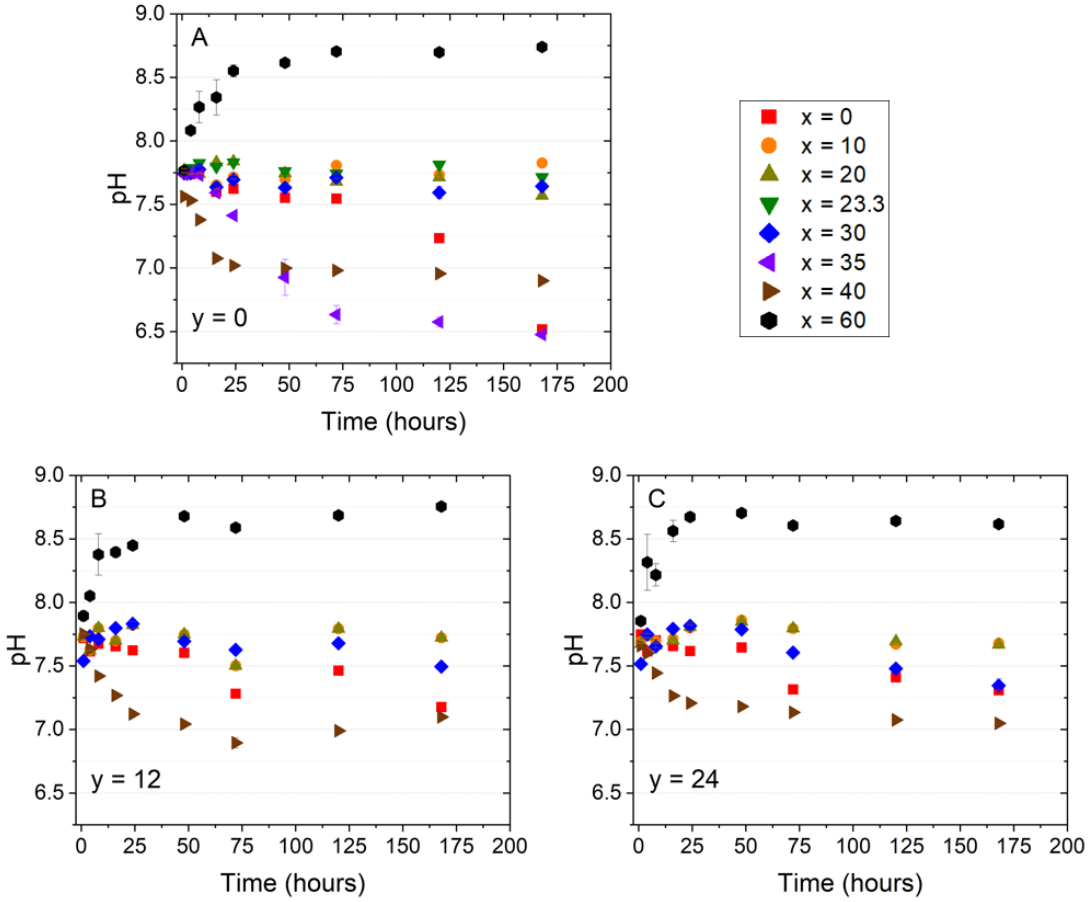

Figure 5. The solution pH over time for the 300mg samples (250-500µm) reacted in SBF of the $16Na_2O$-(24-y)CaO-ySrO-xB_2O_3-(60-x)P_2O_5 compositional series, where y = 0 (A), 12 (B) and 24 (C). All experiments were carried out in a shaker bath set to 37°C.

XRD analyses of particles recovered after 168 hours in SBF showed the presence of crystalline brushite for the x = 35 and 40/y=0 samples (Figure 6), but all other recovered particles, including the x=40/y=12 and x=40/y=24 samples, were x-ray amorphous.

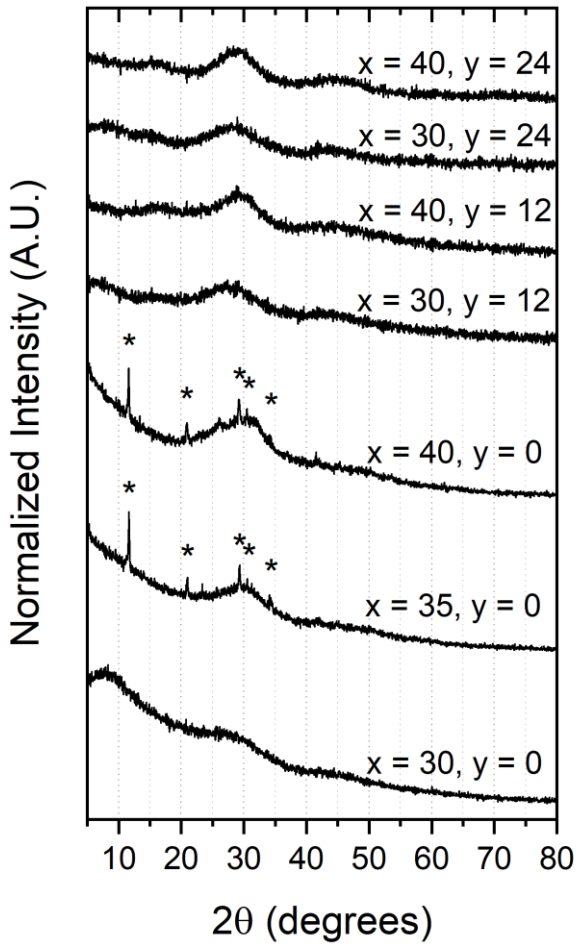

Figure 6. XRD analyses of glass particles after immersion in SBF at 37°C for 168 hr. Primary peaks for brushite, $Ca(HPO_4)\cdot 2H_2O$ (ICCD # 00-001-0395) are noted by asterisks.

Figure 7 shows the Raman spectra collected from several different glasses, before (left) and after (right) 168 hours in SBF. The broad peaks shown in the as-prepared glasses have been assigned to the vibrational modes of the phosphate and borate moieties that constitute the network structures of the glasses and are described in detail in reference [40]. The sharp peaks between about 900 and 1200 cm^{-1} in the spectra from the

reacted particles can be assigned to the vibrational modes of different phosphate species that constitute the calcium phosphate layer that formed on the surfaces of those particles. The Raman spectra from glasses that fully reacted in 168 hrs (x=35/y=0 and x=40/y=0, x=40/y=12, and x=40/y=24) have only sharp peaks associated with the reaction layer, whereas the spectra from the partially reacted glasses (x=30/y=0) have sharp peaks from the reaction product overlaid on the broader peaks from the unreacted glass.

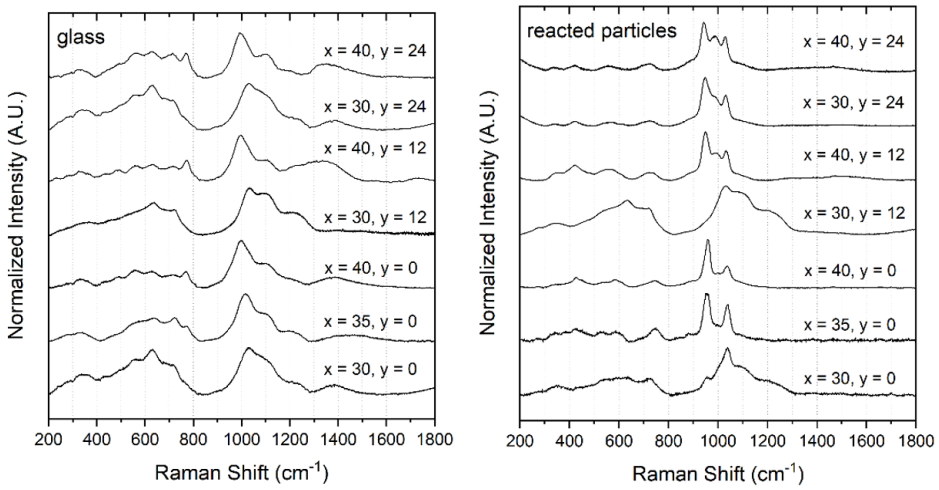

Figure 7. Raman spectra collected $16Na_2O$-(24-y)CaO-ySrO-xB_2O_3-(60-x)P_2O_5 glasses before (left, from [40]) and after (right) immersion in SBF at 37°C for 168 hrs.

4. DISCUSSION

4.1. DISSOLUTION RATES AND GLASS STRUCTURE

The dissolution rate kinetics of the weight loss data in Figure 3 were analyzed using the contracting volume model (CVM) [42], which defines the linear dissolution kinetics for spherical particles as:

$$k_{CVM}t = 1 - (1 - \alpha)^{\frac{1}{3}} \quad [1]$$

where α is the mass fraction of a particle that has reacted in time t, and k_{CVM} is the temperature-dependent reaction rate parameter. One assumption of the contracting volume model is that the dissolution kinetics are linear, generally controlled by a reaction between the solvent and reactant. Linear dissolution kinetics have been observed for borate glasses in water [22], but the initial dissolution kinetics of phosphate glasses in water have been reported to be parabolic, controlled by the initial diffusion of water into the glass surface [4]. Linear weight loss rates were noted for a Ca-borophosphate glass in solutions with pH values ranging from 2 to 14 [43].

Figure 8 shows the weight-loss data from the SrO-free (y=0) glasses with their respective fits to Equation 1. Similar fits were done to the first 24 hours of weight-loss data from the y=12 and y=24 series and these are shown in the Appendix. These analyses were limited to the first 24 hours of reaction to reduce the complications created by the precipitation of calcium phosphate phases on the x=40 samples.

Figure 9 shows the reaction rate constants for the three series of glasses calculated from their respective weight loss measurements. For all three series, the initial replacement of P_2O_5 by B_2O_3 reduced the dissolution rate by an order of magnitude, with the slowest dissolving glasses having a nominal P_2O_5:B_2O_3 ratio of 40:20. Further replacement of P_2O_5 by B_2O_3 increased the dissolution rates by over two orders of magnitude, with the x=60 composition the fastest dissolving glass in each series. In general, the mixed alkaline earth series (y=12) had the slowest dissolution rates and the

SrO-free series (y=0) had the fastest dissolution rates across the compositional series. The sensitivity of dissolution rates to the choice of alkaline earth oxide may indicate that the cations preferentially neutralize the phosphate anions in the glass, as substituting strontium for calcium has been shown to decrease dissolution rates in phosphate glasses [43] and increase dissolution rates in borate glasses [10]. This preference has been observed in other studies of alkali borophosphate glasses [32].

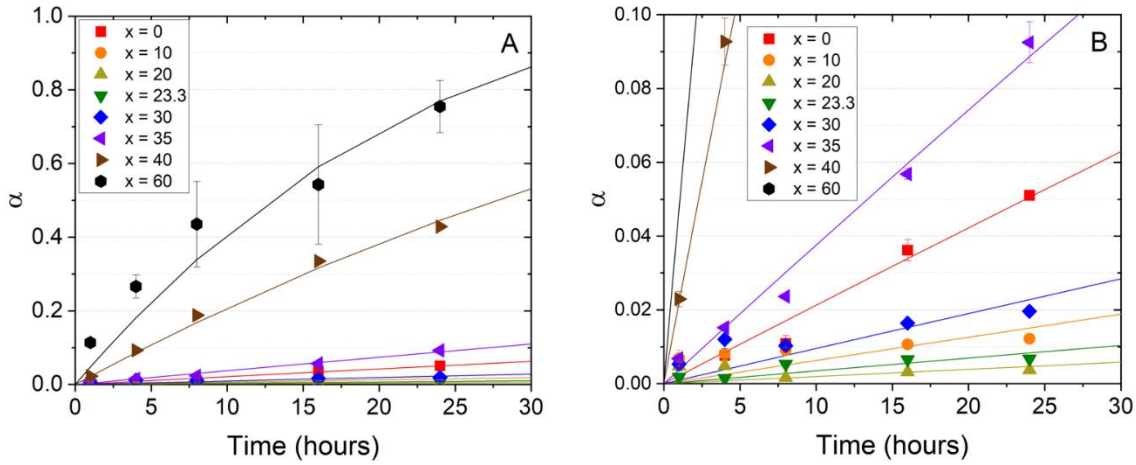

Figure 8. Fraction weight loss (α) data for glass particles in 37°C SBF. The solid lines are fits of the first 24 hours of data to the contracting volume model (Equation 1). The data on the right has an expanded y-axis to better show the results from the slower dissolving glasses.

To understand the different reactions that might control the overall glass dissolution rates, the compositional-dependence of the glass structures must be considered. The structures of these glasses are described in detail elsewhere [40] and can be summarized by considering the phosphate and borate sites that constitute the network structures. Freudenberger et al. used the term P_{jB}^{i} to describe phosphate tetrahedra

bonded to "i" total P- and B-polyhedra and to "j" B-polyhedra, and B_{jP}^{i} to describe B-polyhedra bonded to "i" total P- and B-polyhedra and to "j" P-tetrahedra. The compound BPO_4, isostructural to silica, thus has a structure based on P_{4B}^{4} and B_{4P}^{4} tetrahedra. For the present series of glasses, the borate-free (x=0) ultraphosphate glasses have structures based on P_{0B}^{3} and P_{0B}^{2} tetrahedra, with the latter anionic sites charge-balanced by the alkali and alkaline earth cations. The phosphate-free (x=60) glasses have structures based principally on B_{0p}^{3} triangles and B_{0P}^{4} tetrahedra, with a small number of anionic B_{0p}^{2} triangles. Those triangles and the anion tetrahedral sites are charge-balanced by the alkali and alkaline earth cations.

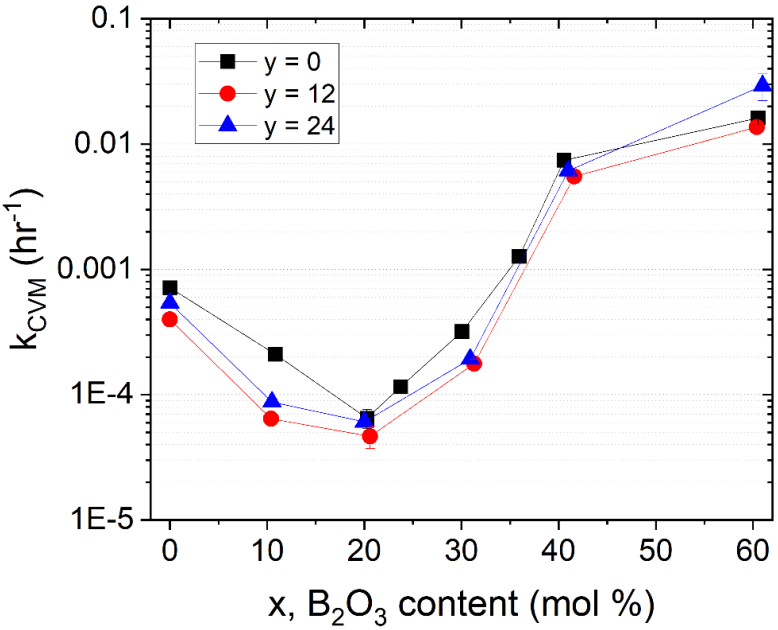

Figure 9. Reaction rate constants (k_{CVM}) for the dissolution of particles from the three series of $16Na_2O$-(24-y)CaO-ySrO-xB_2O_3-(60-x)P_2O_5 (mol%) glasses in 37°C SBF.

With increasing B_2O_3 content in the glass series, the dominant network units change as indicated here [40]:

$$P_{0B}^{3},(P_{0B}^{2}) \rightarrow (P_{2B}^{3}),(P_{xB}^{2}), B_{4P}^{4} \rightarrow (P_{2B}^{3}),(P_{xB}^{2}), \left(B_{(4-x)P}^{4}\right), B_{0P}^{3} \rightarrow (B_{0P}^{4}), B_{0P}^{3}, (B_{0P}^{2})$$

The value of 'x' in the subscript increases with increasing B_2O_3 content, although it may be different for each unit. Units in parantheses are anionic and will be charge balanced by the alkali and alkaline earth ions.

Figure 10 summarizes some of the quantitative nuclear magnetic resonance (NMR) results from Freudenberger, et al. to show how the relative fractions of the bridging oxygens (Ø) that link the various network units change with composition. The initial replacement of P_2O_5 by B_2O_3 creates tetrahedral B_{4P}^{4} sites in the phosphate glass network, replacing bridging P-Ø-P bonds with bridging P-Ø-B bonds. Because these B_{4P}^{4} sites are charge-neutral, the metal cations (Na^{+}, Ca^{2+}, Sr^{2+}) must charge balance the nonbridging oxygens on anionic P_{xB}^{3}- and P_{xB}^{2}-tetrahedra. The fraction of B_{4P}^{4} units reaches a maximum near x=20 and further additions of B_2O_3 create trigonal B_{0P}^{3} sites, including those that link to tetrahedral $B_{(4-x)P}^{4}$ sites, producing increasing fractions of B-Ø-B bonds. Anionic B_{0P}^{4} sites also form in the borate-rich glasses and these are charge-balanced by the metal cations as the relative fraction of anionic phosphate sites decreases.

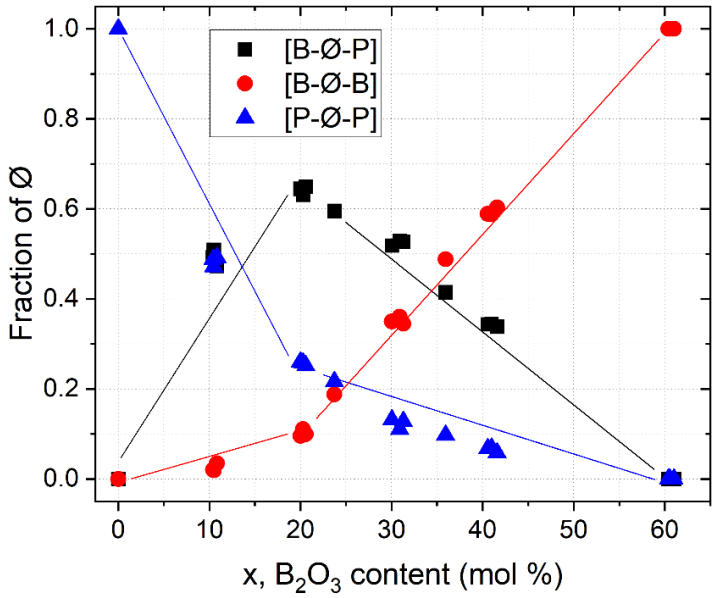

Figure 10. Bridging oxygen (Ø) speciation for the three series of $16Na_2O$-(24-y)CaO-ySrO-xB_2O_3-(60-x)P_2O_5 glasses calculated from borate and phosphate speciation reported in reference [40].

We can now consider different reactions between water and the different constituents of the glass structure. Consider first the hydration of bonds between the alkali or alkaline earth ions and the phosphate and borate anions that they charge-balance. For example, alkali and alkaline earth cations link neighboring phosphate anions through bonds with the nonbridging oxygens on those cations. Ma et al. [6] summarized the general hydration reactions of two phosphate anions with n and n' polyhedra charge-balanced by (n+2) and (n'+2) metal cations (M^+), respectively, as

$$(P_nO_{3n+1})(M)_{(n+n'+4)}(P_{n'}O_{3n'+1}) + \frac{(n+n'+4)}{2}H_2O \rightarrow$$

$$H_{2+n}(P_nO_{3n+1}) + H_{2+n'}(P_nO_{3n'+1}) + (n+n'+4)MOH \qquad [2]$$

where the resulting polyphosphoric acids and metal hydroxides are then released to solution after hydration.

For borate glasses, one type of hydration reaction involves the metal cations that charge balance anionic tetrahedral units, as summarized by:

$$(B\emptyset_4)^- M^+ + H_2O \rightarrow (B\emptyset_4)^- H^+ + MOH \qquad [3]$$

Here, Ø represents a bridging oxygen that links a neighboring borate anion. Protonated borate tetrahedra are unstable and convert to more stable protonated trigonal sites [44,45] so that the net hydration reaction of a metal cation bonded to a borate tetrahedron is:

$$(B\emptyset_4)^- M^+ + H_2O \rightarrow (B\emptyset_2OH) + MOH \qquad [4]$$

A second type of reaction involves the hydrolysis of the bridging oxygens between network forming phosphate and borate polyhedra. Under pH-neutral conditions, like those associated with SBF-solutions, the hydrolysis of bridging P-Ø-P bonds in linear phosphate anions is relatively slow, compared to hydrolysis in more acidic solutions [46]. Hydrolysis reactions of the bridging oxygens that constitute the structures of a borate glass may involve the protonated trigonal species created after the hydration

of a metal cation-tetrahedral borate site (reactions 3 and 4), summarized by reaction 5, or the bridging oxygens associated with trigonal borate sites, as shown in reaction 6:

$$(B\emptyset_2OH) + H_2O \rightarrow B(OH)_3 \quad [5]$$

$$2B^3_{0P} + 3\mathrm{H_2O} \rightarrow 2\mathrm{B(OH)_3} \quad [6]$$

In both of these reactions, soluble boric acid is released into the solution, along with the metal hydroxide from the original hydration reaction (Eq. 4).

In the present study, the analyses of ions released from the phosphate glasses (x=0) into water (Figure 2) show similar ratios as those in the original glass, indicating that the network hydrolysis and subsequent hydration reactions lead to congruent glass dissolution. Similar results have been reported from dissolution studies of other alkali-alkaline earth phosphate glasses [4,6,12]. The analyses of ions released to water from the borate (x=60) glass in Figure 2 also reveal congruent dissolution, implying that the hydration and hydrolysis reactions occur simultaneously, as reported elsewhere [22].

Similar hydration and hydrolysis reactions can be proposed for the borophosphate glasses studied here. Figure 10 shows that for the x=10 and x=20 glasses, significant fractions of P-Ø-B bonds are present in the glass network and so their relative hydrolysis rate would affect the overall dissolution rates of these glasses. In water, these glasses also dissolve congruently (Figure 2), and in SBF, their dissolution rates are considerably lower than those for either the phosphate or borate end members. In fact, the

compositional dependence of the dissolution rates shown in Figure 9 are inversely proportional to the relative fractions of B-Ø-P bonds that constitute the glass network, as shown in Figure 10, implying that the incorporation of tetrahedral B_{4P}^{4} sites in the glass network improves the chemical stability of these glasses in SBF. Similar observations have been made in other dissolution studies borophosphate glasses in aqueous solutions 29,37,47,48].

Freudenberger et al. reported finding similar distributions of phosphate anions from quantitative chromatographic and ^{31}P NMR analyses, after accounting for the hydrolysis of the P_{2B}^{3} species [40]. Since those chromatographic samples were produced by dissolving the glasses in a slightly basic solution where P-Ø-P bond hydrolysis rates are very slow, the borophosphate glasses had to dissolve by the hydrolysis of the P-Ø-B bonds to release a polyphosphate anion and boric acid, along with the hydrated alkali and alkaline earth ions that were charge balancing the phosphate anion in the glass.

Figure 11 shows the anion distributions calculated from the chromatography data reported by Freudenberger et al., including chromatographs collected by dissolving the x=0 glass [40]. This latter data could not be used to analyze the original structures of the x=0 glasses because of the hydrolysis of the P_{0B}^{3} sites, which released into the chromatographic solution large concentrations of both orthophosphate anions (P_1) and anions with more than three P-tetrahedra. Increasing the borate content of the borophosphate glasses decreased the relative concentrations of longer anions, and increased the relative concentrations of smaller anions until at x=40, >98% of the phosphate anions released to solution were orthophosphate anions.

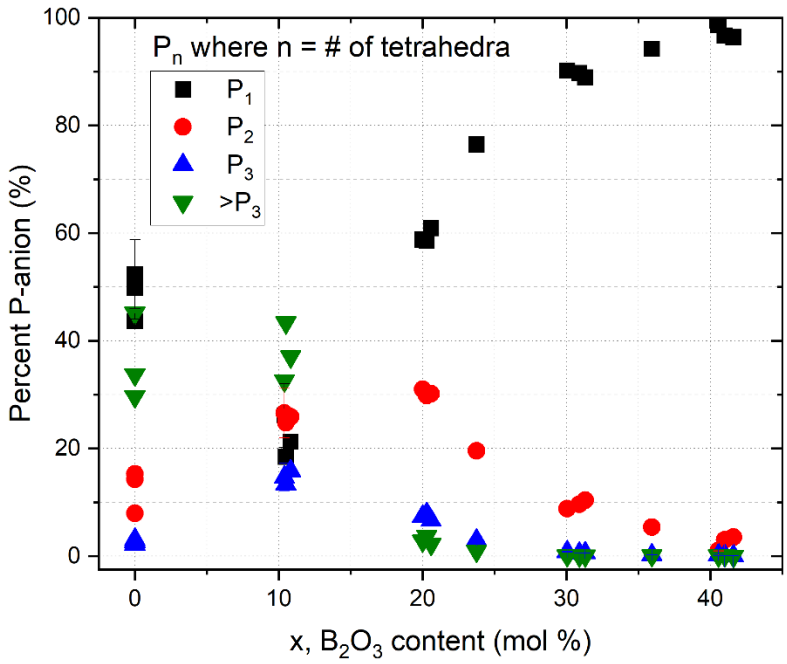

Figure 11. P-anion distributions for the three series (y=0, 12, and 24) of glasses determined by ion chromatography [41]. Hydrolysis of the ultraphosphate network of the x=0 glasses (0 B_2O_3) produced an anion distribution that is not representative of the original glass structure.

The long-term weight loss data from glasses in SBF, shown in Figure 3.3, have plateaus near 40-60% after about 48 hours for the three x=40 (y=0, 12, 24) glasses, with the final weight loss fraction decreasing systematically when SrO replaces CaO in the glass composition. The plateau time corresponds to the full release of borate into the respective solutions (Figure 4). The total weight lost from the x=35 (y=0) glass at the completion of one week on test is also about 60% and, again, corresponds to the full release of borate from the glass to the solution. Similar plateaus exist in the Ca- and P-release data from the x=40 (y=0) glass in water (Figure 2).

The plateaus in the weight loss and ion release data are associated with the development of precipitation phases on the respective glass surfaces. For example, the formation of an insoluble partially crystalline brushite ($CaHPO_4 \cdot 2H_2O$) phase, identified by XRD, on the surfaces of the SrO-free x=40 glass particles reacted in both water and SBF, as well on the SrO-free x=35 particles in SBF, accounts for both the plateaus in the respective weight change data as well as the lower release rates of Ca and P to water. The development of other x-ray amorphous precipitation products likely explains the weight change plateaus for the x=40/y=12 and x=40/y=24 particles in SBF. In fact, the systematic decrease in total weight loss with the replacement of CaO by SrO in the x=40 compositions is consistent with the development of a precipitation product with increasing concentrations of heavier Sr-ions.

The Raman spectra in Figure 7 provide some additional information about the nature of the precipitation phases that form on these glasses after exposure to SBF. The sharp peaks near 960 cm^{-1} in the spectra of the reacted x=35/y=0 and x=40/(y=0,12,24) glasses can be assigned to the symmetric stretching mode of an orthophosphate anion. Amorphous calcium phosphates (ACP) and octocalcium phosphate (OCP, $Ca_8(HPO_4)_2(PO_4)_4 \cdot 2H_2O$) have sharp Raman peaks near 960 cm^{-1} [49-51] whereas the peak frequency for crystalline brushite is near 985 cm^{-1} [52,53]. This indicates that the crystalline brushite detected by XRD is a small fraction of the precipitated material from the x=35/y=0 and x=40/y=0 samples, that most of precipitated phase is in the form of an amorphous phosphate, including the phases that form on the x=40/y=12 and x=40/y=24 samples. Indeed, ACP and OCP are precursors to the precipitation of brushite and

hydroxyapatite in phosphate solutions [49], and the XRD results provide some indication of the progress of that transformation.

There are potentially several overlapping contributions to the intensity of second sharp peak in the Raman spectra, near 1030 cm^{-1}, including an asymmetric stretching mode of the orthophosphate anion [52,53] and stretching modes from carbonate species [54-56], which can be incorporated into phosphate phases that precipitate from SBF on the surfaces of bioactive glasses [57]. More likely, though, is that the 1030 cm^{-1} peak is due to symmetric stretching modes of pyrophosphate units incorporated into the phosphate precipitation layer [58,59]. The ratio of the intensities of the 1030 and 960 cm^{-1} peaks increases for the y=0 glasses in the order (x=40)<(x=35)<(x=30) as does the relative intensity of the peak at 750 cm^{-1}, assigned to the symmetric stretching modes of oxygens that bridge phosphate tetrahedra in a pyrophosphate anion [60]. The relative concentrations of pyrophosphate anions found in the network structures of the base glasses increases in the same compositional order [40]. For example, Figure 11 shows that the pyrophosphate (P2)-to-orthophosphate (P1) ratio increased from 2:98 for the (x=40/y=0) glass to 8:90 for the (x=30/y=0) glass. The presence of pyrophosphate anions in solution is known to inhibit the nucleation and crystallization of orthophosphate phases like brushite or hydroxyapatite [61,62] and this is consistent with the amorphous XRD patterns associated with samples with relatively greater pyrophosphate components, as revealed by the Raman spectra.

There is a third peak, near 1000 cm^{-1}, in the Raman spectra from the reacted Sr-containing glasses (x=40/y-12 and x=40/y=24) that does not appear in the spectra of the

reacted Sr-free glasses. This peak might be due to the incorporation of Sr-ions into an calcium phosphate layer or to the presence of HPO_4^{2-} anions in the layer [63].

In summary then, the compositional dependence of the initial reaction rate constant data shown in Figure 9 can be related to the systematic changes in the network structure of the glass. The initial replacement of P_2O_5 by B_2O_3 replaces reactive P_{0B}^{3}-sites with chemically durable B_{4P}^{4}-sites, the concentration of which is maximized near x=20. Further replacement of P_2O_5 by B_2O_3 reduces the relative fractions of more durable P-Ø-B bonds with more reactive B-Ø-B bonds, particularly those associated with the readily hydrolysable borate trigonal sites. The fastest dissolving glasses are those with the lowest phosphate contents. The precipitation of insoluble phases on the surfaces of the reacting glasses does not appear to affect the rates of release of soluble species from the glass, but the nature of that insoluble phase does depend on the original glass composition.

4.2. SOLUTION pH

Equations 2-6 indicate some of the reactions that can occur when the alkali-alkaline earth borophosphate glasses react with water. Those reactions can produce borate and phosphate acids and alkali and alkaline earth hydroxides, and the relative concentrations and acid dissociation constants (pKa) will determine the solution pH. Table 1 lists room temperature dissociation constants for some of the species expected to be present in solution when these borophosphate glasses dissolve in water. The base dissociation constants (pK_b) for several of the metal cations were calculated by subtracting the acid dissociation constant from the dissociation constant of water (pK_{water} = 13.995) [64].

Table 1. Acid dissociation constants (pKa) for possible species in solution containing Na, Ca, B, and P ions. [64,65]

Aqueous acid-base equilibria	Step	T (°C)	pK_a (pK_b)
$B(OH)_3 + H_2O \leftrightarrow B(OH)_4^- + H^+$	1	20	9.27
$B(OH)_4^- + H_2O \leftrightarrow B(OH)_5^{2-} + H^+$	2	20	> 14
$Ca^{2+} + 2H_2O \leftrightarrow Ca(OH)_2 + 2H^+$		25	12.6 (1.4)
$H_2CO_3 \leftrightarrow (HCO_3)^- + H^+$	1	25	6.35
$(HCO_3)^- \leftrightarrow (CO_3)^{2-} + H^+$	2	25	10.33
$H_3PO_4 \leftrightarrow (H_2PO_4)^- + H^+$	1	25	2.16
$(H_2PO_4)^- \leftrightarrow (HPO_4)^{2-} + H^+$	2	25	7.21
$(HPO_4)^{2-} \leftrightarrow (PO_4)^{3-} + H^+$	3	25	12.32
$H_4P_2O_7 \leftrightarrow (H_3P_2O_7)^- + H^+$	1	25	0.91
$(H_3P_2O_7)^- \leftrightarrow (H_2P_2O_7)^{2-} + H^+$	2	25	2.10
$(H_2P_2O_7)^{2-} \leftrightarrow (HP_2O_7)^{3-} + H^+$	3	25	6.70
$(HP_2O_7)^{3-} \leftrightarrow (P_2O_7)^{4-} + H^+$	4	25	9.32
$Na^+ + H_2O \leftrightarrow NaOH + H^+$		25	14.8 (-0.81)
$Sr^{2+} + 2H_2O \leftrightarrow Sr(OH)_2 + 2H^+$		25	13.2 (0.79)

A smaller dissociation constant indicates a stronger acid or base. Boric acid (pK_a = 9.27) is a much weaker acid than the phosphoric acid (pK_{a1} = 2.16) and this explains why the phosphate-rich glasses produced much more acidic solutions when dissolved in water than did the borate-rich glasses (Figure 1). The pH of the solutions created by the dissolution of the borophosphate glasses in water increased with the borate-content of the glass. The final pH of the solution created by the dissolution of the x=40 was about 7.2, similar to the second dissociation constant of phosphoric acid and so indicating that this solution may be controlled by the following buffer reaction:

$$(H_2PO_4)^- \leftrightarrow (HPO_4)^{2-} + H^+ \qquad [7]$$

The dissolution of borophosphate glasses in SBF produced smaller changes in solution pH (Figure 6), reflecting the more complex solution chemistries and generally slower dissolution kinetics of the glasses. The dissolution of the x=60 borate glass increased the pH of the SBF solution to a value of about 8.7 after the first 24-48 hours, after which the glasses were completed dissolved (Figure 5). The SBF pH values from the fast-reacting x=40 glasses leveled off near 7.0 and most of the solutions from the slower reacting glasses remained in the range 7.2 to 7.7. One exception is the drop in SBF pH for the CaO-analog of the x=0 glass after about 60 hours on test. Chromatographic analyses of this glass (Figure 11) reveals that long phosphate anions are released to solution [40] and when these anions hydrolyze, they produce phosphoric acid, which then accelerates the hydrolysis reactions [12]. High field strength cations, like Ca^{2+}, also catalyze the hydrolysis of phosphate anions in solution [7], and this may explain why the pH values of SBF at the conclusion of the one-week dissolution experiments increased in the order (y=0)<(y=12)<(y=24) for the x=0 glass (Figure 6), despite the slightly lower pK_b of SrO compared to CaO (Table 1).

5. CONCLUSION

The dissolution kinetics of glasses from the $16Na_2O$-(24-y)CaO-ySrO-xB_2O_3-(60-x)P_2O_5 (mol%) compositional series, where $0 \leq x \leq 60$ and y=0, 12, and 24, were measured in 37°C water and in simulated body fluid (SBF). A minimum in dissolution rate (x = 20) can be related to a maximum in number of B-Ø-P linkages in the original glass, indicating a correlation between dissolution rate and tetrahedral $B(ØP)_4$ sites. Above

about 20 mole% B_2O_3, trigonal borate sites begin to be incorporated in the borophosphate glass structure and an increase in the relative numbers of hydrolyzable B-Ø-B contributes to the increasing dissolution rates in both SBF and water. The release of Na-, Ca-, and Sr-hydroxides from hydration of the metal ion sites and boric and phosphoric acid from hydrolysis of borate and phosphate bonds affects the solution pH, however it ultimately depends on buffering reactions between the soluble species. Insoluble phosphate phases precipitate on the surfaces of the faster reacting borophosphate glasses. Crystalline brushite was detected on Ca-glasses with 35 and 40 mole% B_2O_3, but the dominant material on both the Ca- and Sr-glasses is an amorphous combination of orthophosphate and pyrophosphate species.

The dissolution rates can be controlled by several orders of magnitude by varying the phosphate-to-borate ratio of the glass, and this may be of value for biomedical applications that require controlled ion release rates. Likewise, control over the local pH created by the dissolution of the borophosphate glasses may prove useful for biomedical applications where the alkalinity of conventional bioactive glasses is a problem.

ACKNOWLEDGEMENTS

This work was supported by the Graduate Assistance in Areas of National Need (GAANN) fellowship from the US Department of Education. The authors would like to thank Alana Buznego for her assistance with a portion of the dissolution experiments, and Dr. Eric Bohannan for his insights into the X-ray diffraction data.

REFERENCES

1. Islam MT, Felfel RM, Abou Neel EA, Grant DM, Ahmed I, Hossain KMZ. Bioactive calcium phosphate–based glasses and ceramics and their biomedical applications: A review. *J Tissue Eng*. 2017;8:1 –16. https://doi.org/10.1177/2041731417719170

2. Ahmed I, Collins CA, Lewis MP, Olsen I, Knowles JC. Processing, characterisation and biocompatibility of iron-phosphate glass fibres for tissue engineering. *Biomaterials*. 2004;25(16):3223–3232. https://doi.org/10.1016/J.BIOMATERIALS.2003.10.013.

3. Shah R, Sinanan ACM, Knowles JC, Hunt NP, Lewis MP. Craniofacial muscle engineering using a 3-dimensional phosphate glass fibre construct. *Biomaterials*. 2005;26(13):1497–1505. https://doi.org/10.1016/J.BIOMATERIALS.2004.04.049

4. Bunker BC, Arnold GW, Wilder JA. Phosphate glass dissolution in aqueous solutions. *J Non Cryst Solids*. 1984;64(3):291–316. https://doi.org/10.1016/0022-3093(84)90184-4.

5. Salih V, Franks K, James M, Hastings GW, Knowles JC, Olsen I. Development of soluble glasses for biomedical use part II: The biological response of human osteoblast cell lines to phosphate-based soluble glasses. *J Mater Sci Mater Med*. 2000;11(10):615–620. https://doi.org/10.1023/A:1008901612674

6. Ma L, Brow K, Schlesinger ME. Dissolution behaviour of sodium calcium polyphosphate glasses. 2018;59(5):205–212. https://doi.org/10.13036/17533562.59.5.018

7. Ahmed I, Parsons AJ, Rudd CD, *et al.* Comparison of phosphate-based glasses in the range $50P_2O_5$-(50– x)CaO-xNa_2O prepared using different precursors. *Glass Technology-European Journal of Glass Science and Technology Part A*. 2008;49:63–72.

8. YP Peng, DE Day, High Thermal Expansion Glasses, Part 1. *Glass Technology*, 32[5] 166-173 (1991)

9. Thilo E, Wieker W. Study of Degradation of Polyphosphates in Aqueous Solution. *Journal of Polymer Science*. 1961;53:55–59.

10. Salazar DAA, Bellstedt P, Miura A, Oi Y. Unravelling the dissolution mechanism of spectroscopy : ligand competition and. *Dalton Transactions*. 2021;45–47. https://doi.org/10.1039/d0dt03381b

11. Ma L, Brow RK, Schlesinger ME. Dissolution behavior of Na_2O–FeO–Fe_2O_3–P_2O_5 glasses. *J Non Cryst Solids*. 2017;463:90–101. https://doi.org/10.1016/J.JNONCRYSOL.2017.02.022

12. Döhler F, Mandlule A, van Wüllen L, Friedrich M, Brauer DS. ^{31}P NMR characterisation of phosphate fragments during dissolution of calcium sodium phosphate glasses. *J Mater Chem B*. 2015;3(6):1125–1134. https://doi.org/10.1039/c4tb01757a

13. O'Donnell MD, Hill RGG, O'Donnell MD, Hill RGG. Influence of strontium and the importance of glass chemistry and structure when designing bioactive glasses for bone regeneration. *Acta Biomater*. 2010;6(7):2382–2385. https://doi.org/10.1016/j.actbio.2010.01.006

14. Hurtel-Lemaire AS, Mentaverri R, Caudrillier A, *et al.* The calcium-sensing receptor is involved in Strontium ranelate-induced osteoclast apoptosis new insights into the associated signaling pathways. *Journal of Biological Chemistry*. 2009;284(1):575–584. https://doi.org/10.1074/jbc.M801668200

15. Freudenberger PT, Saitoh A, Ikeda H, *et al.* Characterization of $20Na_2O \cdot 30((1-x)CaO \cdot xSrO) \cdot 50P_2O_5$ glasses for a resorbable optical fiber application. *Int J Appl Glass Sci*. 2019;10(3). https://doi.org/10.1111/ijag.13106

16. Jung SB and Day DE. Conversion kinetics of silicate, borosilicate, and borate bioactive glasses to hydroxyapatite. *Phys. Chem. Glasses* 2009; 50(4):85-88.

17. Fu Q, Rahaman MN, Fu H, and Liu X. Silicate, borosilicate, and borate bioactive glass scaffolds with controllable degradation rate for bone tissue enginneering applications. I. Preapration and in vitro degradation. *J. Biomedical Materials Research A* 2010;95A(1):164-171.

18. Rahaman MN, Day DE, Sonny Bal B, et al. Bioactive glass in tissue engineering. Acta Biomater. 2011;7(6):2355–2373. https://doi.org/10.1016/J.ACTBIO.2011.03.016

19. Ottomeyer M, Mohammadkah A, Day D, Westenberg D. Broad-Spectrum Antibacterial Characteristics of Four Novel Borate-Based Bioactive Glasses. *Adv Microbiol*. 2016;06(10):776–787. https://doi.org/10.4236/aim.2016.610076

20. Jung SB, Day DE, Day T, Stoecker W, Taylor P. Treatment of non-Healing Diabetic Venous Stasis Ulcers with Bioactive Glass Nanofibers. *Wound Repair and Regeneration*. 2011;19(2):A30–A30.

21. Brow RK. The Dissolution of Borate Glasses in Aqueous Solutions. In: Kasuga T, Obata A, Brauer DS, eds. *Phosphate and Borate Bioactive Glasses*. Royal Society of Chemistry; 2022

22. Goetschius KL, Beuerlein MA, Bischo CM, Brow RK. Dissolution behavior of ternary alkali-alkaline earth-borate glasses in water. *J Non Cryst Solids*. 2018;487:12–18. https://doi.org/10.1016/j.jnoncrysol.2018.02.011

23. Veléz MH, Tuller HL, Uhlmann DR. Chemical durability of lithium borate glasses. *Chemical Durability of Lithium Borate Glasses*. 1982;49:351–362. https://doi.org/10.1137/1.9781611970319.ch1

24. Gu Y, Xiao W, Lu L, Huang W, Rahaman MN, Wang D. Kinetics and mechanisms of converting bioactive borate glasses to hydroxyapatite in aqueous phosphate solution. *J Mater Sci*. 2011;46(1):47–54. https://doi.org/10.1007/s10853-010-4792-x

25. Huang W, Li Y, Rahaman M, Day D. Mechanisms for converting bioactive silicate, borate, and borosilicate glasses to hydroxyapatite in dilute phosphate solution. *Physics and Chemistry of Glasses-european Journal of Glass Science and Technology Part B*. 2006;47:647–658.

26. Dorozhkin S v. Calcium orthophosphates ($CaPO_4$): occurrence and properties. *Prog Biomater*. 2016;5(1):9–70. https://doi.org/10.1007/s40204-015-0045-z

27. Fu H, Rahaman MN, Brown RF, Day DE. Acta Biomaterialia Evaluation of bone regeneration in implants composed of hollow HA microspheres loaded with transforming growth factor b 1 in a rat calvarial defect model. *Acta Biomater*. 2013;9(3):5718–5727. https://doi.org/10.1016/j.actbio.2012.11.017

28. Massera J, Shpotyuk Y, Sabatier F, *et al.* Processing and characterization of novel borophosphate glasses and fibers for medical applications. *J Non Cryst Solids*. 2015;425:52–60. https://doi.org/10.1016/j.jnoncrysol.2015.05.028

29. Sharmin N, Hasan MS, Parsons AJ, *et al.* Effect of boron addition on the thermal, degradation, and cytocompatibility properties of phosphate-based glasses. *Biomed Res Int*. 2013;2013. https://doi.org/10.1155/2013/902427

30. Abo-Naf SM, Khalil ESM, El-Sayed ESM, Zayed HA, Youness RA. In vitro bioactivity evaluation, mechanical properties and microstructural characterization of Na_2O-CaO-B_2O_3-P_2O_5 glasses. *Spectrochim Acta A Mol Biomol Spectrosc*. 2015;144:88–98. https://doi.org/10.1016/j.saa.2015.02.076

31. Raskar D, Rinke MT, Eckert H. The Mixed-Network Former Effect in Phosphate Glasses: NMR and XPS Structural Studies of the Connectivity Distribution in the Glass System (NaPO3)1-x(B2O3)x. *The Journal of Physical Chemistry C*. 2008;112:12530–12539. https://doi.org/10.1039/c0cp01590c

32. Rinke MT, Eckert H. The mixed network former effect in glasses: Solid state NMR and XPS structural studies of the glass system (Na2O)x(BPO 4)1-x. *Physical Chemistry Chemical Physics*. 2011;13(14):6552–6565. https://doi.org/10.1039/c0cp01590c

33. Koudelka L, Mošner P. Borophosphate glasses of the ZnO–B_2O_3–P_2O_5 system. *Mater Lett*. 2000;42(January):194–199.

34. Koudelka L, Mošner P, Pospíšil J, Montagne L, Palavit G. Structure and properties of titanium-zinc borophosphate glasses. *J Solid State Chem*. 2005;178(6):1837–1843. https://doi.org/10.1016/j.jssc.2005.03.025

35. Christensen R, Olson G, Martin SW. Structural Studies of Mixed Glass Former $0.35Na_2O+ 0.65[xB_2O_3+(1-x)P_2O_5]$ Glasses by Raman and ^{11}B and ^{31}P Magic Angle Spinning Nuclear Magnetic Resonance Spectroscopies. *J Phys Chem B*. 2013;117(7):2169–2179. https://doi.org/10.1021/jp308494a

36. Muñoz-Senovilla L, Tricot G, Muñoz F. Kinetic fragility and structure of lithium borophosphate glasses analysed by 1D/2D NMR. *Physical Chemistry Chemical Physics*. 2017;19(34):22777–22784. https://doi.org/10.1039/c7cp04171c

37. Lim JW, Schmitt ML, Brow RK, Yung SW. Properties and structures of tin borophosphate glasses. *J Non Cryst Solids*. 2010;356(28–30):1379–1384. https://doi.org/10.1016/j.jnoncrysol.2010.02.019

38. Abokefa, N. In vitro and in vivo response to a novel borophosphate bioactive glass (2021). *Masters Theses Missoori S&T.* 7972. https://scholarsmine.mst.edu/masters_theses/7972.

39. Zhang D., Lepparanta O., Munukka E., Ylanen H, Viljanen MK, Eerola E., Hpa M., and Hupa, L. Antibacterial effects and dissolution behavior of six bioactive glasses. *J. Biomedical Materials Research A* 2010;93 (2):475-483.

40. Freudenberger PT, Blatt RL, Youngman RE, and Brow RK, "Network Structures and the Properties of Na-Ca-Sr-Borophosphate Glasses," *Journal of Non-Crystalline Solids*, 600 121966 (2023).

41. Kokubo T, Kushitani H, Sakka S, Kitsugi T, Yamamuro T. Solutions able to reproduce in vivo surface-structure changes in bioactive glass-ceramic A-W3. *J Biomed Mater Res*. 1990;24(6):721–734.

42. Khawam A, Flanagan DR. Solid-State Kinetic Models: Basics and Mathematical Fundamentals. *Journal of Physical Chemistry B*. 2006;110(35):17315–17328.

43. Mascaraque N, Bauchy M., and Smedskjaer MM. Corelating the Network Topology of Oxide Glasses with their Chemical Durability. *J. Phys. Chem. B* (2017);121(5):1139-1147., et al. (2017)

44. Zapol P, He H, Kwon KD, Criscenti LJ. First-principles study of hydrolysis reaction barriers in a sodium borosilicate glass. *Int J Appl Glass Sci*. 2013;4(4):395–407. https://doi.org/10.1111/ijag.12052

45. Geneste G, Bouyer F, Gin S. Hydrogen-sodium interdiffusion in borosilicate glasses investigated from first principles. *J Non Cryst Solids*. 2006;352(28–29):3147–3152. https://doi.org/10.1016/j.jnoncrysol.2006.04.023

46. McCullough JF, Van Wazer JR, and Griffith, EJ. Structure and Properties of the Condensed Phosphates. XI. Hydrolytic Degradation of Graham's Salt. *J. Amer. Chem. Soc*. 1956;78:4528-4533.

47. Koudelka L and Mosner P. Study of the Structure and Properties of Pb-Zn Borophosphate Glasses. *J. Non-Cryst. Solids* 2001;293-295:635-641.

48. Takebe H, Kobatake T, and Saitoh A. Dissolutiojn Behaviour of $SnO-P_2O_5$ and $SnO-P_2O_5-B_2O_3$ Glasses in Water. *Phys. Chem. Glasses B* 2013;54(4) 182-186.

49. Montes-Hernandez G and Renard F. Nucleation of Brushite and Hydroxyapatite from Amorphous Calcium Phosphate Phases Revealed by Dynamic *In Situ* Raman Spectroscopy. *J. Phys. Chem. C* 2020;124:15302-15311.

50. Seah RKH, Garland M, Loo JSC, and Widjaja E. Use of Raman Microscopy and Multivariate Data Analysis to Observe the Biomimetic Growth of Carbonated Hydroxyapatite on Bioactive Glas. Anal. Chem. 2009;81:1442-1449.

51. Bannerman A, Williams RL, Cox SC, and Grover LM. Visualizing phase change in a brushite-based calcium phosphate ceramic. *Scientific Reports* 2016; 6:32671 | DOI: 10.1038/srep32671

52. Louati B, Guidara K, Gargouri M, and Fourati M. ^{1}H NMR, ^{31}P NMR and Raman Study of $CaHPO_4$ and $SrHPO_4$. *Z. Naturforsch*. 2005;60a:121–126.

53. Frost RL, Xi Y, Pogson RE, Millar GJ, Tan K, and Palmer SJ. Raman spectroscopy of synthetic $CaHPO_4 \cdot 2H_2O$ and in comparison with the cave mineral brushite. *J. Raman Spectroscopy* 2011; 43(4):571-576.

54. Kazanci M, Fratzl P, Klaushofer K, and Pascalis EP. Complementary Information on In Vitro Conversion of Amorphous (Precursur) Clcium Phosphate to Hydroxyapatite from Raman Microspectroscopy and Wide-Angle X-Ray Scattering. *Calcif. Tissue Int.* 2006;79:354-359.

55. Awonusi A, Morris MD, and Tecklenburg MMJ. Carbonate Assignment and Calibration in the Raman Spectrum of Apatite. *Calcif. Tissue Int*. 2007;81:46-52.

56. Penel G, Leroy N, Rey C, Lemaitre P, Van Landuyt P, Ghanty N, and Leroy G. Qualitative and Quantitative Investigation of Calcium Phosphate of Biological Interest by Raman Microspectrometry. Recent Res. Devel. Appl. Spectroscopy 1999;2:137-146.

57. Vallet-Regi M and Ramila A. New Bioactive Glass and Changes in Porosity during the Growth of a Carbonate Hydroxyapatite Layer on Glass Surfaces. Chem. Mater. 2000;12(4):961-965.

58. Chen K-H, Li M-J, Cheng W-T, Balic-Zunic T, and Lin S-Y. Identification of monoclinic calcium pyrophosphate dihydrate and hydroxyapatite in human scelra using Raman microspectroscopy. Int. J. Experimental Pathology 2009;90(1):74-78. https://doi.org/10.1111/j.1365-2613.2008.00614.x

59. Hughes EAB, Jones-Salkey O, Forey P, Chipara M, and Grover LM. Exploring the Formation of Calcium Orthophosphate-Pyrophosphate Chemical Gardens. *ChemSystemsChem* 2021;3:2000062.

60. Cornilsen BC. Solid State Vibrational Spectra of Calcium Pyrophosphate Dihydrate. *J. Molec. Structure* 1984;117(1-2):1-9.

61. Francis MD. The Inhibition of Calcium Hydroxyapatite Crystal Growth by Polyphosphonates and Polyphosphates. *Calcified Tissue Research* 1969;3:151-162.

62. Orriss IR, Arnett TR, and Russell RGG. Pyrophosphate: A Key Inhibitor of Mineralisation. *Curr. Opinion in Pharmacology* 2016;28;57-68.

63. Shi H, He F., and Ye J. Synthesis andstructure of iron- and strontium substituted octacalcium phosphate: effects of ionic charge and radius. *J. Materials Chemistry B* 2016;4:1712-1719.

64. Lide DR, Haynes WM. CRC *Handbook of Chemistry and Physics*. 90th ed. 2010

65. Kochkodan V, Darwish N bin, Hilal N. The Chemistry of Boron in Water. *Boron Separation Processes*. 2015:41–43.

SECTION

3. CONCLUSIONS AND RECOMMENDATIONS

Because the intent of the characterization of zinc borophosphate (ZBP) glasses in the Paper section was to determine the effect that B_2O_3 has on the properties and structure of ZBP glasses with fixed oxygen to phosphorus (O/P) ratios, there were gaps in the terminal oxygen to boron ratio (TO/[B]) when performing the structural analysis with the structural model proposed by Hoppe. The interest in the O/P ratio of 3.25 was due to previous experiments in which wave-guiding structures were written into zinc phosphate (ZP) and zinc aluminophosphate (ZAP) glasses using fs laser writing.[81-83] The prevailing notion is that this was due to structural similarities in the ZP and ZAP glasses to vitreous silica, i.e. a tetrahedrally connected structure.[84] If this project were to be continued, a broader range of compositions based on TO/[B] is recommended to better understand the deviation of borophosphate compositions from Hoppe's terminal oxygen model. The assumption that zinc remains in a tetrahedral coordination for these glasses should be confirmed for these compositions, along with developing a similar understanding of the evolution of borate species in transition metal borophosphate compositions as what is described by Hermansen's structural model for alkali-alkaline earth borophosphate glasses. Furthermore, there has been no comprehensive analysis of the waveguide-forming capabilities of the ZBP compositions.

As a side note, the sample preparation techniques that were developed in the collaboration with colleagues from Nippon Electric Glass for the Na-Ca/Sr-

borophosphate glasses described in the Paper section should be applied to the preparation of the ZBP glasses. Zinc metaphosphate can be used as a raw material to add phosphate to the composition rather than phosphoric acid, pure platinum crucibles should be used rather than platinum-rhodium alloys, and the melt can be stirred using a platinum stir rod to achieve a homogenous melt with less potential for discoloration from the crucible.

In the Paper section, the metaphosphate glass compositions were designed and proven to have similar characteristic temperatures but different refractive indices to produce a core-clad fiber combination. Moreover, a fiber was demonstrated to transmit 632 nm light when submerged in a phosphate buffer solution at 21°C for a demonstrable lifetime. Continuation of this project would involve designing and testing an actual device.

In addition to comparing the data to literature, the ^{11}B and ^{31}P MAS NMR analysis for alkali-alkaline earth borophosphate glasses in the Paper section was related to results from High Pressure Liquid Chromatography and Raman Spectroscopy, and the charge balance for associated cation and anion species was calculated using the analyzed composition to confirm spectral fitting. While this generated a high confidence in the analysis, further investigation using other 2D NMR techniques would help clarify the nature of the trigonal borate species; e.g., identifying sites with non-bridging oxygens. With an understanding of how a direct substitution of borate for phosphate in the glass composition affects structure, there should be a shift in focus to observing the effects of varied alkali modifier content, both in comparison to one another and to glass forming oxides to further validate Hermansen's Structural model and the connection between breaks in properties with the critical composition identified by the model.

The current study on the dissolution of alkali borophosphate glasses focused on the effects of structure in the bulk glass on dissolution, resulting in a narrow analysis of short-term dissolution, particularly within the first 24 hours. Therefore, to continue the development of these glasses for biomedical applications, it is suggested that future efforts drive towards further understanding of the mechanisms of reaction layer formation, including both solution chemistry and glass surface analysis for long times (at least up to 2 weeks) to compare to industry standard compositions such as 1393-B3 and 45S5.[85]

In the study by Liu *et al.*, the formation of crystalline species on 1393-B3 fibers was not identified until 7 days of predominately static (shaken once a day) dissolution, which was the longest time point for dissolution in the shaker bath experiment reported in the Paper section. Of note, the borophosphate composition ($16Na_2O$-$24CaO$-$40B_2O_3$-$20P_2O_5$, mol%) analyzed in the Paper section demonstrated promising results in angiogenesis and muscle regeneration experiments. Residual fines in solution were observed qualitatively in Simulated Body Fluid (SBF) after 168 hours at 37°C in a shaker bath for only this composition, emphasizing that steps to characterize solution and surface chemistry of these glasses should be taken. This would include quantitative analyses of the calcium phosphate precipitation products, such as amorphous calcium phosphate, brushite, and hydroxyapatite. In doing so, however, it is recommended that the procedure for dissolution be modified away from glass particles in nylon satchels, as the surface of the particles can be disturbed during removal from the satchels; bulk glass samples or fibers, as in Liu *et al*., is suggested.[85]

Concurrently with experimental analyses, there should be some effort towards identifying useful solution chemistry predictions, as the calculations using FactSage (Appendix) provided some insight but were limited by assumptions used by the software. Once found, this tool could potentially be used to quantify the roles and contributions of phosphate anion hydration and borate network hydrolysis on the dissolution kinetics, as this work was only able to make qualitative observations of the link between these structures and dissolution rate.

APPENDIX A.

SUPPLEMENTARY INFORMATION FOR PAPER III

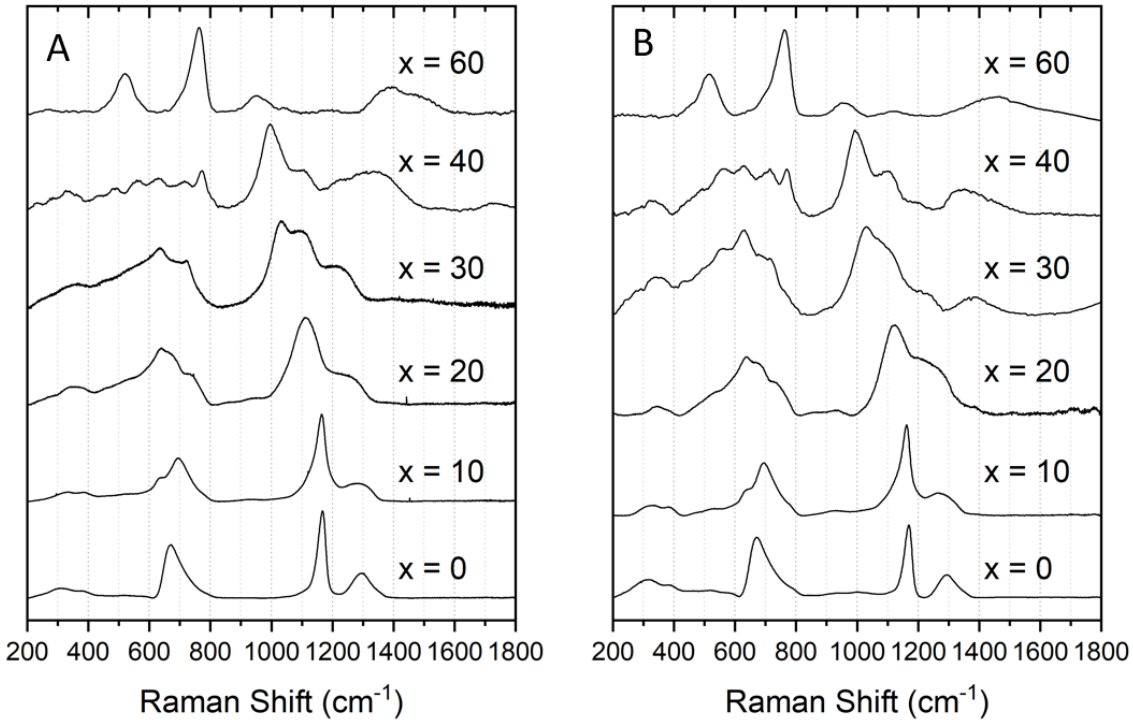

Figure A.1. Raman spectra from glasses in the mixed alkali (y=12, A) and CaO-free (y=24, B) nominal molar compositional series 16Na2O-(24-y)CaO-ySrO-xB_2O_3-(60-x)P_2O_5. The intensity of each spectrum was normalized to the most intense peak in that spectrum for visual comparison.

Table A.1. Summary of phosphate units determined by ^{31}P MAS NMR analysis for glasses of the nominal compostion $16Na_2O$-(24-y)CaO-ySrO-xB_2O_3-(60-x)P_2O_5.

Composition		**Fraction NFU**						
y	*x*	*P4,4B*	*P3,0B*	*P3,2B*	*P2,0B*	*P2,1B*	*P2,2B*	*P1,1B*
0	0	0.0	39.6	0.0	60.4	0.0	0.0	0.0
	10	5.4	11.8	7.7	30.4	26.9	0.0	0.0
	20	4.1	0.0	26.0	14.2	22.7	0.0	0.0
	23.3	2.7	0.0	35.6	10.3	11.3	2.3	0.0
	30	0.4	0.0	35.3	2.6	0.2	11.9	0.8
	35	0.0	0.0	26.9	1.5	0.0	12.7	1.6
	40	0.0	0.0	20.8	0.0	0.0	11.2	2.3
	60	0.0	0.0	0.0	0.0	0.0	0.0	0.0
12	0	0.0	36.6	0.0	63.4	0.0	0.0	0.0
	10	6.4	10.7	4.1	29.9	31.7	0.0	0.0
	20	3.3	0.0	30.7	12.7	20.1	0.0	0.0
	30	0.3	0.0	34.3	2.6	0.2	12.2	0.6
	40	0.0	0.0	17.9	0.0	0.0	12.5	2.6
	60	0.0	0.0	0.0	0.0	0.0	0.0	0.0
24	0	0.0	35.7	0.0	64.3	0.0	0.0	0.0
	10	7.6	6.2	7.3	36.0	25.8	0.0	0.0
	20	3.6	0.0	28.0	13.5	22.5	0.0	0.0
	30	0.2	0.0	30.1	1.5	0.2	17.2	1.0
	40	0.0	0.0	21.4	0.0	0.0	11.1	1.6
	60	0.0	0.0	0.0	0.0	0.0	0.0	0.0

Table A.2. Summary of borate units determined by ^{11}B MAS NMR analysis for glasses of the nominal compostion $16Na_2O$-(24-y)CaO-ySrO-xB_2O_3-(60-x)P_2O_5.

Composition		**Fraction NFU**					
y	*x*	*B4,0P*	*B4,1P*	*B4,2P*	*B4,3P*	*B4,4P*	*B3*
0.0	0	0.0	0.0	0.0	0.0	0.0	0.0
	10	0.0	0.0	0.0	9.3	8.5	0.0
	20	0.0	0.4	6.2	16.1	9.2	1.1
	23.3	0.0	1.9	10.5	22.3	0.0	3.2
	30	0.6	8.1	16.4	11.2	0.0	12.5
	35	1.1	16.8	11.6	5.9	0.0	22.0
	40	1.9	20.2	8.6	3.9	0.0	31.1
	60	44.9	0.0	0.0	0.0	0.0	55.1
12.0	0	0.0	0.0	0.0	0.0	0.0	0.0
	10	0.0	0.0	0.0	5.3	11.8	0.0
	20	0.0	0.0	6.7	13.4	12.0	1.1
	30	0.0	7.2	18.5	12.0	0.0	12.1
	40	2.0	21.0	9.3	3.8	0.0	31.0
	60	44.8	0.0	0.0	0.0	0.0	55.2
24.0	0	0.0	0.0	0.0	0.0	0.0	0.0
	10	0.0	0.0	0.0	5.1	11.9	0.0
	20	0.0	0.0	5.8	14.4	11.2	0.8
	30	0.0	7.4	18.9	11.0	0.0	12.5
	40	2.4	21.3	8.9	3.8	0.0	29.5
	60	45.7	0.0	0.0	0.0	0.0	54.3

1. CHARGE BALANCE

The charge (q_{comp}) from the anionic (B^i_{jP} and P^i_{jB}) units for each composition necessary to balance the contribution from the cations (Na^+ and Ca^{2+}) was determined using Eqn. A.1:

$$q_{comp} = -([Na^+] + 2[Ca^{2+}] + 2[Sr^{2+}]) \quad \text{A.1}$$

Where $[Na^+]$, $[Ca^{2+}]$, and $[Sr^{2+}]$ are the concentrations of the cations determined from the analyzed compositions by ICP-OES. The charge contribution from each type of anionic unit is listed in Table A.1.

Table A.1. The charges associated with each borate (B^i_{jP}) and phosphate (P^i_{jB}) unit.

Borate Unit	Charge (q)	Phosphate Unit	Charge (q)
B^4_{4P}	0	P^4_{4B}	0
B^4_{3P}	-0.25	P^3_{0B}	0
B^4_{2P}	-0.5	P^3_{2B}	-0.5
B^4_{1P}	-0.75	P^2_{0B}	-1
B^4_{0P}	-1	P^2_{1B}	-1.25
B^3	0	P^2_{2B}	-1.5
B^2	-1	P^1_{0B}	-2
		P^1_{1B}	-2.25
		P^0_{0B}	-3

The expected charge from compsition (q_{comp}) is plotted against what was determined using the fraction of anionic units identified by ^{11}B and ^{31}P MAS NMR (Table A.1) in Figure A.1. In an attempt to confirm the presence of anionic trigonal borate sites, two sets of calculations were carried out: 1) including anionic trigonal sites (include B^2 units) and 2) assuming all trigonal sites are neutral (no B^2 units). While the presence of anionic trigonal sites is confirmed using this method for the borate (x=60) composition, these calculations were unable to clearly confirm or deny the presence of anionic trigonal sites in borophosphate (x=30, 35, 40) compositions.

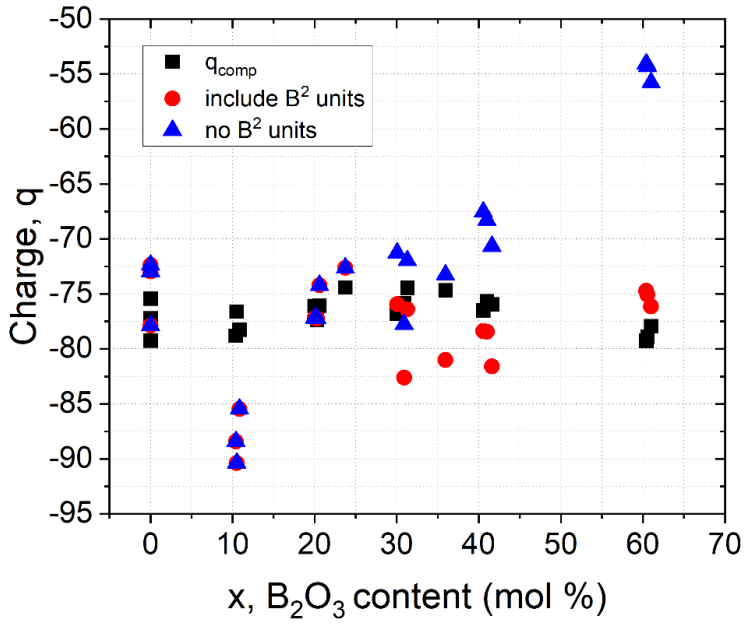

Figure A.1. The anionic charge from glasses with the nominal molar composition $16Na_2O$-(24-y)CaO-ySrO-xB_2O_3-(60-x)P_2O_5, where y=0, y=12, and y=24. The analyzed charges were determined using fractions of phosphate and borate units by ^{31}P and ^{11}B MAS NMR and the unit charges, including anionic B^2 units (red circles) and excluding anionic B^2 units (blue triangles).

APPENDIX B.

SUPPLEMENTARY INFORMATION FOR PAPER IV

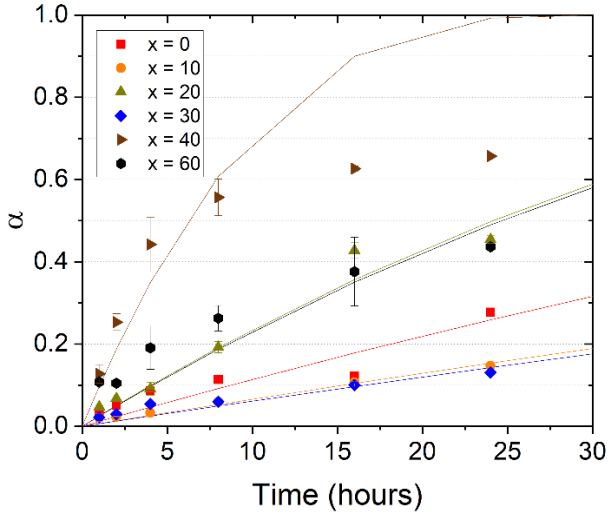

Figure B.2. The Contracting Volume Model fitted to the first 24 hours of weight loss data for the the 150mg samples (75-150 mm) in deionized water for the $16Na_2O$-$24CaO$-xB_2O_3-$(60-x)P_2O_5$ (SrO-free) compositional series. All experiments were carried out in a shaker bath set to 37°C.

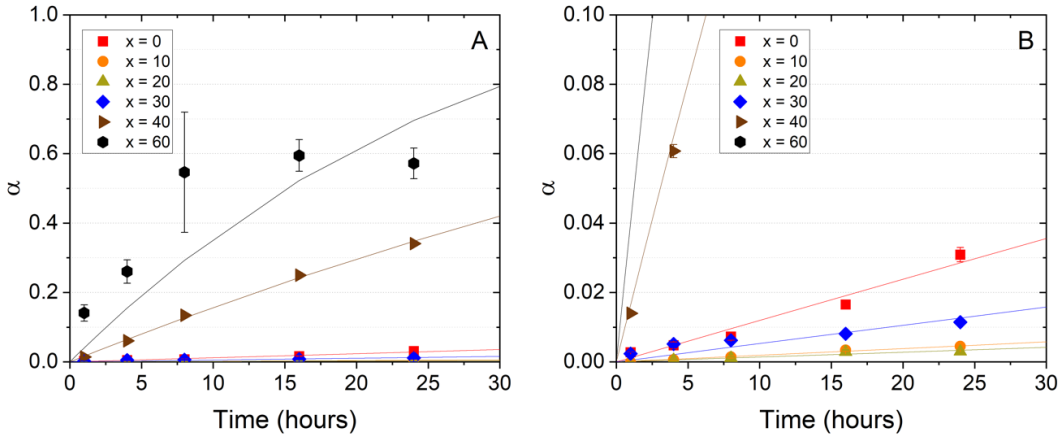

Figure B.3. The Contracting Volume Model fitted to the first 24 hours of weight loss data for the 300mg samples (250-500mm) in SBF for the $16Na_2O$-$12CaO$-$12SrO$-xB_2O_3-$(60-x)P_2O_5$ (mixed alkali) compositional series (A). The insert (B) clarifies the fits for compositions that dissolve much more slowly. All experiments were carried out in a shaker bath set to 37°C.

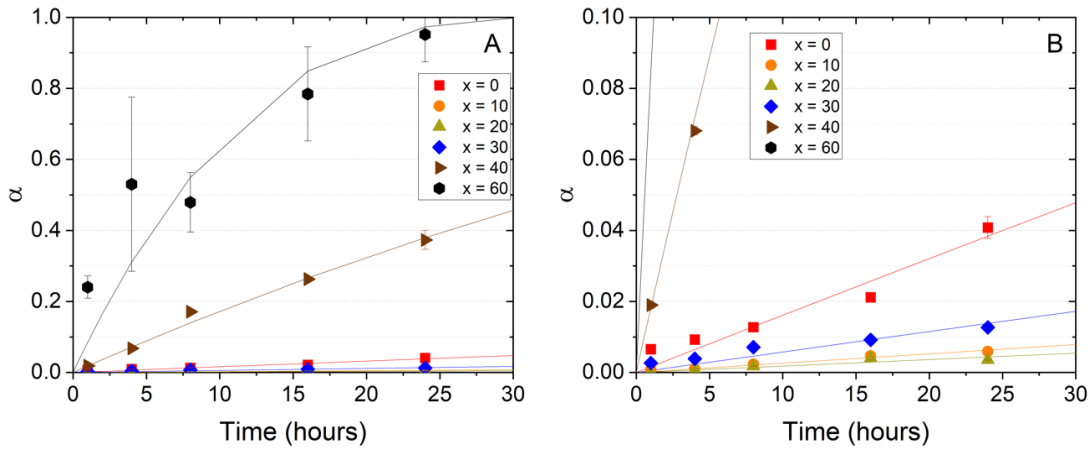

Figure B.4. The Contracting Volume Model fitted to the first 24 hours of weight loss data for the 300mg samples (250-500mm) in SBF for the $16Na_2O$-$24SrO$-xB_2O_3-$(60-x)P_2O_5$ (CaO free) compositional series (A). The insert (B) clarifies the fits for compositions that dissolve much more slowly. All experiments were carried out in a shaker bath set to 37°C.

1. FACTSAGE CALCULATIONS

Solution speciation reactions were calculated using the Equilib module of FactSage™ 7.2, a thermochemical database and computing system. The ion concentrations from the ICP-OES measurements were used to predict the solution pH and precipitation products for both the deionized water and SBF experiments, the latter after including thermochemical information for tris(hydroxymethyl)aminomethane, a component in SBF. In the case of the SBF experiments, ion concentrations were estimated assuming the glasses dissolved congruently and using the boron release data by ICP-OES for glasses containing boron. For the borate-free glass, the weight loss data was used. The results are presented in Figure B.1 and Figure B.2.

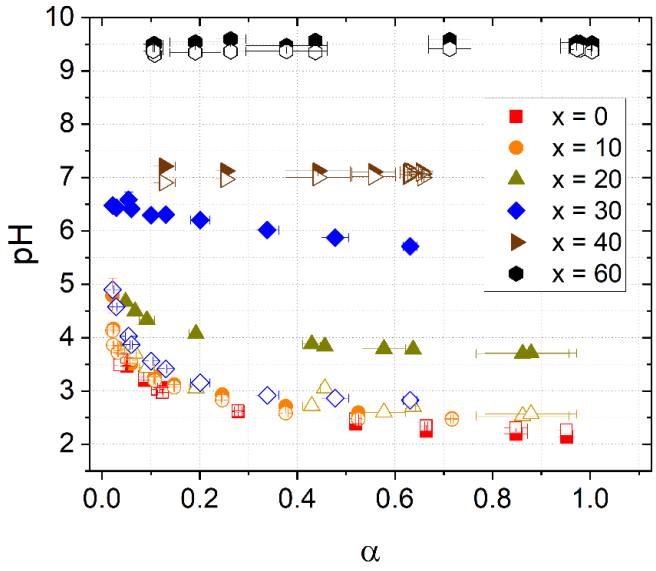

Figure B.1. The calculated solution pH using FactSage (open symbols) compared to experimental data (solid symbols) for the SrO-free (y=0) $16Na_2O$-$24CaO$-xB_2O_3-$(60-x)P_2O_5$ compositional series used in the 150mg (75-150 µm particles) deionized water experiment with respect to the fraction of glass reacted determined by weight loss (x=0) or B release (x≥10) data.

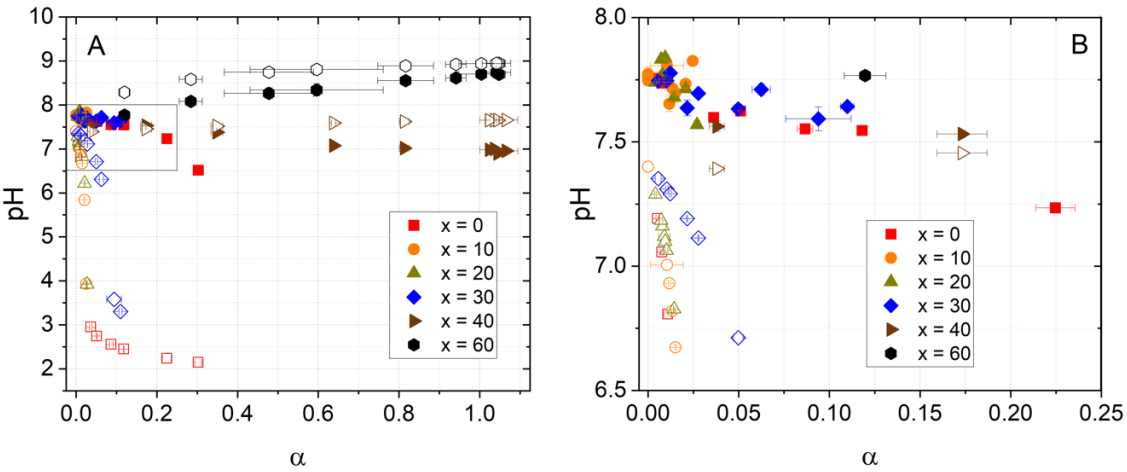

Figure B.2. The calculated solution pH using FactSage (open symbols) compared to experimental data (solid symbols) for the SrO-free (y=0) $16Na_2O$-$24CaO$-xB_2O_3-$(60-x)P_2O_5$ compositional series used in the 300mg (250-500µm particles) SBF experiment. The fraction of glass reacted determined by weight loss was used for x=0 and B release data was used for x≥10. The box in A denotes the expanded section in B.

Based on the estimated activities of possible species in solution, calculations using FactSage™ determined that disodium calcium pyrophosphate ($Na_2CaP_2O_7$) was expected to form in acidic (<7.0) environments. In deionized water, the x = 60 glass was expected to fully dissolve with no reaction products, though hydroxyapatite was expected to form for glasses having higher B_2O_3 content (x =40) and in SBF. In contrast, the conversion to brushite on of the x = 40 composition and the formation of an amorphous Ca-phosphate layer on the x = 30 sample was observed, the latter of which is a non-equilibrium phase and therefore not predicted by FactSage™. Though the calculations using FactSage™ did not accurately depict the formation of reaction products during dissolution, there are some insights to be had in the way that the program estimates solution pH, particularly with regards to the phosphate species in solution.

Simulated Body Fluid acts as a complexing agent in hydrolysis, and this effect is not accounted for by the Debye-Huckel equation, which is used by the FactSage™ software to calculate species' activities and assumes that all solutes are fully dissociated. For the deionized water experiment in Figure B**.1**, however, there is an autocatalyzing effect on the hydrolysis due to the acidic pH, creating a similar ion environment to that which is assumed by the Debye-Huckel equation. This leads to a calculated pH value that is in good agreement with the measured pH (~2.2) for the x = 0 composition in deionized water. The borophosphate compositions (x = 20 and 30) in deionized water have significantly higher measured pH (3.6, 5.7) compared to the calculated pH (<3.0). In the case of the x = 40 composition in deionized water, there are more depolymerized phosphate species being released into solution, and therefore match the pH calculations

by FactSage^{TM}. FactSage^{TM} may be a useful tool in the consideration of phosphate glass dissolution in water or glasses having predominantly orthophosphate species.

2. SEMI-QUANTITATIVE ANALYSIS

An estimation of bond strengths can be made by evaluating the contribution of valence units (V.U.) of cations through bond valence analysis. Tetrahedral boron contributes 0.75 V.U. to the Ø, and 1 V.U. is contributed by trigonal boron. Phosphorus typically contributes 1 V.U. to the Ø between phosphate tetrahedra, and the remaining charge is redistributed between the NBO. While heteroatomic bonds to the Ø (1.75 V.U.) are not necessarily stronger than those between phosphate tetrahedra (2.0 V.U.) and mixed borate species (1.75 V.U.), the relationship between [BØP] and [BØB] is an indicator of the role of phosphate tetrahedra in balancing tetrahedral borate species, delaying the formation of trigonal borate units.

With increasing [BØP], the phosphate chains are shortened and charge balanced by the modifying cations, increasing their resistance to hydration through stronger bonds to the NBOs. Furthermore, Ma *et al.* found that the dissolution rate in both the parabolic and linear stages of sodium and calcium polyphosphate glasses decreases by an order of magnitude as the phosphate chain length ($\bar{n}$) decreases. Additionally, an increase in ratio of trigonal to tetrahedral borate species, signaled by increasing [BØB] above x = 20, has been directly related to increasing borate glass dissolution rates.

The dissolution rate can be related to these changes in glass structure by using the fraction of P_{jB}^2 units to quantify chain length and the fraction of B^3 units to empirically calculate a Network Structure Factor (NSF):

$$Network\ Structure\ Factor\ (NSF) = 5\left[P_{jB}^2\right] + [B^3] \qquad \text{B.1}$$

The log of the dissolution rates is plotted against this Network Structure Factor in Figure B.1, demonstrating a clear positive trend in dissolution rates and P_{jB}^2 and B^3 unit concentrations. Additional research is necessary to assign a physical meaning to the coefficient, though the increase in P_{jB}^2 units appears to have a greater effect on this NSF, and the dissolution rate by proxy, as trigonal borate species.

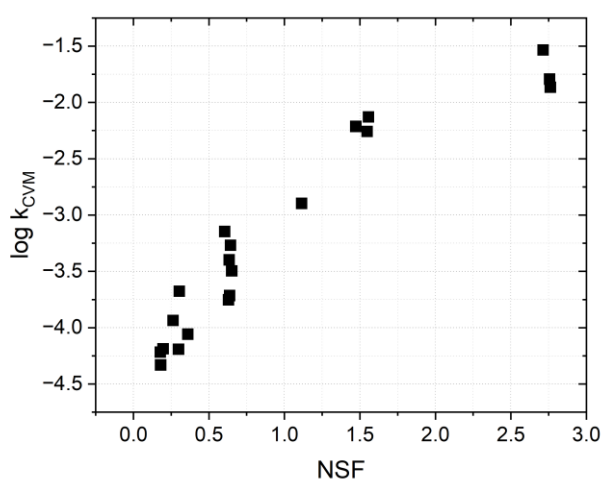

Figure B.1. The dependence of the dissolution rate (k_{CVM}, CVM) on the Network Structure Factor established by Equation B.1 for glasses of the system $16Na_2O$-(24-y)CaO-ySrO-xB_2O_3-(60-x)P_2O_5.

BIBLIOGRAPHY

1. Hoppe U. A structural model for phosphate glasses. Journal of Non-Crystalline Solids. 1996;195(1–2):138–147. https://doi.org/10.1016/0022-3093(95)00524-2.

2. Smith CE, Brow RK, Montagne L, Revel B. The structure and properties of zinc aluminophosphate glasses. Journal of Non-Crystalline Solids. 2014;386:105–114. https://doi.org/10.1016/j.jnoncrysol.2013.11.042

3. Hermansen C, Mauro JC, Yue Y. A model for phosphate glass topology considering the modifying ion sub-network. Journal of Chemical Physics. 2014;140(15). https://doi.org/10.1063/1.4870764

4. Hermansen C, Youngman RE, Wang J, Yue Y. Structural and topological aspects of borophosphate glasses and their relation to physical properties. Journal of Chemical Physics. 2015;142(18). https://doi.org/10.1063/1.4919798

5. Dorozhkin S v. Calcium orthophosphates ($CaPO_4$): occurrence and properties. Progress in Biomaterials. 2016;5(1):9–70. https://doi.org/10.1007/s40204-015-0045-z

6. Kirsti L, E. K. Metabolic phases during the development of granulation tissue. 1967;4. https://doi.org/10.1042/bj1050333

7. Ye RC. The Relationship of pH of the Granulation Tissue and the Take of the Skin Graft. Meeting of the Society of Plastic and Reconstructive Surgery. Miami Beach: 1956:213–217.

8. Hench LL, Splinter RJ, Allen WC, Greenlee TK. Bonding mechanisms at the interface of ceramic prosthetic materials. Journal of Biomedical Materials Research. 1971;5:117.

9. Jones JR, Brauer DS, Greenspan DC, Consulting S, Court B, Augustine S. Bioglass and Bioactive Glasses and Their Impact on Healthcare. 2016;434:423–434. https://doi.org/10.1111/ijag.12252

10. Carr BI. Hepatic Arterial 90Yttrium Glass Microspheres (Therasphere) for Unresectable Hepatocellular Carcinoma: Interim Safety and Survival Data on 65 Patients. Liver Transplantation. 2004;10(2):107–110. https://doi.org/10.1002/lt.20036

11. Fu H, Rahaman MN, Brown RF, Day DE. Acta Biomaterialia Evaluation of bone regeneration in implants composed of hollow HA microspheres loaded with transforming growth factor b 1 in a rat calvarial defect model. Acta Biomaterialia. 2013;9(3):5718–5727. https://doi.org/10.1016/j.actbio.2012.11.017

12. Earl JS, Leary RK, Muller KH, Langford RM, Greenspan DC. Physical and chemical characterization of dentin surface following treatment with NovaMin technology. Journal of Clinical Dentistry. 2011;22(3):62–67.

13. Himene DAC, Ennox KIKL, Aunas RORK, Aharwar AKKG. Advanced Bioinks for 3D Printing : A Materials Science Perspective. 2016;44(6):2090–2102. https://doi.org/10.1007/s10439-016-1638-y

14. Jung SB, Day DE, Day T, Stoecker W, Taylor P. Treatment of non-Healing Diabetic Venous Stasis Ulcers with Bioactive Glass Nanofibers. Wound Repair and Regeneration. 2011;19(2):A30–A30.

15. Kokubo T, Kushitani H, Sakka S, Kitsugi T, Yamamuro T. Solutions able to reproduce in vivo surface-structure changes in bioactive glass-ceramic A-W3. Journal of Biomedical Materials Research. 1990;24(6):721–734.

16. Islam MT, Felfel RM, Abou Neel EA, Grant DM, Ahmed I, Hossain KMZ. Bioactive calcium phosphate–based glasses and ceramics and their biomedical applications: A Review. Journal of Tissue Engineering. 2017;8:1 –16. https://doi.org/10.1177/2041731417719170

17. Macon ALB, Kim TB, Valliant EM, et al. A unified in vitro evaluation for apatite-forming ability of bioactive glasses and their variants. Journal of Materials Science: Materials in Medicine. 2015;26(115). https://doi.org/10.1007/s10856-015-5403-9

18. Hench LL, Andersson Ö. An Introduction to Bioceramics. World Scientific Publishing; 1993

19. Rahaman MN, Day DE, Sonny Bal B, et al. Bioactive glass in tissue engineering. Acta Biomaterialia. 2011;7(6):2355–2373. https://doi.org/10.1016/J.ACTBIO.2011.03.016

20. Ottomeyer M, Mohammadkah A, Day D, Westenberg D. Broad-Spectrum Antibacterial Characteristics of Four Novel Borate-Based Bioactive Glasses. Advances in Microbiology. 2016;06(10):776–787. https://doi.org/10.4236/aim.2016.610076

21. Ahmed I, Lewis M, Olsen I, Knowles JC. Phosphate glasses for tissue engineering: Part 1. Processing and characterisation of a ternary-based P_2O_5-CaO-Na_2O glass system. Biomaterials. 2004;25(3):501–507. https://doi.org/10.1016/S0142-9612(03)00547-7

22. Ahmed I, Lewis M, Olsen I, Knowles JC. Phosphate glasses for tissue engineering: Part 2. Processing and characterisation of a ternary-based P_2O_5–CaO–Na_2O glass fibre system. Biomaterials. 2004;25(3):501–507. https://doi.org/10.1016/S0142-9612(03)00547-7

23. Franks K, Abrahams I, Knowles JC. Development of soluble glasses for biomedical use part I: In vitro solubility measurement. Journal of Materials Science: Materials in Medicine. 2000;11(10):609–614. https://doi.org/10.1023/A:1008949527695

24. Salih V, Franks K, James M, Hastings GW, Knowles JC, Olsen I. Development of soluble glasses for biomedical use part II: The biological response of human osteoblast cell lines to phosphate-based soluble glasses. Journal of Materials Science: Materials in Medicine. 2000;11(10):615–620. https://doi.org/10.1023/A:1008901612674

25. Brow RK. Review: the structure of simple phosphate glasses. Journal of Non-Crystalline Solids. 2000;263–264:1–28. https://doi.org/10.1016/S0022-3093(99)00620-1

26. Smith CE, Brow RK, Montagne L, Revel B. The structure and properties of zinc aluminophosphate glasses. Journal of Non-Crystalline Solids. 2014;386:105–114. https://doi.org/10.1016/j.jnoncrysol.2013.11.042

27. Sales BC, Boatner LA, Ramey JO. Chromatographic studies of the structures of amorphous phosphates: a review. Journal of Non-Crystalline Solids. 2000;263–264:155–166. https://doi.org/10.1016/S0022-3093(99)00644-4

28. Hoppe U. A structural model for phosphate glasses. Journal of Non-Crystalline Solids. 1996;195(1–2):138–147. https://doi.org/10.1016/0022-3093(95)00524-2

29. Hoppe U, Walter G, Kranold R, Stachel D, Barz A. The dependence of structural peculiarities in binary phosphate glasses on their network modifier content. Journal of Non-Crystalline Solids. 1995;192–193:28–31. https://doi.org/10.1016/0022-3093(95)00325-8

30. Hudgens JJ, Martin SW. Glass Transition and Infrared Spectra of Low-Alkali, Anhydrous Lithium Phosphate Glasses. Journal of the American Ceramic Society. 1993;76(7):1691–1696. https://doi.org/10.1111/j.1151-2916.1993.tb06636.x

31. Alam TM, Conzone S, Brow RK, Boyle TJ. ^{6}Li, ^{7}Li nuclear magnetic resonance investigation of lithium coordination in binary phosphate glasses. Journal of Non-Crystalline Solids. 1999;258(1–3):140–154. https://doi.org/10.1016/S0022-3093(99)00481-0

32. Muruganandam K, Seshasayee M, Patnaik S. An X-ray RDF study of $Li_2O \cdot P_2O_5 \cdot LiCl$ glasses. Solid State Ionics. 1996;89(3–4):313–319. https://doi.org/10.1016/0167-2738(96)00344-X

33. Hoppe U. Short-range order of phosphate glasses studied by a difference approach using X-ray diffraction results. Journal of Non-Crystalline Solids. 1995;183(1–2):85–91. https://doi.org/10.1016/0022-3093(94)00632-6

34. Hoppe U, Herms G, Gerike W, Sakowski J. The increased intensity of the first sharp diffraction peak of a $NaPO_3$ melt. Journal of Physics Condensed Matter. 1996;8(43):8077–8087. https://doi.org/10.1088/0953-8984/8/43/006

35. Brow RK, Click CA, Alam TM. Modifier coordination and phosphate glass networks. Journal of Non-Crystalline Solids. 2000;274:9–16.

36. Bunker BC, Arnold GW, Wilder JA. Phosphate glass dissolution in aqueous solutions. Journal of Non-Crystalline Solids. 1984;64(3):291–316. https://doi.org/10.1016/0022-3093(84)90184-4

37. Shelby JE. Introduction to Glass Science and Technology. 2nd ed. The Royal Society of Chemistry; 2005

38. Shelby JE. Thermal Expansion of Alkali Borate Glasses. Journal of the American Ceramic Society. 1983;66(3):225–227.

39. Youngman RE, Haubrich ST, Zwanziger JW, Janicke MT, Chmelka BF. Short- and Intermediate-Range Structural Ordering in Glassy Boron Oxide. 1995;269:1416–1420.

40. Shelby JE. Thermal Expansion of Alkali Borate Glasses. Journal of the American Ceramic Society. 1983;66(3):225–227.

41. Bunker BC, Arnold GW, Day DE, Bray PJ. The Effect of Molecular Structure on Borosilicate Glass Leaching. Journal of Non-Crystalline Solids. 1986;87:226–253.

42. Veléz MH, Tuller HL, Uhlmann DR. Chemical durability of lithium borate glasses. Chemical Durability of Lithium Borate Glasses. 1982;49:351–362. https://doi.org/10.1137/1.9781611970319.ch1

43. Goetschius KL, Beuerlein MA, Bischo CM, Brow RK. Dissolution behavior of ternary alkali-alkaline earth-borate glasses in water. Journal of Non-Crystalline Solids. 2018;487:12–18. https://doi.org/10.1016/j.jnoncrysol.2018.02.011

44. Bray PJ, Leventhal M, Hooper HO. Nuclear Magnetic Resonance Investigations of Structure of Alkali Borate Glasses. Physics and Chemistry of Glasses. 1963;4(2):37–46.

45. Michaelis VK, Aguiar PM, Kroeker S. Probing alkali coordination environments in alkali borate glasses by multinuclear magnetic resonance. Journal of Non-Crystalline Solids. 2007;353:2582–2590.

46. Michaelis VK, Aguiar PM, Kroeker S. Probing alkali coordination environments in alkali borate glasses by multinuclear magnetic resonance. Journal of Non-Crystalline Solids. 2007;353:2582–2590.

47. Kroeker S, Stebbins JF. Three-coordinated boron-11 shifts in borates. Inorganic Chemsitry. 2001;40(24):6239–6246.

48. Bray PJ. NMR and NQR studies of boron in vitreous and crystalline borates. Inorganica Chimica Acta. 1999;289(1):158–173. https://doi.org/https://doi.org/10.1016/S0020-1693(99)00066-3

49. Bray PJ. NMR and NQR studies of boron in vitreous and crystalline borates. Inorganica Chimica Acta. 1999;289(1):158–173. https://doi.org/https://doi.org/10.1016/S0020-1693(99)00066-3

50. Kroeker S, Feller SA, Affatigato M, O'Brien CP, Clarida WJ, Kodama M. Multiple four coordinated boron sites in caesium borate and their relation to medium range order. Physics and Chemistry of Glasses. 2003;44(2):54–58.

51. Saranti A, Koutselas I, Karakassides MA. Bioactive glasses in the system CaO-B_2O_3-P_2O_5: Preparation, structural study and in vitro evaluation. Journal of Non-Crystalline Solids. 2006;352(5):390–398. https://doi.org/10.1016/j.jnoncrysol.2006.01.042

52. Christensen R, Olson G, Martin SW. Structural Studies of Mixed Glass Former $0.35Na_2O + 0.65[xB_2O_3+(1–x)P_2O_5]$ Glasses by Raman and ^{11}B and ^{31}P Magic Angle Spinning Nuclear Magnetic R. The Journal of Physical Chemistry B. 2013;117(7):2169–2179. https://doi.org/10.1021/jp308494a

53. Brow RK, Tallant DR. Structural design of sealing glasses. Journal of Non-Crystalline Solids. 1997;222:396–406.

54. Koudelka L, Mošner P. Borophosphate glasses of the ZnO – B_2O_3 – P_2O_5 system. Materials Letters. 2000;42(January):194–199.

55. Koudelka L, Mošner P, Pospíšil J, Montagne L, Palavit G. Structure and properties of titanium-zinc borophosphate glasses. Journal of Solid State Chemistry. 2005;178(6):1837–1843. https://doi.org/10.1016/j.jssc.2005.03.025

56. Svenson MN, Youngman RE, Yue Y, et al. Volume and Structure Relaxation in Compressed Sodium Borate Glass. Phys Chem Chem Phys Physical Chemistry Chemical Physics Physical Chemistry Chemical Physics Accepted Manuscript. 2016;18:29879–29891. https://doi.org/10.1039/C6CP06341A

57. Carta D, Qiu D, Guerry P, et al. The effect of composition on the structure of sodium borophosphate glasses. Journal of Non-Crystalline Solids. 2008;354(31):3671–3677. https://doi.org/10.1016/j.jnoncrysol.2008.04.009

58. Lim JWW, Schmitt MLL, Brow RKK, Yung SWW. Properties and structures of tin borophosphate glasses. Journal of Non-Crystalline Solids. 2010;356(28–30):1379–1384. https://doi.org/10.1016/j.jnoncrysol.2010.02.019

59. Raskar D, Rinke MT, Eckert H. The Mixed-Network Former Effect in Phosphate Glasses: NMR and XPS Structural Studies of the Connectivity Distribution in the Glass System $(NaPO_3)_{1-x}(B_2O_3)_x$. The Journal of Physical Chemistry C. 2008;112:12530–12539. https://doi.org/10.1039/c0cp01590c

60. Massera J, Shpotyuk Y, Sabatier F, et al. Processing and characterization of novel borophosphate glasses and fibers for medical applications. Journal of Non-Crystalline Solids. 2015;425:52–60. https://doi.org/10.1016/j.jnoncrysol.2015.05.028

61. Casey WH, Bunker BC. Leaching of Mineral and Glass Surfaces During Dissolution. Mineral-Water Interface Geochemistry. 1990:397–426. https://doi.org/https://doi.org/10.1515/9781501509131-014

62. Van Wazer JR. Phosphorus and its Compounds. New York, NY: Interscience; 1958

63. Abrajano Jr TA, Bates JK, Byers CD. Aqueous Corrosion of Natural and Nuclear Waste Glasses. Journal of Non-Crystalline Solids. 1986;84:251–257.

64. Zoitos BK, Clark DE. Corrosion of glass, ceramics and ceramic superconductors: Principles, testing, characterization and applications. Park Ridge, NJ: Noyes Publications; 1992

65. Van Wazer JR. Phosphorus and its Compounds. New York, NY: Interscience; 1958

66. Thilo E, Wieker W. Study of Degradation of Polyphosphates in Aqueous Solution. Journal of Polymer Science. 1961;53:55–59.

67. Ma L, Brow K, Schlesinger ME. Dissolution behaviour of sodium calcium polyphosphate glasses. 2018;59(5):205–212. https://doi.org/10.13036/17533562.59.5.018

68. Van Wazer JR, Campanella DA. Structure and Properties of the Condensed Phosphates. IV. Complex Ion Formation in Polyphosphate Solutions. Journal of the American Ceramic Society. 1950;72(2):655–663. https://doi.org/10.1021/ja01158a004

69. Delahaye F, Montagne L, Palavit G, Touray JC, Baillif P. Acid dissolution of sodium-calcium metaphosphate glasses. Journal of Non-Crystalline Solids. 1998;242(1):25–32. https://doi.org/10.1016/S0022-3093(98)00784-4

70. Ahmed I, Parsons AJ, Rudd CD, et al. Comparison of phosphate-based glasses in the range $50P_2O_5$-(50-x)CaO-xNa_2O prepared using different precursors. Glass Technology - European Journal of Glass Science and Technology Part A. 2008;49(2):63–72.

71. Ma L, Brow K, Schlesinger ME. Dissolution behaviour of sodium calcium polyphosphate glasses. 2018;59(5):205–212. https://doi.org/10.13036/17533562.59.5.018

72. Dorozhkin S V. Calcium orthophosphates ($CaPO_4$): occurrence and properties. Progress in Biomaterials. 2016;5(1):9–70. https://doi.org/10.1007/s40204-015-0045-z

73. Boskey AL, Posner AS. Magnesium stabilization of amorphous calcium phosphate: A kinetic study. Materials Research Bulletin. 1974;9(7):907–916. https://doi.org/https://doi.org/10.1016/0025-5408(74)90169-X

74. Goetschius KL, Beuerlein MA, Bischo CM, Brow RK. Dissolution behavior of ternary alkali-alkaline earth-borate glasses in water. 2018;487(February):12–18. https://doi.org/10.1016/j.jnoncrysol.2018.02.011

75. Zapol P, He H, Kwon KD, Criscenti LJ. First-principles study of hydrolysis reaction barriers in a sodium borosilicate glass. International Journal of Applied Glass Science. 2013;4(4):395–407. https://doi.org/10.1111/ijag.12052

76. Bunker BC, Arnold GW, Day DE, Bray PJ. The Effect of Molecular Structure on Borosilicate Glass Leaching. Journal of Non-Crystalline Solids. 1986;87:226–253.

77. Brow RK. The Dissolution of Borate Glasses in Aqueous Solutions. In: Kasuga T, Obata A, Brauer DS, eds. Phosphate and Borate Bioactive Glasses. Royal Society of Chemistry; 2022

78. George JL, Brow RK. In-situ characterization of borate glass dissolution kinetics by μ -Raman spectroscopy. Journal of Non-Crystalline Solids. 2015;426:116–124. https://doi.org/10.1016/j.jnoncrysol.2015.07.003

79. Gu Y, Xiao W, Lu L, Huang W, Rahaman MN, Wang D. Kinetics and mechanisms of converting bioactive borate glasses to hydroxyapatite in aqueous phosphate solution. Journal of Materials Science. 2011;46(1):47–54. https://doi.org/10.1007/s10853-010-4792-x

80. Huang W, Li Y, Rahaman M, Day D. Mechanisms for converting bioactive silicate, borate, and borosilicate glasses to hydroxyapatite in dilute phosphate solution. Physics and Chemistry of Glasses-european Journal of Glass Science and Technology Part B. 2006;47:647–658.

81. Fletcher LB, Witcher JJ, Troy N, Reis ST, Brow RK, Krol DM. Direct femtosecond laser waveguide writing inside zinc phosphate glass. Optics Express. 2011;19(9):7929. https://doi.org/10.1364/OE.19.007929

82. Hernandez-Rueda J, Semenov V, Troy N, Smith CE, Brow RK, Krol DM. All-optical characterization of fs-laser induce refractive index changes in bulk and at the surface of zinc phosphate glasses. Proceedings of SPIE. 2015

83. Hernandez-Rueda J, Troy NW, Freudenberger P, Brow RK, Krol DM. Femtosecond laser-matter interactions in ternary zinc phosphate glasses. Optical Materials Express. 2018;8(12):3622. https://doi.org/10.1364/ome.8.003622

84. Krol DM, Chan JW, Huser TR, Risbud SH, Hayden JS. Fs Laser Fabrication of Photonic Structures in Glass: the Role of Glass Composition. UCRL-PROC. 2004;30–39. https://doi.org/10.1117/12.595762

85. Liu X, Rahaman MN, Day DE. Conversion of melt-derived microfibrous borate (13-93B3) and silicate (45S5) bioactive glass in a simulated body fluid. Journal of Materials Science: Materials in Medicine. 2013;24:583–595.

VITA

Parker Tracy Freudenberger was born to Richard and Laurie Freudenberger on April 15, 1991 in Portland, Maine. She graduated from D.W. Daniel High School in June 2009, and enrolled at Clemson University in August 2009. During her undergraduate career, she played piccolo in Tigerband (the band that shakes the Southland!), served as Day Away Committee Chair in Alpha Omega Epsilon, and also served as President of Keramos. She graduated with a B.S. in Ceramic Materials and Engineering in June 2014. From there, she enrolled at Missouri University of Science and Technology in August 2014. After surviving teaching and a global pandemic, she received her Ph.D. in Materials Science and Engineering in May 2023 from Missouri University of Science and Technology under the supervision of Dr. Richard K. Brow.